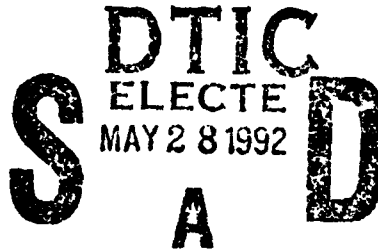




**RELIABILITY AND FAILURE ANALYSES OF 2-D
CARBON-CARBON STRUCTURAL COMPONENTS:**

VOLUME 2.

**R.A. Heller
S. Thangjitham
I. Yeo**



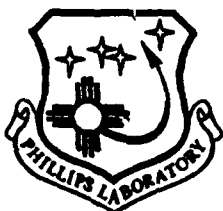
**Department of Engineering Science and Mechanics
Virginia Polytechnic Institute and State University
Blacksburg VA 24061-0219**

April 1992

Final Report

APPROVED FOR PUBLIC RELEASE; DISTRIBUTION UNLIMITED.

92-13879



**PHILLIPS LABORATORY
Propulsion Directorate
AIR FORCE SYSTEMS COMMAND
EDWARDS AIR FORCE BASE CA 93523-5000**



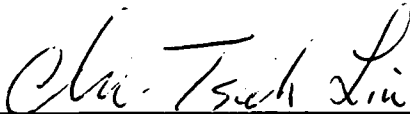
NOTICE

When U.S. Government drawings, specifications, or other data are used for any purpose other than a definitely related Government procurement operation, the fact that the Government may have formulated, furnished, or in any way supplied the said drawings, specifications, or other data, is not to be regarded by implication or otherwise, or in any way licensing the holder or any other person or corporation, or conveying any rights or permission to manufacture, use or sell any patented invention that may be related thereto.

FOREWORD

This Final 3 Volume Report was prepared by the Department of Engineering Science and Mechanics, Virginia Polytechnic Institute and State University, Blacksburg VA, under contact F04611-87-K-0010 for Operating Location AC, Phillips Laboratory (AFSC), Edwards AFB CA 93523-5000. OLAC PL Project Manager was Chi T. Liu.

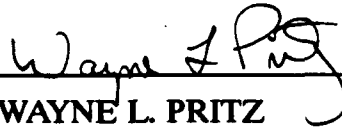
This report has been reviewed and is approved for release and distribution in accordance with the distribution statement on the cover and on the SF Form 298.



CHI T. LIU
Project Manager



BERNARD E. WILKERSON, CAPT, USAF
Chief, Propellants Branch



WAYNE L. PRITZ
Director,
Components Engineering Division



RANNEY G. ADAMS
Public Affairs Director

REPORT DOCUMENTATION PAGE

Form Approved
OMB No. 0704-0188

Public reporting burden for this collection of information is estimated to average 1 hour per response, including the time for reviewing instructions, searching existing data sources, gathering and maintaining the data needed, and completing and reviewing the collection of information. Send comments regarding this burden estimate or any other aspect of this collection of information, including suggestions for reducing this burden, to Washington Headquarters Services, Directorate for Information Operations and Reports, 1215 Jefferson Davis Highway, Suite 1204, Arlington, VA 22202-4302, and to the Office of Management and Budget, Paperwork Reduction Project (0704-0188), Washington, DC 20503.

1. AGENCY USE ONLY (Leave blank)		2. REPORT DATE April 1992		3. REPORT TYPE AND DATES COVERED Technical Report 5/1/87-6/30/91	
4. TITLE AND SUBTITLE Reliability and Failure Analysis of 2D Carbon-Carbon Structural Components				5. FUNDING NUMBERS C: F04611-87-K-001/P0001 PR: 3059 TA: 004G	
6. AUTHOR(S) Heller, R. A., Yeo, I., and Thangjitham, S.					
7. PERFORMING ORGANIZATION NAME(S) AND ADDRESS(ES) Department of Engineering Science and Mechanics Virginia Polytechnic Institute and State University Blacksburg, VA 24061-0219				8. PERFORMING ORGANIZATION REPORT NUMBER	
9. SPONSORING/MONITORING AGENCY NAME(S) AND ADDRESS(ES) Department of the Air Force OLAC, Phillips Lab (AFSC) Edwards AFB, CA 90523-5000 Dr. C. T. Liu, OLAC/PL/RCP				10. SPONSORING/MONITORING AGENCY REPORT NUMBER PL-TR-91-3068 V2	
11. SUPPLEMENTARY NOTES This is the second part of a three part report. COSATI Codes: 07/02: 13/08					
12a. DISTRIBUTION/AVAILABILITY STATEMENT Public Release; Distribution Unlimited				12b. DISTRIBUTION CODE	
13. ABSTRACT (Maximum 200 words) The strength of brittle materials is characterized by a wide scatter. Such materials are also afflicted by size effects. Size effects in brittle composite structures such as beams and plates with and without stress raisers are investigated experimentally and analytically. A methodology for reliability analysis of carbon-carbon composites is presented. The model is based on Weibull statistics which was extended to account for the three-dimensional stress field including interlaminar stresses. Failure criteria for bi-directional orthotropic lamina are developed and failure analysis in the non-probabilistic sense (f.e., First-ply-failure analysis) is performed. Comparisons are made with existing failure criteria, with the results of the reliability analysis and also with experiments.					
14. SUBJECT TERMS Carbon-carbon, Reliability, First Ply Failure, Weakest Link, Weibull Distribution, Beams, Plates				15. NUMBER OF PAGES 138	
				16. PRICE CODE	
17. SECURITY CLASSIFICATION OF REPORT Unclassified		18. SECURITY CLASSIFICATION OF THIS PAGE Unclassified		19. SECURITY CLASSIFICATION OF ABSTRACT Unclassified	
				20. LIMITATION OF ABSTRACT SAR	

TABLE OF CONTENTS

ABSTRACT.....	ii
ACKNOWLEDGEMENTS.....	v
Dedication.....	vi
LIST OF TABLES.....	xi
LIST OF FIGURES.....	xiv
INTRODUCTION	1
Objectives.....	1
Literature Review.....	1
SIZE EFFECT ANALYSIS	4
Analytical Study of Size Effect	4
* <i>Weakest Link</i> * Analysis.....	4
Experimental Study on Size Effect.....	6
Tension and Compression Tests	6
In-plane Shear Tests.....	7
Interlaminar Shear Tests.....	7
Beam Bending Tests	7
Plate Bending Tests	8
Determination of Weibull Distribution Parameters.....	21
STRESS ANALYSIS OF COMPOSITE BEAMS AND PLATES	23
Isotropic Beams under Four Point Bending	23
Composite Beams under Four Point Bending.....	23
Composite Plates under In-plane Loading.....	26
Composite Plates under Transverse Loading	26
RELIABILITY ANALYSIS OF COMPOSITE BEAMS AND PLATES	34
Reliability of Beams under Four Point Bending	34
Isotropic Beams	34
Unnotched Beams.....	34
Notched Beams.....	38
Composite Beams	49
Reliability of Composite Plates under Transverse Loading	55
Extension of * <i>Weakest Link</i> * Reliability to Account for	
Interlaminar Shear Stresses τ_{zx} and τ_{zy}	55
Square Plates under Transverse Loading.....	56
Square Plate without a Hole.....	56
Square Plate with a Hole.....	56
Rectangular Plates under Transverse Loading.....	56
Rectangular Plate without a Hole.....	56
Rectangular Plate with a Hole.....	56
FAILURE ANALYSIS.....	76

Modeling of Failure in a Laminated Composite Plate	76
Review of Failure Criteria	76
Category I Failure Criteria	76
Category II Failure Criteria	77
Development of Three-Dimensional Failure Criteria for a Bi-Directional Composite Lamina	80
Proposed Failure Criteria for an Orthotropic Composite Lamina	81
Failure Analysis	82
First-Ply-Failure Analysis of Carbon-Carbon Composite Plates	82
Comparison of the Proposed Criteria with Other Criteria	88
Comparison of Reliability Analysis with First-Ply-Failure Analysis and Experiments	95
Composite Beams	95
Composite Plates	95
CLOSURE	98
Discussions	98
Future Work	99
REFERENCES	100
Appendix-A	104
Formulation of Finite Element Program <u>F2DELAST</u>	107
Finite Element Formulation for Nonlinear Bending of a Laminated Composite Plate with Shear Deformation	111
Element Stiffness Matrix and Force Vector for Nonlinear Plate Bending Formulation	123

LIST OF TABLES

Table 1	Four Point Bending Test Results	12
Table 2	Plate Bending Test Data	18
Table 3	Normalized Tension Strength Data and Three Weibull Parameters.....	22
Table 4	Dimension and strength parameters used in the computation of reliability of an isotropic beam.....	44
Table 5	Comparison of experimental and analytical results for an isotropic beam.....	44
Table 6	Material properties and strength parameters of a composite beam.....	50
Table 7	Comparison of experimental and analytical results for a composite beam	51
Table 8	Material properties and strength parameters of composite plates	61
Table 9	First-ply-failure load, mode, and location of a carbon-carbon square plate with a hole under uniform transverse load predicted by the proposed failure criteria	84
Table 10	First-ply-failure load, mode, and location of a carbon-carbon rectangular plate without a hole under uniform transverse load predicted by the proposed failure criteria.....	85
Table 11	First-ply-failure load, mode, and location of a carbon-carbon rectangular plate with a hole under uniform transverse load predicted by the proposed failure criteria.....	86
Table 12	Comparison of normalized first-ply-failure pressure, mode, and location predicted by the proposed criteria with those of other criteria for a [0/90] _s graphite-epoxy square plate with aspect ratio 10 under sinusoidal load.	92
Table 13	Comparison of normalized first-ply-failure pressure, mode, and location predicted by the proposed criteria with those of other criteria for a [0/90] _s graphite-epoxy square plate with aspect ratio 100 under sinusoidal load.....	93
Table 14	Comparison of failure loads predicted by reliability analysis, first-ply-failure analysis and experiment for carbon-carbon composite beam under 4-point bending.....	96
Table 15	Comparison of failure loads predicted by reliability analysis, first-ply-failure analysis based on the proposed failure criteria and experiment for carbon-carbon composite plate under uniform transverse load.....	97
Table A.1	Average tension and compression data.....	104
Table A.2	In-plane shear data.....	105
Table A.3	Interlaminar shear data.....	106
Table A.4	Average Mechanical Parameters.....	121



v

Accession For	
NTIS CRA&I	<input checked="" type="checkbox"/>
DTIC TAB	<input type="checkbox"/>
Unannounced	<input type="checkbox"/>
Justification	
By	
Distribution /	
Availability Codes	
Dist	Availability for Special
A-1	

LIST OF FIGURES

Fig. 1	Typical arrangements of specimens cut from a 10 x 6.5 x 0.5 " plate.....	9
Fig. 2	Loading configuration for four point bending specimens.....	10
Fig. 3	Test fixture for four point bending tests.....	10
Fig. 4	Four point bending test configuration.....	11
Fig. 5	Failure modes of unnotched four point bending specimens.....	13
Fig. 6	Failure modes of notched four point bending specimens.....	14
Fig. 7	Plate bending specimen.....	15
Fig. 8	Plate bending test fixture.....	16
Fig. 9	Simply supported boundary condition used in the experiment and stress analysis.....	17
Fig. 10	Load-deflection curve for rectangular plates (1 & 2, with a hole, 3, with no hole	19
Fig. 11	Load-deflection curve for a square plate with a hole.....	20
Fig. 12	Finite element mesh of an unnotched isotropic beam.....	24
Fig. 13	Finite element mesh of a notched isotropic beam.....	24
Fig. 14	Finite element mesh of an unnotched composite beam.....	25
Fig. 15	Finite element mesh of a notched composite beam.....	25
Fig. 16	Geometry and dimension of a square plate under in-plane loading (a) uni-axial loading (b) bi-axial loading.....	27
Fig. 17	Finite element mesh of a square plate with a hole for $d/w=0.05$	28
Fig. 18	Finite element mesh of a rectangular plate with a hole for aspect ratio $L/w=5$ and hole-diameter-to-width ratio $d/w=0.1$	29
Fig. 19	Typical 2-D finite element domain.....	30
Fig. 20	Node and Gauss point numbering scheme in a 9-node element.....	30
Fig. 21	Geometry and coordinate system of a laminate.....	31
Fig. 22	Diagram of resultant forces and moments in a laminate.....	32
Fig. 23	Geometry and layer number of a multi-layered laminate.....	33
Fig. 24	Four point bending diagram on an unnotched isotropic beam.....	35
Fig. 25	Reliability of an isotropic unnotched beam under 4-point bending as a function of load.....	39
Fig. 26	Reliability of an isotropic notched beam under 4-point bending as a function of load.....	39
Fig. 27	Comparison of reliabilities of an isotropic unnotched and notched beam due to tensile stresses alone as a function of load.....	41
Fig. 28	Comparison of reliabilities of an isotropic unnotched and notched beam due to tensile and compressive stresses combined as a function of load.....	41
Fig. 29	Reliability of an isotropic unnotched beam under 4-point bending as a function of maximum principal stress.....	42
Fig. 30	Reliability of an isotropic notched beam under 4-point bending as a function of maximum principal stress.....	42
Fig. 31	Comparison of reliabilities of an isotropic unnotched and notched beam due to tensile stresses alone as a function of maximum principal stress	43
Fig. 32	Comparison of reliabilities of an isotropic unnotched and notched beam due to tensile stresses and compressive stresses combined as a function of maximum principal stress	43
Fig. 33	Reliability contour of an isotropic unnotched beam under 4-point bending due to tensile stresses at 0.5 (kip) load.....	45
Fig. 34	Reliability contour of an isotropic unnotched beam under 4-point bending	

	due to tensile & compressive stresses combined at 0.5 (kip) load.....	46
Fig. 35	Reliability contour of an isotropic notched beam under 4-point bending due to tensile stresses at 0.25 (kip) load.....	47
Fig. 36	Reliability contour of an isotropic notched beam under 4-point bending due to tensile & compressive stresses combined at 0.25 (kip) load.....	48
Fig. 37	Reliability of an unnotched composite beam under 4-point bending as a function of load.....	52
Fig. 38	Reliability of a notched composite beam under 4-point bending as a function of load.....	52
Fig. 39	Comparison of reliabilities of an unnotched and notched composite beam due to tensile stresses alone as a function of load	54
Fig. 40	Comparison of reliabilities of an unnotched and notched composite beam due to tensile, compressive and interlaminar stresses combined as a function of load	54
Fig. 41	Reliability of an unnotched composite beam under 4-point bending as a function of maximum principal stress.....	57
Fig. 42	Reliability of a notched composite beam under 4-point bending as a function of maximum principal stress.....	57
Fig. 43	Comparison of reliabilities of an unnotched and notched composite beam due to tensile stresses alone as a function of maximum principal stress.....	58
Fig. 44	Comparison of reliabilities of an unnotched and notched composite beam due to tensile, compressive and interlaminar stresses combined as a function of maximum principal stress	58
Fig. 45	Reliability contour of an unnotched composite beam under 4-point bending due to tensile stresses alone at 0.20 (kip).....	59
Fig. 46	Reliability contour of a notched composite beam under 4-point bending due to all stress components at 0.20 (kip).....	60
Fig. 47	Reliability of a carbon-carbon square plate without a hole under transverse loading as a function of pressure.....	63
Fig. 48	Reliability of a carbon-carbon square plate with a hole under transverse loading as a function of pressure.....	63
Fig. 49	Reliability of a carbon-carbon square plate without a hole under transverse loading as a function of load.....	64
Fig. 50	Reliability of a carbon-carbon square plate with a hole under transverse loading as a function of load.....	64
Fig. 51	Reliability of a carbon-carbon square plate without a hole under transverse loading as a function of maximum stress.....	65
Fig. 52	Reliability of a carbon-carbon square plate with a hole under transverse loading as a function of maximum stress.....	65
Fig. 53	Reliability of a carbon-carbon rectangular plate without a hole under transverse loading as a function of pressure.....	66
Fig. 54	Reliability of a carbon-carbon rectangular plate with a hole under transverse loading as a function of pressure.....	66
Fig. 55	Reliability of a carbon-carbon rectangular plate without a hole under transverse loading as a function of load.....	67
Fig. 56	Reliability of a carbon-carbon rectangular plate with a hole under transverse loading as a function of load.....	67
Fig. 57	Reliability of a carbon-carbon rectangular plate without a hole under transverse loading as a function of maximum stress.....	68
Fig. 58	Reliability of a carbon-carbon rectangular plate with a hole under transverse loading as a function of maximum stress.....	68
Fig. 59	Comparison of reliabilities of carbon-carbon square and rectangular plates with and without a hole as a function of pressure.....	69
Fig. 60	Comparison of reliabilities of carbon-carbon square and rectangular plates with and without a hole as a function of load.....	69

Fig. 61	Comparison of reliabilities of carbon-carbon square plates with and without a hole as a function of maximum stress in x-direction.....	70
Fig. 62	Comparison of reliabilities of carbon-carbon rectangular plates with and without a hole as a function of maximum stress in y-direction.....	70
Fig. 63	Reliability contour at top matrix layer of a carbon-carbon square plate with a hole due to 3-D stresses at 100 psi uniform transverse loading	71
Fig. 64	Reliability contour at top matrix layer of a carbon-carbon rectangular plate without a hole due to 3-D stresses at 100 psi uniform transverse loading	72
Fig. 65	Reliability contour at bottom fiber layer of a carbon-carbon rectangular plate without a hole due to 3-D stresses at 100 psi uniform transverse loading ..	73
Fig. 66	Reliability contour at top matrix layer of a carbon-carbon rectangular plate with a hole due to 3-D stresses at 100 psi uniform transverse loading	74
Fig. 67	Reliability contour at bottom fiber layer of a carbon-carbon rectangular plate with a hole due to 3-D stresses at 100 psi uniform transverse loading.....	75
Fig. 68	Comparison of FPF loads predicted by the proposed criteria and failure loads at 0.5 reliability level with experimental failure loads for carbon-carbon square and rectangular plates under uniform transverse loading	83
Fig. 69	Comparison of FPF loads predicted by various criteria with those obtained by reliability analysis and experiment for carbon-carbon rectangular plates without a hole under uniform transverse loading.....	87
Fig. 70	Comparison of FPF pressures predicted by various failure criteria for a graphite-epoxy square plate under sinusoidal transverse loading.....	90
Fig. 71	Comparison of normalized FPF pressures predicted by various failure criteria for a graphite-epoxy square plate under sinusoidal transverse loading.....	91
Fig. 72	Comparison of normalized FPF pressures predicted by various failure criteria including Brewer-Lagace's delamination criteria for a graphite-epoxy square plate under sinusoidal transverse loading.....	94

INTRODUCTION

Objectives

One of the most important areas in research on composite materials is the area of failure analysis. Unfortunately, most of this research is deterministic and does not account for the variability inherent in material properties and in environmental loading conditions. It is a well-known fact that there is a wide scatter in strength data for composite materials. While for some materials the deterministic stress/failure analysis may suffice, for others such as brittle composites, the deterministic stress analysis alone is not enough and must be supplemented by some statistical theory of failure.

Most brittle materials are afflicted by the so-called "size effect" in some way or another. To establish this effect, it is necessary to test components of widely varying sizes, obtain properties and to infer from these the necessary information about the size effect. It is, however, often very costly and impractical or even impossible to conduct experiments on full scale structures. It is, therefore, necessary to scale lab specimen results to the real, larger size structural component as the lab test results are not directly applicable to such full scale structures. One of the objectives of this research is to investigate the size effect of composite materials both analytically and experimentally and to establish a methodology of assessing the probability of failure (or reliability) of structures made of brittle composite materials. The procedure is applied to 2-D woven carbon-carbon composites. Detailed experimental data are available on tension and compression tests, off-angle tension tests, in-plane and interlaminar shear tests, 4-point bending on isotropic and composite beams with and without stress concentrations, and bending tests on composite plates of various shapes, aspect ratios, and stress concentrations [Heller et al, 1991].

Another objective is to perform the failure analysis in non-probabilistic sense because the reliability analysis does not give information about failure modes and failure locations. New failure criteria are developed and proposed. These criteria are compared with existing ones found in the literature.

Literature Review

Reliability Analysis

A statistical theory of strength of materials was developed by Weibull [1938, 1939, 1951] based on the "Weakest Link" hypothesis. The starting point of the theory was the notion that the strength of a material may be represented as the weakest strength of a large number of components. Assuming that the components have independent random strengths, a consistent family of probability distributions was derived. Since Weibull proposed a probability function for brittle materials in 1939, it has been found to adequately describe their behavior.

In the 1970's, several researchers studied the probabilistic failure analysis of brittle structures using Weibull's distribution function [Stanley, Sivill and Fessler, 1974; Margetson, 1976; Stanley and Margetson, 1977; Margetson, 1980]. However, all work was performed for isotropic, orthotropic or anisotropic materials and none was devoted to structures made of composites. Statistical theory of size effect was reviewed and some deterministic strength theories on orthotropic and composite materials were proposed by several authors [Hahn, 1975; Yamada and Sun, 1978].

In 1981, an attempt was made by Wetherhold [1984] to obtain statistical information for failure of composite materials by the use of a closed-form expansion of the maximum distortion energy failure criterion and also by the use of a Monte Carlo simulation method on the same failure criterion [1985]. Only one orthotropic layer was considered, and not a composite structure. Heller et al. [Heller, Schmidt and Denninghoff, 1984; Heller, Thangjitham and Wall, 1986] applied the weakest link theory to a proof-loaded isotropic material and to a composite plate with a hole. Recently, Thangjitham and Heller [1987] worked on the reliability analysis of an infinite composite plate with a hole under a randomly oriented load, and Heller et al. [Heller, Thangjitham and Yeo, 1990] investigated size effects of brittle composites and worked on the reliability analysis of composite beams with stress concentrations. The reliability of composite beams and plates with and without stress concentrations based on these considerations is discussed in detail by Yeo [Yeo, 1991].

Failure Analysis

Failure theories existed since the time of Galileo. In his famous experiment, he subjected rock specimens to tension and observed that the strength depends on cross-sectional area but is independent of length. He concluded that failure would occur when the "absolute resistance to fracture," i.e. critical stress, was reached. This appears to be the first suggestion of the maximum normal stress theory for predicting fracture of brittle materials [Rowlands, 1985].

Since then numerous failure criteria were developed for isotropic materials. Though it is informative to review these in more detail, this review is concerned with those applicable to anisotropic composite materials.

In 1948, Hill [1948, 1950] introduced a strength criterion for an orthotropic material based on the observation that under large deformation, the micro-mechanical structure of isotropic materials becomes anisotropic. He assumed that the yield stresses are the same in both tension and compression. While it is not common to use Hill's criterion in its original form for composite materials, it nonetheless forms the basis of several composite strength criteria. For an isotropic material, Hill's criterion has the same form as the von Mises' distortion energy yield criterion.

Hill's criterion was further generalized by Hoffman in 1967 [Hoffman, 1967]. Based on the features of the Mises' isotropic yield condition and Hill's orthotropic yield condition, Hoffman proposed a fracture condition for orthotropic brittle materials which contains nine material parameters that can account for widely differing tensile and compressive strengths in various directions by introduction of linear stress terms.

Tsai [1968] modified Hill's criterion in 1968 with the assumption that the transverse strengths in the y- and z-directions are the same for fiber reinforced composites. This modification is called the Hill-Tsai failure criterion.

In 1971, influenced by the work of Goldenblat and Kovnop [Goldenblat and Kovnop, 1965], Tsai and Wu [1971] presented a general lamina failure criterion. By taking 1st and 2nd terms (i.e. up to 4th order strength tensors) proposed by Goldenblat and Kovnop and assuming that the powers of them are equal to 1, they proposed a quadratic tensor polynomial failure criterion. Recognizing that the strength theory should be independent of coordinate systems, they assumed that there exists a certain failure surface in stress space. The linear terms in stress are included for possible differences in tensile and compressive strengths, which is similar to Hoffman's work. Even though there is a disadvantage in this criterion in that the determination of the interaction coefficients is impractical and difficult, it is the most general failure criterion which includes most of the other criteria as special cases. The advantages are that (1) it is invariant under rotation of coordinates, (2) it transforms via the established tensor transformation laws, (3)

symmetric strength properties are similar to those of stiffnesses and compliances. Therefore, the mathematical operations with this tensorial failure criterion are relatively easy and straightforward.

In 1973, Hashin and Rotem [1973] proposed a fatigue failure criterion for fiber reinforced materials under static and oscillatory states of combined plane stress. They observed that there are two basically different failure modes – fiber failure and matrix failure. By assuming that the two are independent (which is not unreasonable), they proposed separate criteria for fiber and matrix failure.

In 1980, Hashin [1980] extended his previous work and proposed a three dimensional failure criterion for unidirectional fiber composites. Based on the idea that most of the unidirectional fiber composites are transversely isotropic with respect to fiber direction and the failure criterion must be invariant under any rotation of the axes around the fiber direction, so that the failure criterion can be at most a function of the stress invariant under such rotation, he introduced the most general form for transversely isotropic materials. As he did in his previous paper, he treated the two planar failure modes – fiber mode and matrix mode – separately, and through some physical argument, derived two failure criteria for the two modes. The plane stress version of the criterion showed a good agreement with experiments. Nothing was said about delamination as a failure mode, however.

In 1981, Lee [1981] developed a finite element scheme in which the damaged zone and modes of failure can be identified. Damage accumulation and the ultimate strength of the composite laminate can also be analyzed. He treated fiber failure and matrix failure separately and proposed a simple criterion for each mode.

In 1988, Christensen [1988] developed a three-dimensional failure criterion. He first derived three-dimensional lamination theory in which two restrictions that reduce the five independent properties of a transversely isotropic material to a form involving three independent constants are involved. From the resulting three-dimensional tensor transformation equation, he derived two separate failure criteria: one for direct fiber failure and the other for fiber/matrix interface failure. The basic variable used was strain. The direct fiber mode is the same as one of the maximum strain failure criterion. These criteria were also presented in terms of stresses through the stress-strain relation. He maintained that longitudinal stress in the fiber direction, σ_{11} , cannot be neglected in a failure criterion involving matrix action.

Brewer and Lagace [1988] proposed a criterion for delamination initiation based on the quadratic tensor criterion. They extended the failure criterion proposed by Kim and Soni [1984, 1986], with a reasoning that the predicted initiation stresses should be independent of the sign of the interlaminar shear stresses and by taking only a quadratic term for the interlaminar normal stress component, they came up with a quadratic delamination criterion.

In 1989, Hwang and Sun [1989] proposed three separate failure criteria for fiber breakage, matrix cracking and delamination. The failure criteria for fiber and matrix failures are very close to those of Hashin's but an additional delamination criterion was presented.

It was reported, recently [Tolson and Zabaras, 1991] that for T300/5208 graphite-epoxy laminates with $[\theta_4/0_4/-\theta_4]_s$ layup under uni-axial tension, Hashin's criterion seems to give results which are slightly less accurate than Lee's and maximum stress criteria, but more accurate than Hoffman's and Tsai-Wu's for this particular laminate.

A first-ply-failure analysis applicable to bi-directional orthotropic laminates was developed by Yeo [Yeo, 1991].

SIZE EFFECT ANALYSIS

Analytical Study of Size Effect

As in the case with other composite materials, the quality of larger components can not be controlled as carefully as that of small laboratory specimens. Larger components have more imperfections and volume distributed flaws such as porosity, discontinuous fibers, holes, matrix poor regions, and so on. As a consequence, most brittle materials such as carbon-carbon have size effects. This effect usually results in strength reduction for larger components and therefore the probability of failure for such components increases not only with the magnitude of the applied stresses but with the size of the components. Hence, to accurately assess the reliability of such components, the size effect has to be somehow incorporated in the analysis.

There are various ways to assess the reliability of structural components. The approach based on the strength-stress interference is one example. It considers, however, maximum stress only at a single location, relates it to maximum strength and bases all failures on that one element. It does not take into account any kind of size effect present in the material.

In this work, reliability analysis based on the "weakest link" principle is applied to calculate the reliability of brittle structural components. One disadvantage of this approach is, however, that it essentially uses deterministic stresses.

"Weakest Link" Analysis

Weibull Statistics for Uni-axial Loading

The probability that a material with unit volume survives under the application of uniform stress, S , is given as [Weibull, 1938]

$$L_i(S) = \exp \left[- \left(\frac{S-R_0}{R_c-R_0} \right)^m \right] \quad (1)$$

where $L_i(S)$ is the probability of survival of a material with unit volume, v , R_c is the "characteristic" ultimate strength of the unit volume, v , R_0 is its minimum strength and m is its Weibull shape parameter. These three constants define the three parameter Weibull distribution. The relationships between the mean, μ_R , standard deviation, σ , and the above-mentioned parameters are as follows:

$$\mu_R = (R_c - R_0) \Gamma\left(1 + \frac{1}{m}\right) + R_0 \quad (2)$$

$$\sigma_R = (R_c - R_0) \sqrt{\left[\Gamma\left(1 + \frac{2}{m}\right) - \Gamma^2\left(1 + \frac{1}{m}\right) \right]} \quad (3)$$

where $\Gamma(\cdot)$ is the tabulated gamma function.

The "characteristic strength" has a probability of survival of $L_i(R_c) = e^{-1} = 0.3679$. In this work, the reliability is derived in terms of the characteristic strength rather than the mean strength in contrast to some authors, [Stanley, Sivill and Fessler, 1976; Stanley and Margetson, 1977; Margetson, 1980] because the mean value is not associated with any specific probability level.

A structural component with volume, V , may be regarded as being made up of N elementary volume elements. It is assumed that failure in any one element leads to the failure of the component, or, that the survival of the component requires the survival of every element (*weakest link* hypothesis). It is further assumed that the reliability of a particular element is independent of that of any other element in the component, hence the reliability of the component is obtained as the product of reliabilities of individual volume elements:

$$L = \prod_{i=1}^N L_i \quad (4)$$

where $N = V/v$ is the number of elementary volume elements in the structural component of volume, V , and L_i is defined in (1). Therefore, the reliability under uniform uni-axial stress, S becomes

$$L = \exp \left[-\frac{V}{v} \left(\frac{S-R_0}{R_c-R_0} \right)^m \right] \quad (5)$$

For a material of volume, V , under non-uniform stress, the reliability is obtained by integrating the stresses over the volume:

$$L = \exp \left[-\frac{1}{v} \int_V \left(\frac{S-R_0}{R_c-R_0} \right)^m dV \right] = e^{-\lambda} \quad (6)$$

where the risk of failure, λ , the exponent of e , is called the stressed-volume integral. If S_{\max} is the maximum value of the applied stress throughout the component and V is the total volume, Eq. 6 may be written in terms of dimensionless ratios as [Stanley, Sivill and Fessler, 1976; Stanley and Margetson, 1977; Margetson, 1980]

$$\ln \frac{1}{L} = \lambda = \left(\frac{1}{v_c (1 - 1/v_{\max})} \right)^m \frac{V}{v} \int_{S > R_0} \left(\frac{S}{S_{\max}} - \frac{v_c}{v_{\max}} \right)^m \frac{dV}{V} \quad (7)$$

with the introduction of the two safety factors

$$v_c = \frac{R_c}{S_{\max}} \quad \text{and} \quad v_{\max} = \frac{R_c}{R_0} \quad (8)$$

Integration is carried out only over the volume where stresses exceed R_0 .

Weibull Statistics for Multi-axial Stress States

To analyse the failure of brittle materials subjected to multi-axial stress states, the Weibull statistics can be modified with the aid of the so-called "Principle of Independent Action" [Stanley, Sivill and Fessler, 1974]. It states that the reliability of a given material under a multi-axial stress state is equal to the product of reliabilities of the material subjected to each of the principal stresses in turn. Therefore, Eq. 5 is modified as

$$L = \exp \left[- \sum_{i=1}^3 \left(\frac{S_i - R_{0i}}{R_{Ci} - R_{0i}} \right)^m \frac{V}{v} \right] \quad (9)$$

where S_i are the principal stresses. The R_{Ci} , R_{0i} terms are the characteristic and minimum strengths rotated into the principal stress directions. For a material of volume, V , under non-uniform multi-axial stress state, the reliability becomes

$$L = \exp \left[- \sum_{i=1}^3 \frac{1}{v} \int_V \left(\frac{S_i - R_{0i}}{R_{Ci} - R_{0i}} \right)^{m_i} dV \right] \quad (10)$$

Experimental Study of Size Effect

All experimental results, repeated in this study were originally reported in Part I of this report by Heller et al, 1991.

Tension and Compression Tests

Tension tests were performed on dog-bone shaped specimens to measure the material properties E_1 , E_2 , ... etc., and Weibull parameters R_0 , R_C , and m . The specimens were cut from 10 " x 6.5 " x 0.5 " panels. The detailed arrangement and dimensions of the specimens are shown in Part I of this report.

Average values and standard deviations for modulus, maximum strength and strain measured in the warp (W) and fill (F) directions are presented in Table A.1.

While tension specimens failed in most cases at 90 degrees to the longitudinal axis, compression tests produced diagonal shear failures. Poisson's ratios were determined in some of the tension tests and are also presented in Table A.1.

In-plane Shear Tests

For the shear moduli G_{WF} , G_{FW} , G_{WT} and G_{FT} as well as the shear strengths R_{WF} , R_{FW} , R_{WT} and R_{FT} , tests were performed in a modified Iosipescu type fixture. Specimen dimensions and geometry are available in Part I. Test samples were cut from a panel with their longitudinal dimensions parallel to the warp (W) and fill (F) directions, while their width dimensions were along each of the three directions: warp (W), fill (F), and through-the-thickness (T). Loads were applied in an Instron machine. Shear strains were obtained from strain gauges at 45 ° to the load direction while shear stresses were calculated as the load divided by the cross-sectional area, A ,

$$\gamma = 2 \epsilon_{45} \quad (11)$$

$$\tau_{xy} = P/A \quad (12)$$

The results are tabulated in Table A.2.

Interlaminar Shear Tests

In order to determine the interlaminar shear moduli, G_{TW} , G_{TF} as well as the interlaminar shear strengths R_{TW} , R_{TF} , specially designed specimens were prepared (Part I). Test results are presented in Table A.3.

Why notched beams and plates with holes?

In order to experimentally demonstrate significant strength reduction due to size effect, specimens of widely differing sizes would have to be tested. Because size variations of the order of 1 to 100 would be required, such tests are impractical and can seldom be performed in the laboratory. To circumvent this problem and to simulate specimens of widely varying sizes, structural components containing sharp stress gradients such as notched beams or plates with holes are considered [Heller, Thangjitham and Yeo, 1990]. In this case, high stresses are concentrated over a "small" volume of material while specimens without stress concentrations act as the "large" volume.

Beam Bending Tests

In order to demonstrate the concept of size effect, four point bending tests were performed on carbon-carbon beams with and without notches. The detailed arrangement of the specimens is shown in Fig. 1. Notched specimens have the same geometry as the unnotched specimens with 60° V notches with a depth, $d=0.22h$, where h is the depth of an unnotched specimen. The specimens whose length is in the warp direction are denoted as W (warp) specimens and those whose length is in the fill direction are denoted by F . N indicates notched specimens. The specimens (1- W , 1- F , 1- WN and 1- FN) with the loading direction perpendicular to the layers are designated as Type I, and those (2- W , 2- F , 2- WN and 2- FN) with the loading direction parallel to the layers as Type II.

The two types of specimens are examined in order to model composite beams and isotropic beams, respectively. Type II specimens were placed into the testing machine with their laminae parallel to the loading direction in order to eliminate interlaminar shear effects of short beams and therefore to model them as isotropic beams. Type I specimens were placed with their laminae perpendicular to the loading direction in order to model them as laminated composite beams. The loading configuration and test fixture are shown in Fig. 2 and Fig. 3. Three specimens were tested in each of the eight configurations shown in Fig. 4. Failure modes were observed and the failure loads were measured. Type I beams generally showed the influence of interlaminar stresses and failed by a combination of through-the-thickness fracture and delamination. This type of failure was observed in both unnotched and notched beams. Type II beams fractured more or less as isotropic materials. This failure mode is most pronounced in notched specimens with a straight line fracture through their depth. Their results are presented in Table 1. The figures of the failure modes for the notched and unnotched specimens are shown in Figs. 5-6. These data will be compared to analytical values in the section on reliability analysis of composite beams to, demonstrate the size effect.

Plate Bending Tests

As another means of verifying the size effect concept, plate bending tests were performed on square and rectangular plates with and without a hole. As presented in Fig. 7, plates were instrumented with strain gages placed in the warp (longitudinal) and fill (transverse) directions at the edges of 0.64 in. diameter holes and with 0-90 ° strain rosettes on their diagonals. Similar gauge arrangements were used on a plate without a central hole; a 0-90° strain rosette was placed at the center of the plate. The transverse deflection was measured by a displacement transducer. In some of the tests acoustic emissions were also monitored.

Experiments were carried out on a plate bending fixture illustrated in Part I. (Fig. 8) Plates were simply supported on all four sides and a uniform load was applied through a sand box. Unlike the usual simple-support boundary condition used in the literature, here the plates were simply sitting on top of supports all around the edges, thus allowing in-plane movements in the x- and y-directions. The boundary conditions used in the stress analysis to simulate the support condition are shown in Fig. 9 Plate bending test results are tabulated in Table 2. Attempts were made to detect "first-ply-failures" by monitoring acoustic emissions with a transducer placed under the plates. The transducer, however, picked up a great deal of noise produced by grinding of sand particles and by machine vibrations. As a consequence, the detection of "first-ply-failure" was not successful.

Plate failures originated near the longitudinal diameters of the holes and propagated first along the warp direction, and eventually along the diagonals of the rectangular plates. In the case of the square plate with a hole, after originating near the warp diameter of the hole, cracks propagated radially outward. All plates failed essentially in a brittle manner and no evidence of delamination was observed.

Load-deflection curves are presented in Figs. 10 and 11.

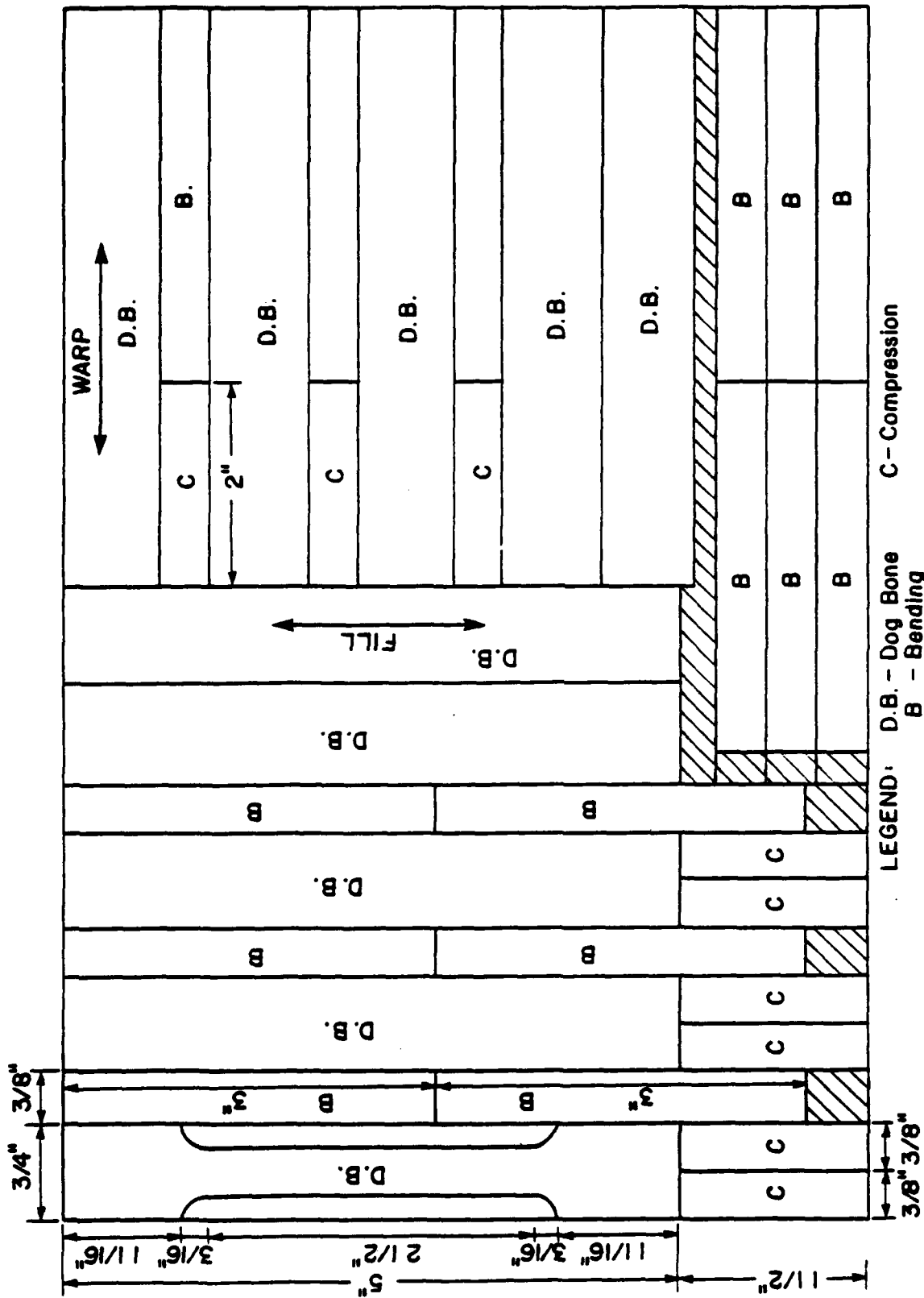


Figure 1

Typical Arrangements of Specimens Cut from a 10 x 6.5 x 0.5 " Panel

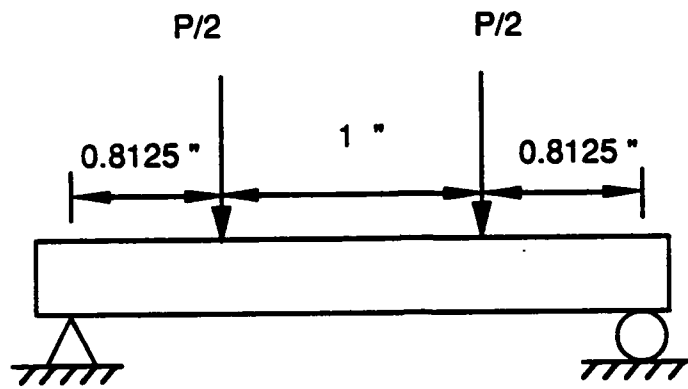


Figure 2

Loading Configuration for Four Point Bending Specimens

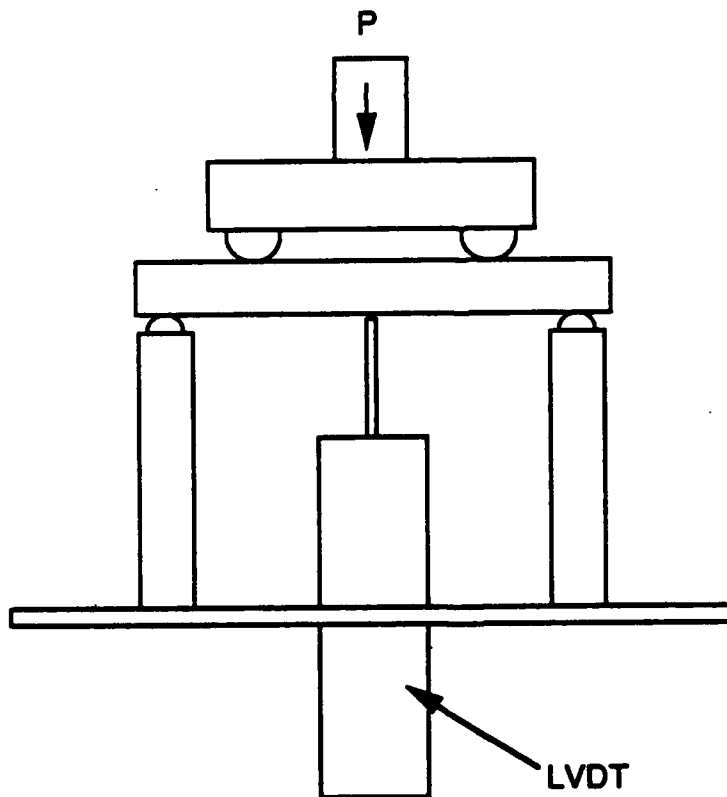


Figure 3

Test Fixture for Four Point Bending Tests

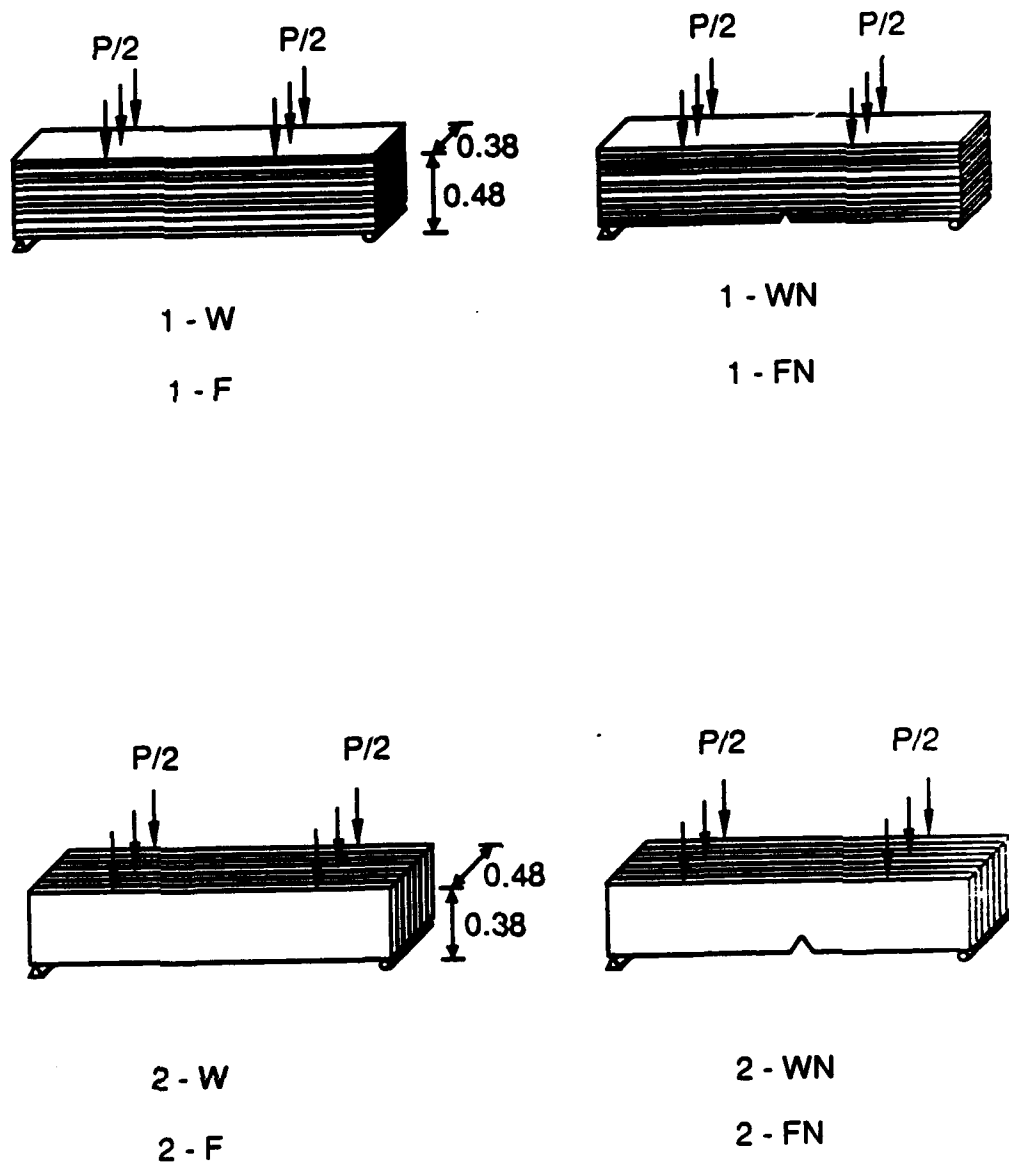


Figure 4
The Four Point Bending Test Configuration

Table 1. Four Point Bending Test Results

No. of Specimens Tested	Type of Specimen	Max. Load P, lbs	σ_p	Max. Stress S, ksi	σ_s	Modulus E ksi $\times 10^3$	σ_E	Max. Strain ϵ in/in $\times 10^{-3}$	σ_ϵ
9	1W	505.9	36.6	15.238	.549	2.468	.1303	6.467	.306
9	2W	493.2	44.9	19.708	.662	2.395	.190	10.079	1.784
9	1F	335.0	5.0	9.198	.190	1.370	.071	9.547	.180
9	2F	288.2	23.1	11.363	.700	1.307	.067	13.759	3.805
9	1WN	288.7	28.2		1.353	2.551	.001	7.516	.462
12	2WN	250.3	11.9		.975	2.367	.077	9.938	.174
10	1FN	177.5	9.0		.532	1.620	.217	11.325	4.649
10	2FN	175.4	3.9		.510	1.655	.250	13.509	3.002

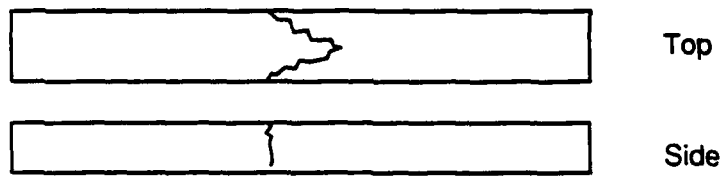
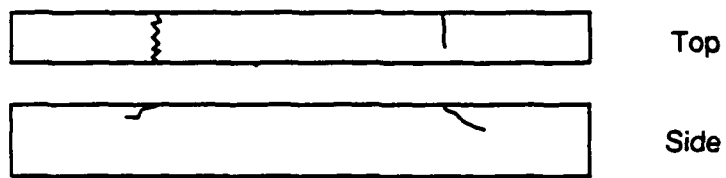
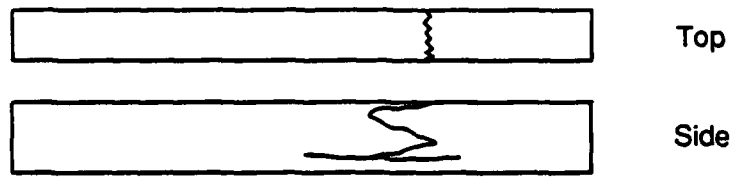


Figure 5

Failure Modes of Unnotched Four Point Bending Specimens

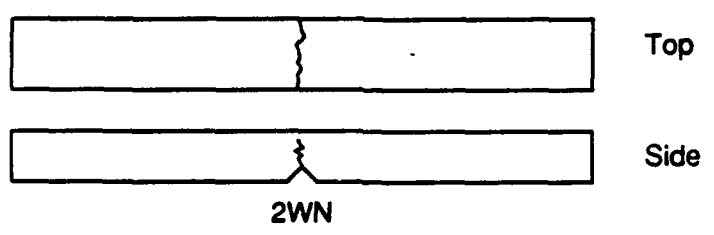
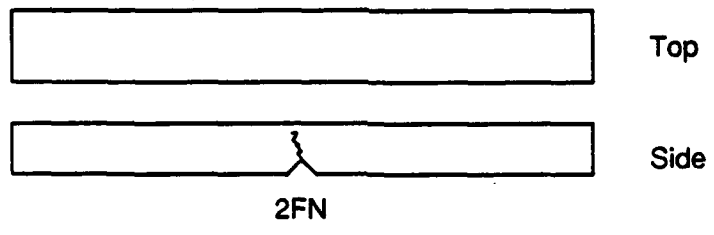
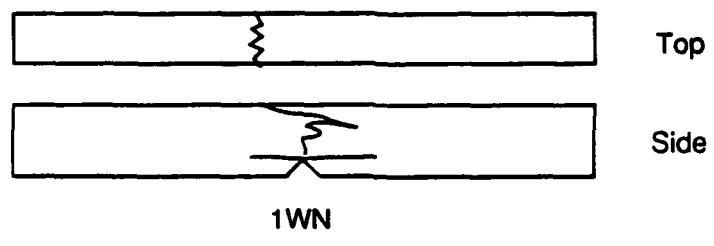
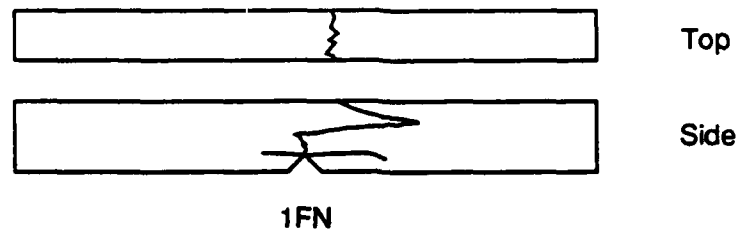


Figure 6
Failure Modes of Notched Four Point Bending Specimens

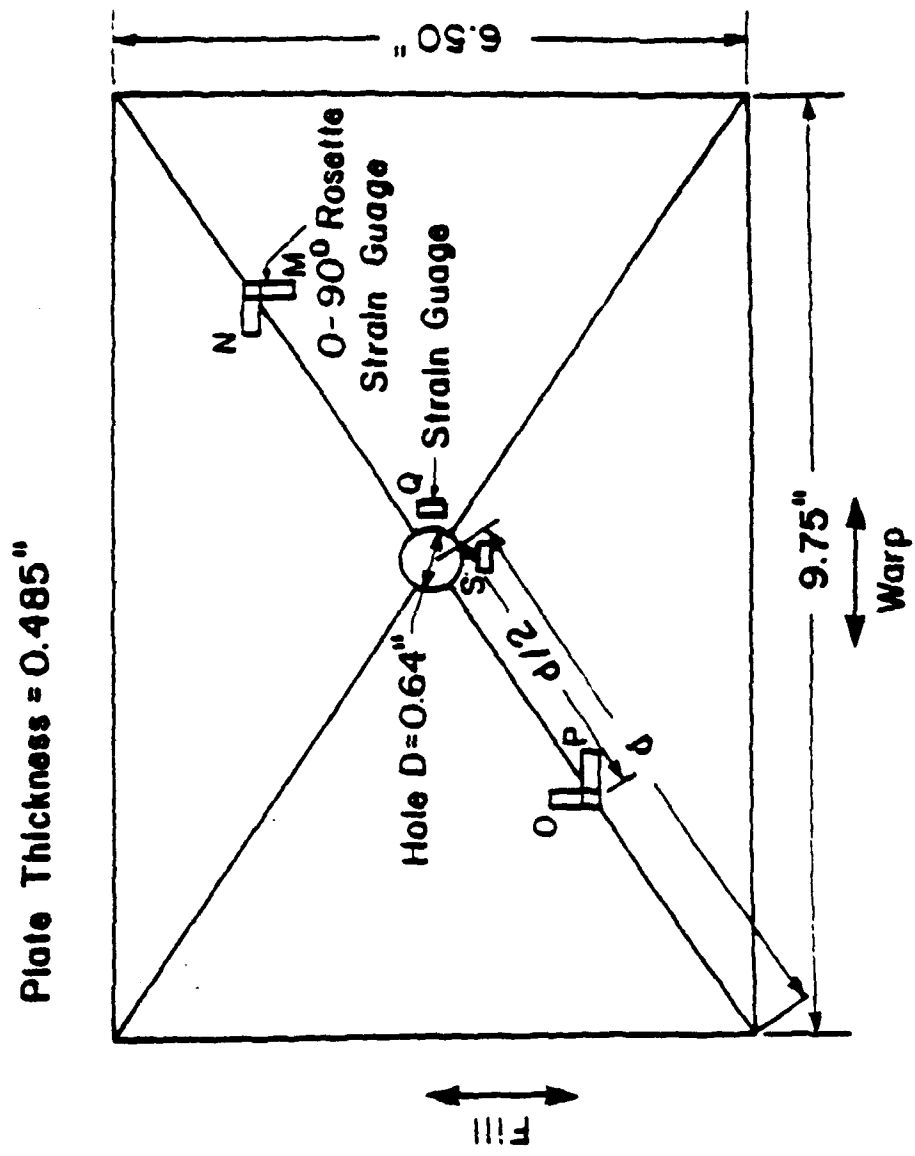


Plate Thickness = 0.485"

Figure 7
Plate Bending Specimen

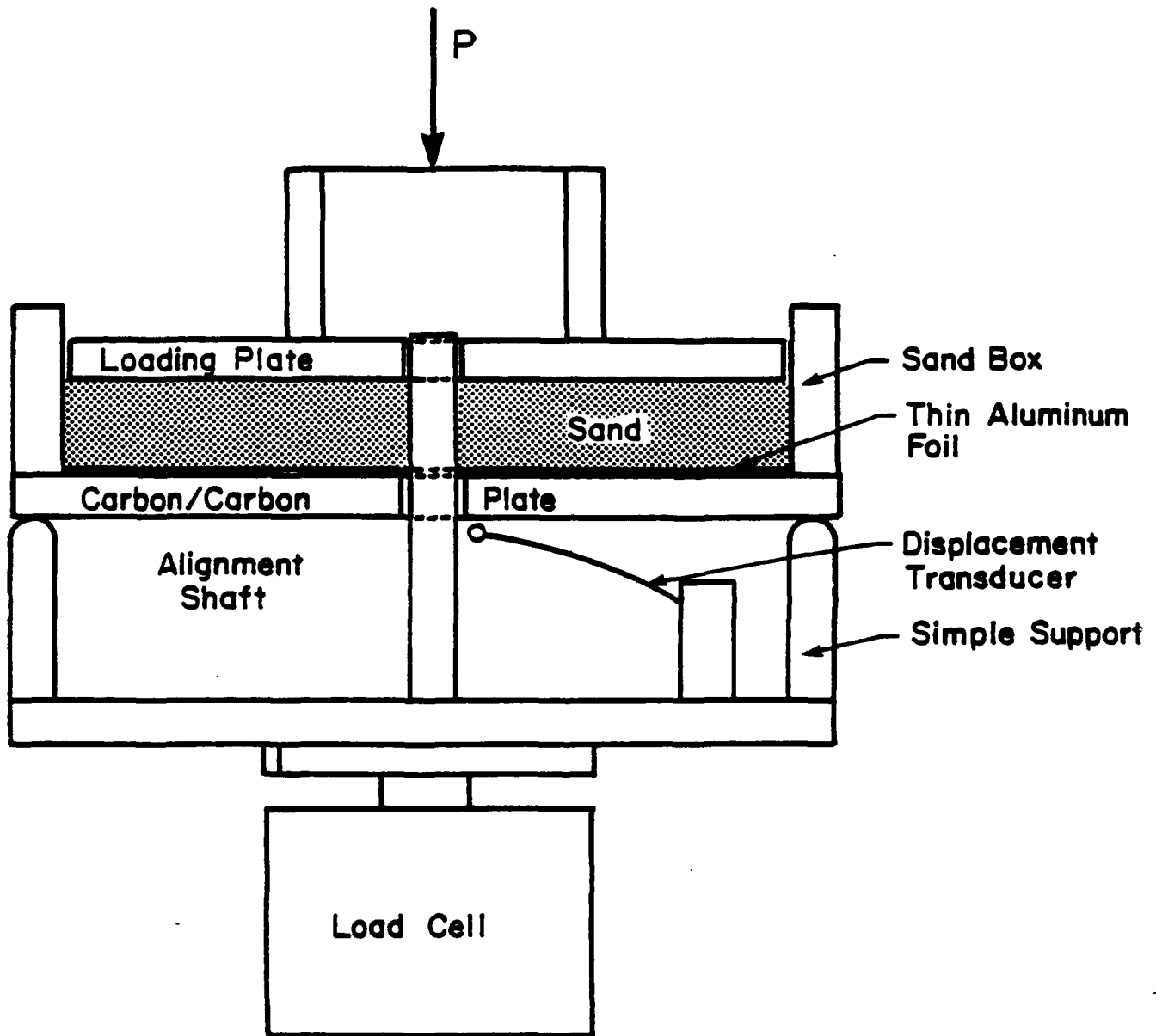
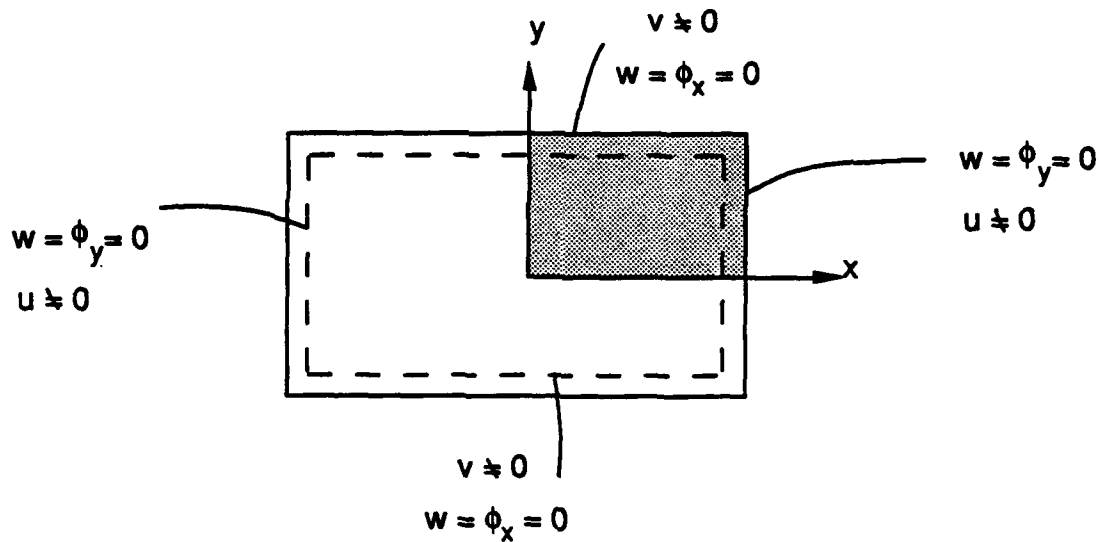
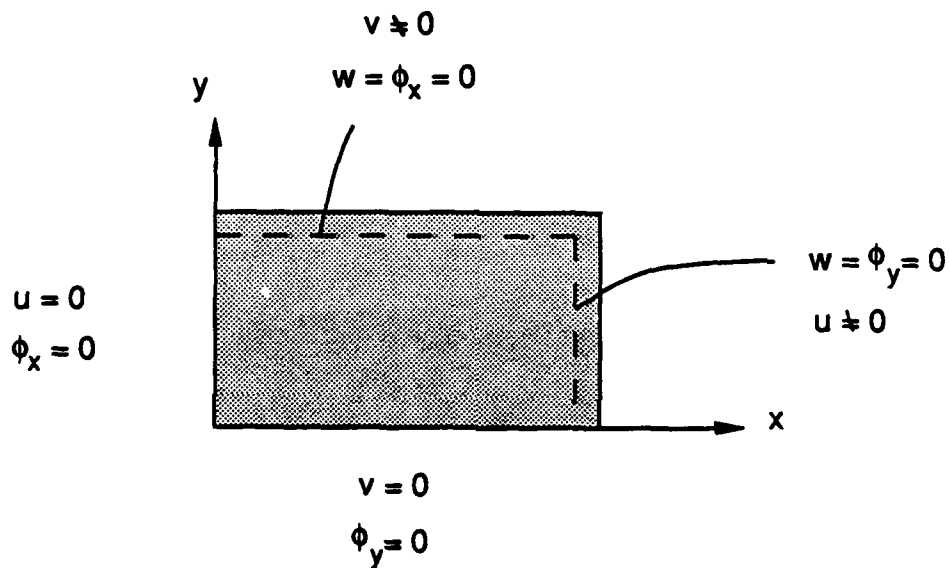


Figure 8
Plate Bending Test Fixture



(a) Simply Supported Boundary Condition Used in Experiment for a Full Plate



(a) Simply Supported Boundary Condition Used in Analysis for a Quarter Plate

Figure 9

Definition of Simply Supported Boundary Condition Used in Experiment and Analysis

Table 2. Plate Bending Test Data

Plate No. --	Type --	Max Load psi	Max. Deflection in
1	*R.H	383	.725
2	R.H	362	.399
3	R.N	360	.286
4	S.H	574	.507

*R = Rectangular Plate
S = Square Plate
H = Plate with Hole
N = Plate without Hole

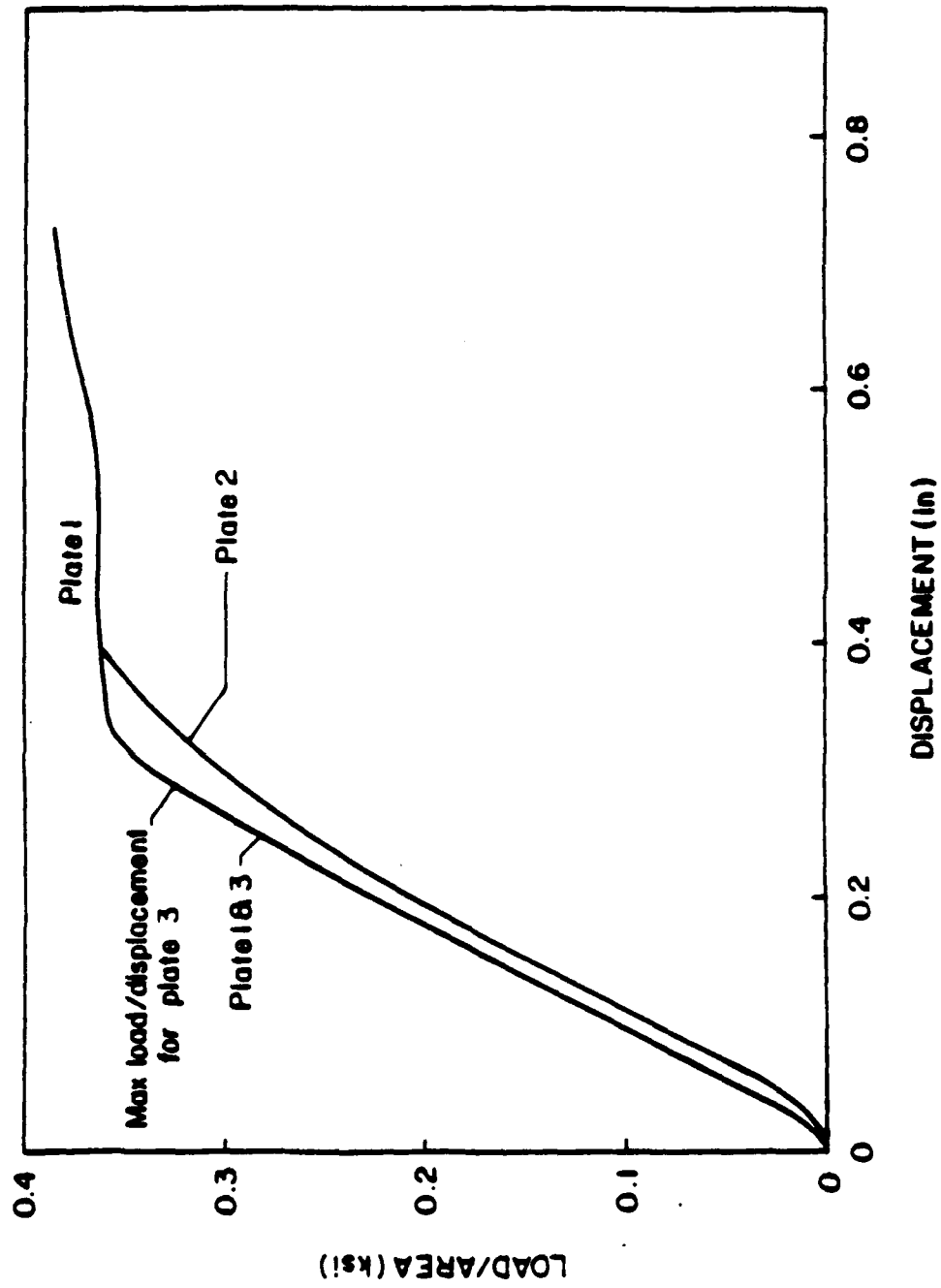


Figure 10

Load - Deflection Curves for Rectangular Plates (1 & 2 with hole, 3 no hole)

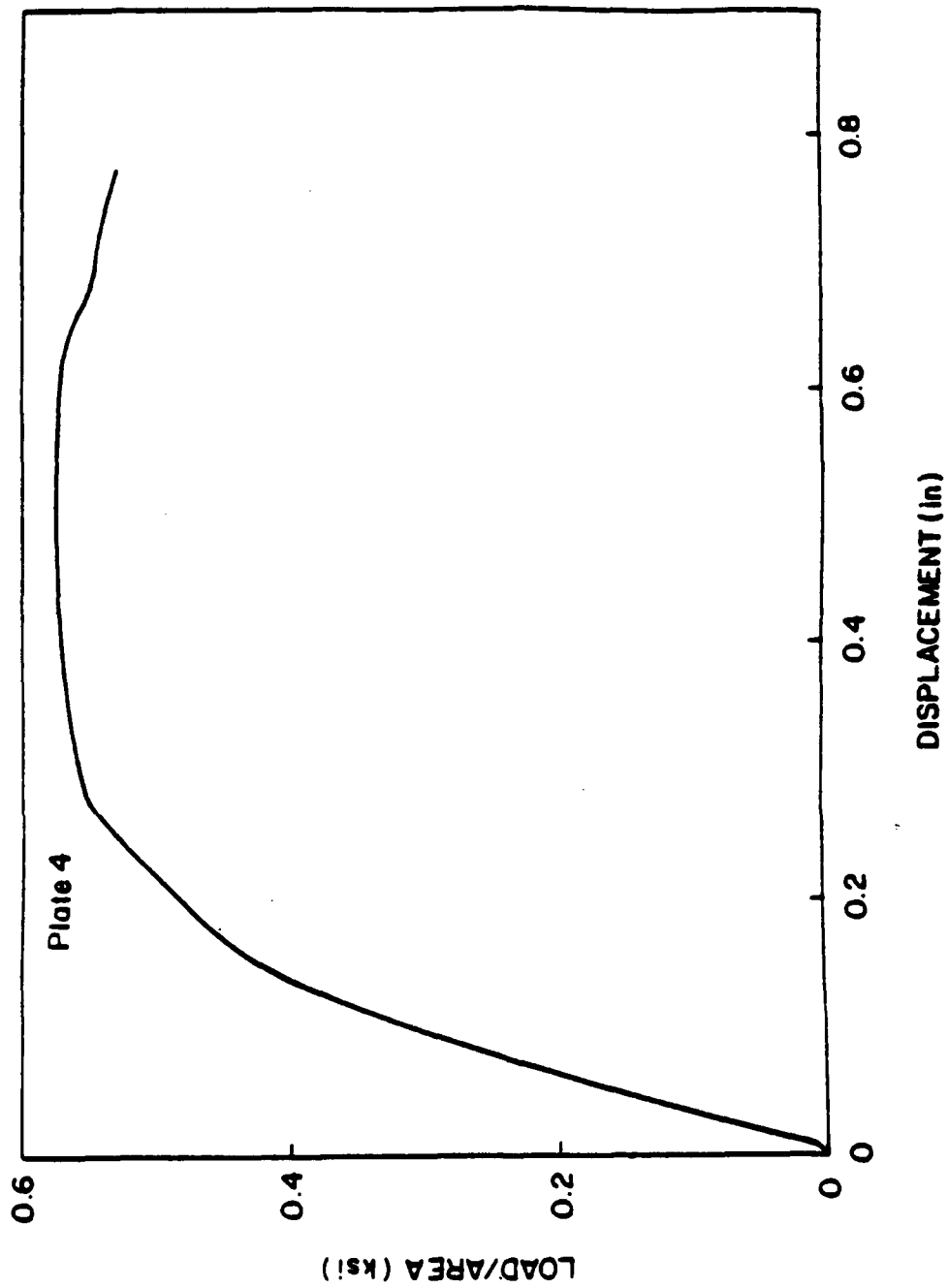


Figure 11

Load - Deflection Curve for a Square Plate with a Hole

Determination of Weibull Distribution Parameters

The basic test results: tension, compression and shear were used to determine the Weibull parameters necessary for the reliability analysis. A three parameter Weibull distribution was fitted to tension strength data. Warp and fill data were combined in order to increase the size of the population. This was accomplished by the introduction of a normalized variable, r , defined as follows:

$$r = \frac{R}{\mu_R} \quad (13)$$

where R is the sample strength and μ_R is the mean strength in the appropriate direction.

For the three parameter Weibull distribution, the probability of exceedance, $L_R(r)$, is written as

$$L_R(S) = \exp \left[- \left(\frac{S-r_0}{r_C-r_0} \right)^m \right] \quad (14)$$

where r_0 is the normalized minimum strength below which no failure is expected, r_C is the normalized characteristic strength with a probability of exceedance of $L(r_C) = e^{-1}$, and m is the shape parameter which is a measure of dispersion.

The following parameters were calculated based on Eqs. 2- 3:

$$m = 6.17, r_0 = 0.61, r_C = 1.03 \quad (15)$$

From these, the distribution parameters for the warp and fill directions become:

$$\begin{array}{l} \text{warp direction} \\ m = 6.17, R_{0W} = 8110 \text{ (psi)}, R_{CW} = 13820 \text{ (psi)} \end{array} \quad (16)$$

$$\begin{array}{l} \text{fill direction} \\ m = 6.17, R_{0W} = 3440 \text{ (psi)}, R_{CW} = 5800 \text{ (psi)} \end{array} \quad (17)$$

The combined data are listed in Table 3.

Table 3. Normalized Tension Strength Data and Three Weibull Parameters

Rank i	Data r_i	$L = 1 - \left(\frac{i}{n+1}\right)$		Rank i	Data r_i	L Reliability L_i
		Reliability L_i				
1	0.7699	0.9825		29	1.0048	0.4912
2	0.8126	0.9649		30	1.0063	0.4737
3	0.8915	0.9474		31	1.0140	0.4561
4	0.9091	0.9298		32	1.0143	0.4386
5	0.9186	0.9123		33	1.0166	0.4211
6	0.9319	0.8947		34	1.0184	0.4035
7	0.9330	0.8772		35	1.0211	0.3860
8	0.9330	0.8596		36	1.0225	0.3684
9	0.9330	0.8421		37	1.0280	0.3509
10	0.9377	0.8246		38	1.0287	0.3333
11	0.9379	0.8070		39	1.0327	0.3158
12	0.9396	0.7895		40	1.0336	0.2982
13	0.9425	0.7719		41	1.0373	0.2807
14	0.9435	0.7544		42	1.0478	0.2632
15	0.9455	0.7368		43	1.0478	0.2456
16	0.9494	0.7193		44	1.0524	0.2281
17	0.9572	0.7018		45	1.0526	0.2015
18	0.9657	0.6842		46	1.0585	0.1930
19	0.9669	0.6667		47	1.0670	0.1754
20	0.9762	0.6491		48	1.0717	0.1079
21	0.9803	0.6316		49	1.0717	0.1404
22	0.9814	0.6140		50	1.0861	0.1228
23	0.9850	0.5965		51	1.1002	0.1053
24	0.9856	0.5789		52	1.1040	0.0877
25	0.9925	0.5614		53	1.1042	0.0702
26	0.9980	0.5439		54	1.1203	0.0526
27	0.9998	0.5263		55	1.1508	0.0351
28	1.0048	0.5088		56	1.1646	0.0175

Shape parameter,
Characteristic value,
Minimum value,

$m = 6.17$
 $r_c = 1.03$
 $r_o = 0.61$

STRESS ANALYSIS OF COMPOSITE BEAMS AND PLATES

Isotropic Beams under Four Point Bending

The 2-W, 2-WN samples presented in Fig. 4 are treated as isotropic beams. Notched beams can not be analyzed in closed form because of their geometric irregularity and consequently should be examined numerically. The finite element method is used as an approximate numerical analysis of stresses. For this purpose, a finite element code **F2DELAST** was written and verified [Yeo, 1991]. A detailed explanation is given later. The beam is modeled by a two dimensional plane elasticity element (plane strain assumption is used). The finite element meshes for both notched and unnotched isotropic beams are presented in Figs. 12 and 13. The number of nodes and elements are 228 and 396 for a beam without a notch and 218 and 380 for a notched beam. The notch depth considered is $0.22h$, where h is a depth of the unnotched beam.

Composite Beams under Four Point Bending

The 1-W, 1-WN samples presented in Fig. 4 are modeled as composite beams. The waviness of the fiber is neglected and the beam is treated as a laminated composite with alternating fiber and matrix layers. The fiber layer is considered to be composed of an orthotropic material and the matrix layer of an isotropic material. The fiber volume fraction, v_f , and matrix volume fraction, v_m , were determined from a microphotograph of the specimen and are 0.6 and 0.4, respectively. Hence the thickness ratio between fiber and matrix layers is 6 to 4. Utilizing the rule of mixtures lamina properties were derived from experimental results on laminates in Part I. The mechanical parameters so obtained are listed in the appendix, Table A4. The number of layers in the beam was also determined from a microphotograph of the specimen, and was 41 layers (21 matrix layers and 20 fiber layers). The matrix layers cover the beam on top and bottom surfaces. The thickness of the matrix layers used in the stress analysis is 0.00951 (in) and that of fiber layers is 0.014265 (in).

As was expected and demonstrated in the experiments [Part I], the interlaminar shear stresses are an important mechanism in the failure of composite beams. The stress analysis of the composite beam was treated as a two dimensional plane elasticity problem with an assumption that there is no variation in stresses in the width direction. The coordinate system of the composite beam and the finite element meshes for the unnotched and notched beams are shown in Figs. 14 and 15. For stress analysis purposes, the finite element code ABAQUS is used. Both the constant stress triangle element CPS3 and 4-node linear rectangular element CPS4 are used in the mesh and the stresses are computed at Gauss points in each element. As the stress gradient in the vicinity of the notch tip is very steep and the stresses in that region are very important in the analysis, the mesh has been refined until there is no appreciable change in the stress field near the notch tip region. The finite element mesh has 2050 elements and 1092 nodes for an unnotched beam and 2001 elements and 1067 nodes for a notched beam. The finite element mesh for composite beams is a lot more refined than that for isotropic beams. This was due to the presence of the thin layers in the composite beam. To obtain reasonably accurate stresses at Gauss points, it is desirable that the elements not be distorted too much. Yet, as one element cannot cover more than one layer because material properties are different for two adjacent layers, finer mesh was dictated.

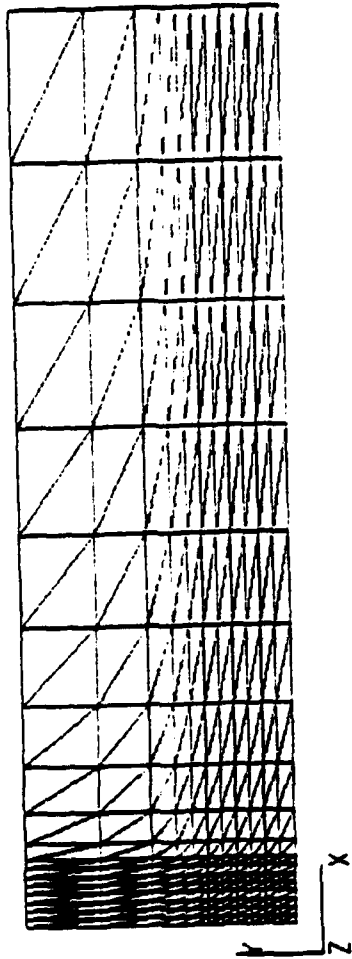


Figure 12
Finite Element Mesh of an Unnotched Isotropic Beam

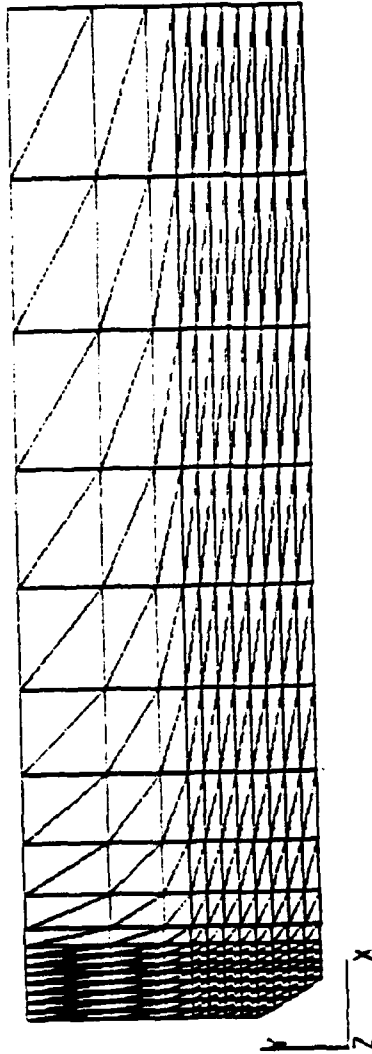


Figure 13
Finite Element Mesh of a Notched Isotropic Beam

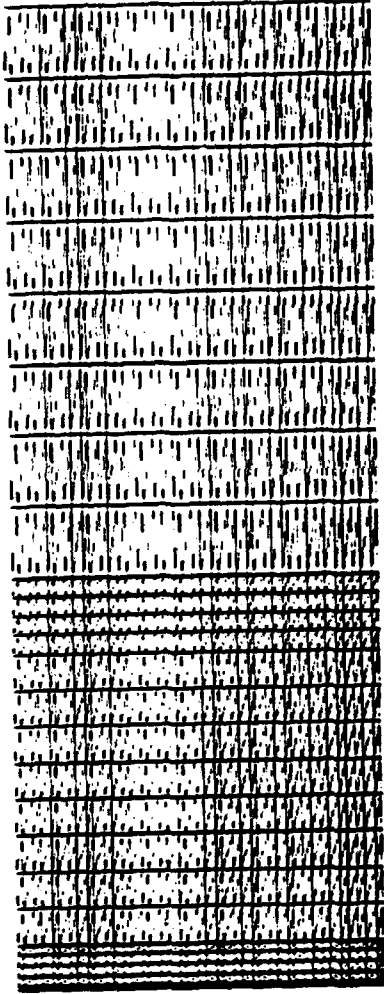


Figure 14

Finite Element Mesh of an Unnotched Composite Beam

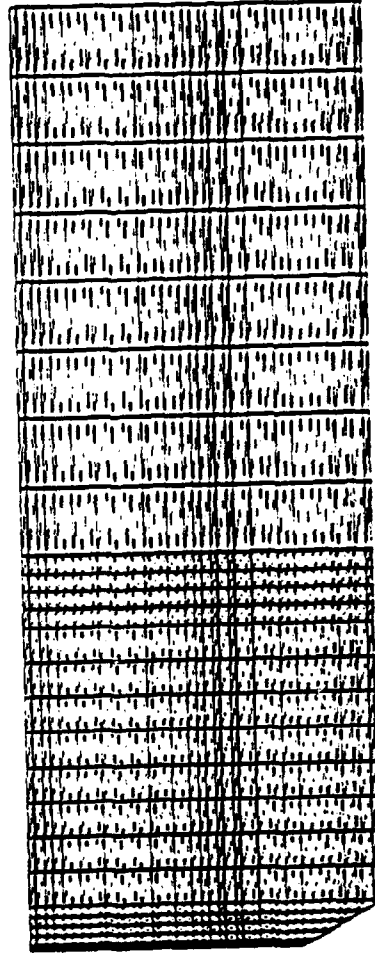


Figure 15

Finite Element Mesh of a Notched Composite Beam

Composite Plates under In-plane Loading

In order to verify the computer codes written for composite plates as well as to compare proposed failure theories presented in the section on 3D failure criteria with published results, graphite-epoxy square laminated plates without and with a hole are analyzed. For a square laminate with a hole, the hole-diameter-to-width ratio, d/w , varies from 0.05 to 0.2. The length-to-thickness ratio, a/h , is 10. The laminate considered is cross-ply symmetric whose stacking sequence is $[0_5/90_5]_S$. The dimension and the geometry of the laminate considered are shown in Fig. 10. In all cases, only a quadrant of the laminate is modeled and analyzed because of symmetry. The typical finite element mesh for $d/w = 0.05$ is presented in Fig. 17.

For rectangular plates under in-plane loading, the material properties and stacking sequence considered are the same as those for the square plates. Only uni-axial loading in the x -direction is considered. The typical finite element mesh is shown in Fig. 18.

Computer program F2DELAST was written for stress analysis of composite plates under in-plane loading based on two dimensional elasticity theory [Yeo, 1991]. The typical domain and a 9-node element considered for the finite element formulation is shown in Figs. 19 and 20. The formulation of the program is explained in the Appendix.

Composite Plates under Transverse Loading

The carbon-carbon plate is modeled as a laminated composite with alternating orthotropic fiber layers and isotropic matrix layers. A nonlinear finite element analysis program ENCOMPLT was developed and verified for the stress/failure analysis of laminated composite plates under transverse loading. The program is based on the first order shear deformable plate theory which accounts for the transverse shear deformation, and it also accounts for the geometrical nonlinearity in the von Karman sense. The displacement finite element model uses iso-parametric Lagrange elements with 5 independent degrees of freedom per node. Reduced integration is used for shear terms to avoid shear locking phenomenon. The Newton-Raphson iterative method is employed for the solution of the nonlinear algebraic equations. The dimension, geometry and coordinate system of the laminate are shown in Fig. 21, laminate resultant forces and moments are shown in Fig. 22 and the geometry and layer number of a multi-layered laminate are presented in Fig. 23. The formulation of the program is presented in detail in the Appendix.

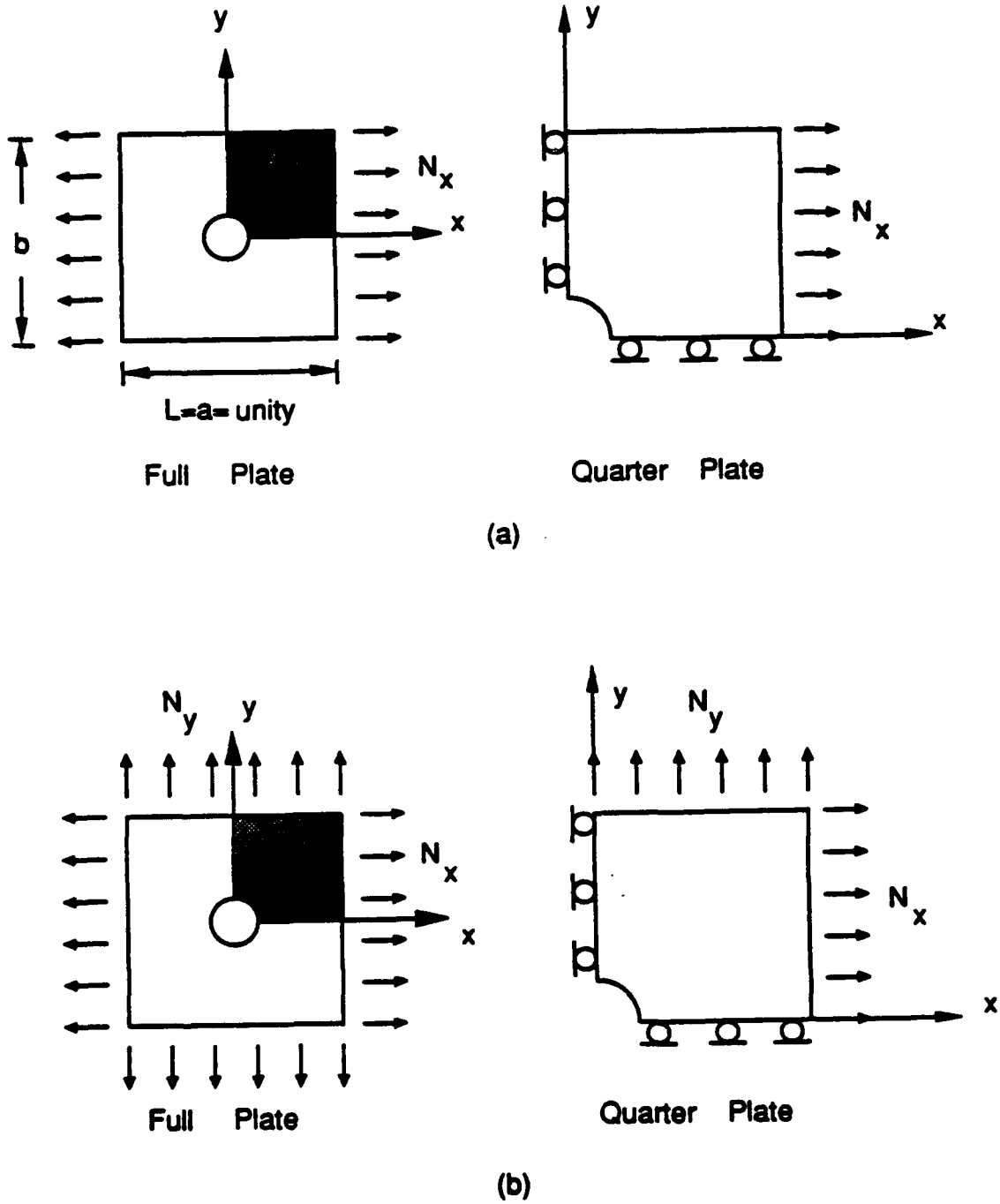


Figure 16

Geometry and Dimension of a Square Plate Under In-plane Loading (a) Uni-axial Loading (b) Bi-axial loading

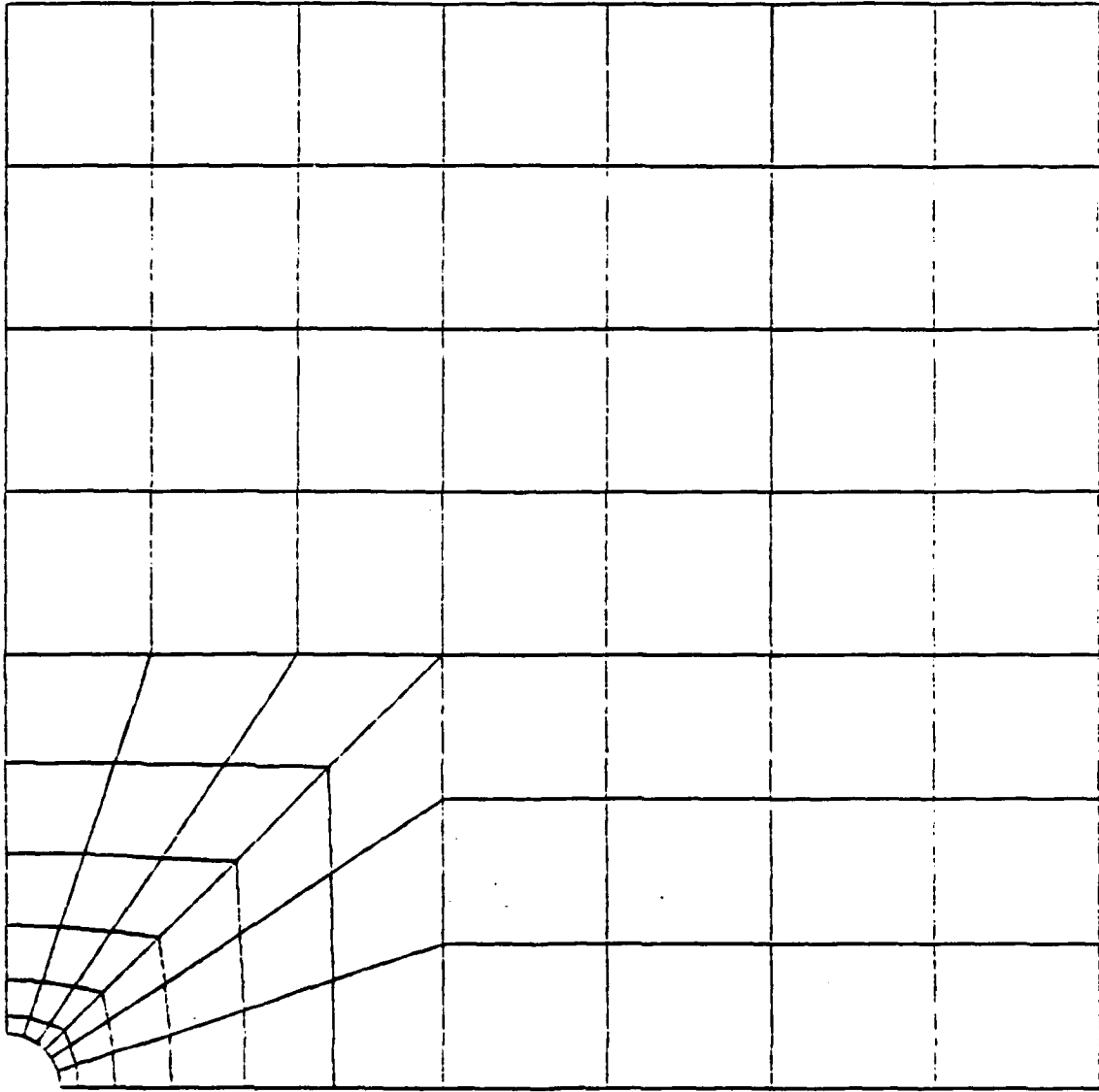


Figure 17
Finite Element Mesh of a Square Plate with a Hole for $d/w= 0.05$

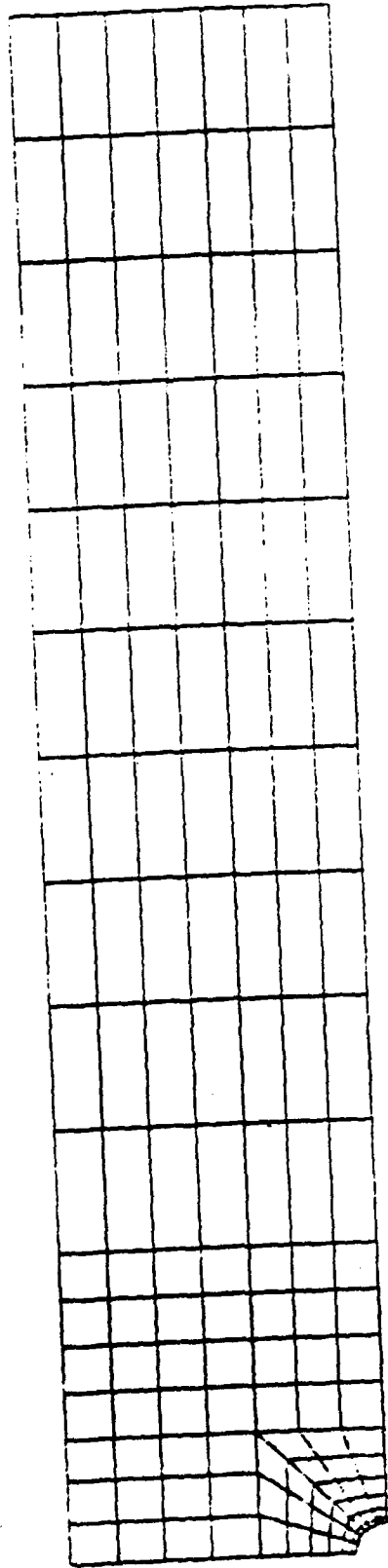


Figure 18

Finite Element Mesh of a Rectangular Plate with a Hole for Aspect Ratio $L/w=5$ and Hole-diameter-to-width Ratio $d/w=0.1$

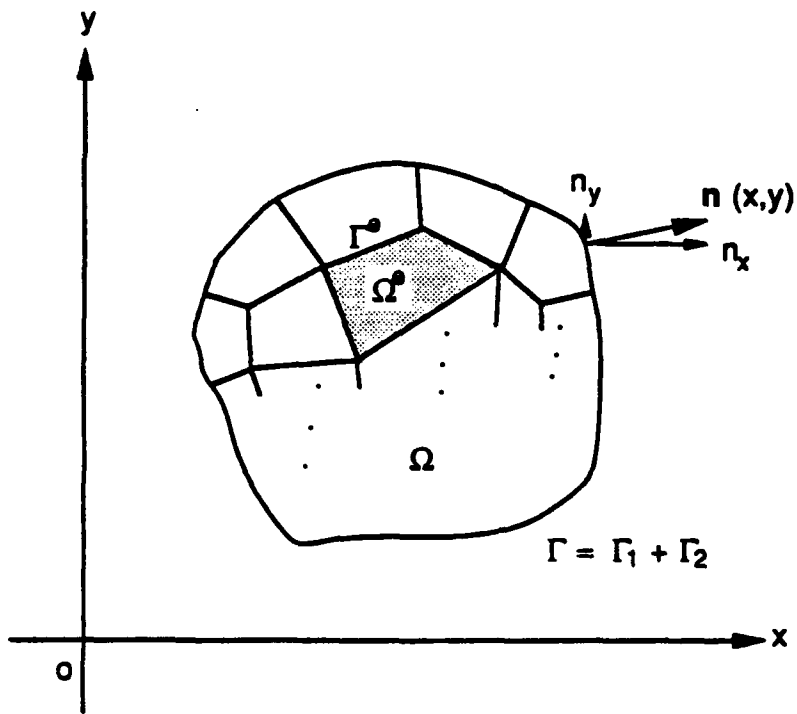


Figure 19

Typical 2-D Finite Element Domain

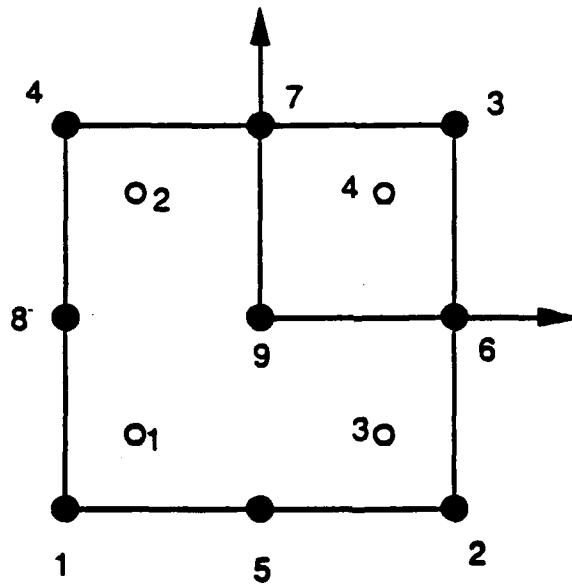


Figure 20

Node and Gauss Point Numbering Scheme in a 9-node Element (●: Nodes, ○: Gauss Points)

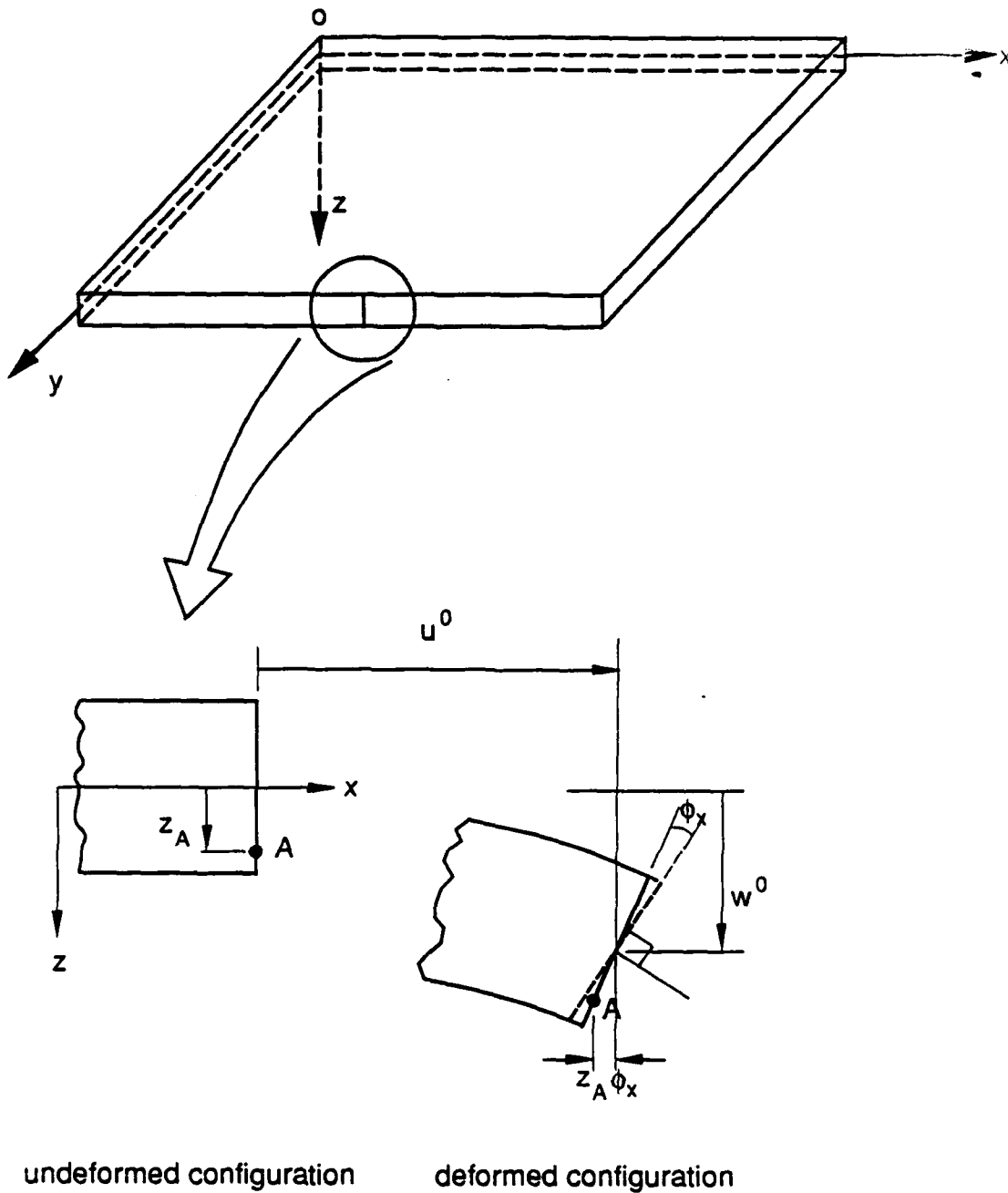


Figure 21
Geometry and Coordinate System of a Laminate

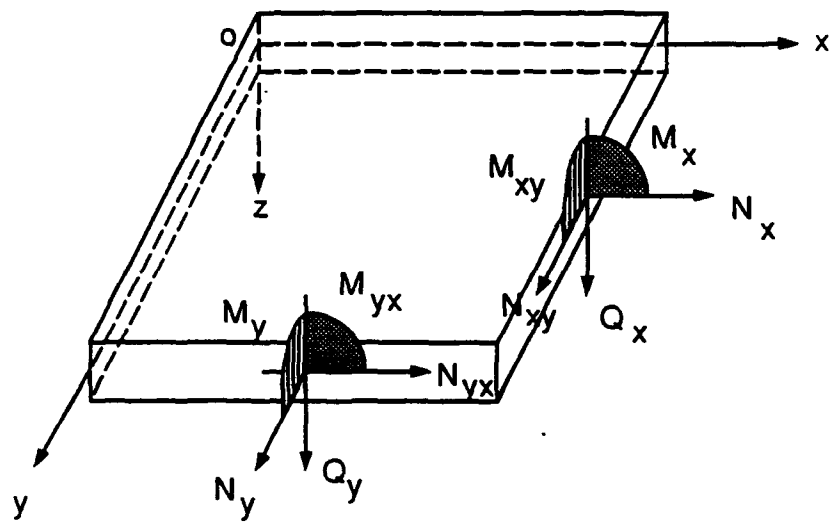


Figure 22

Diagram of Resultant Forces and Moments in a Laminate

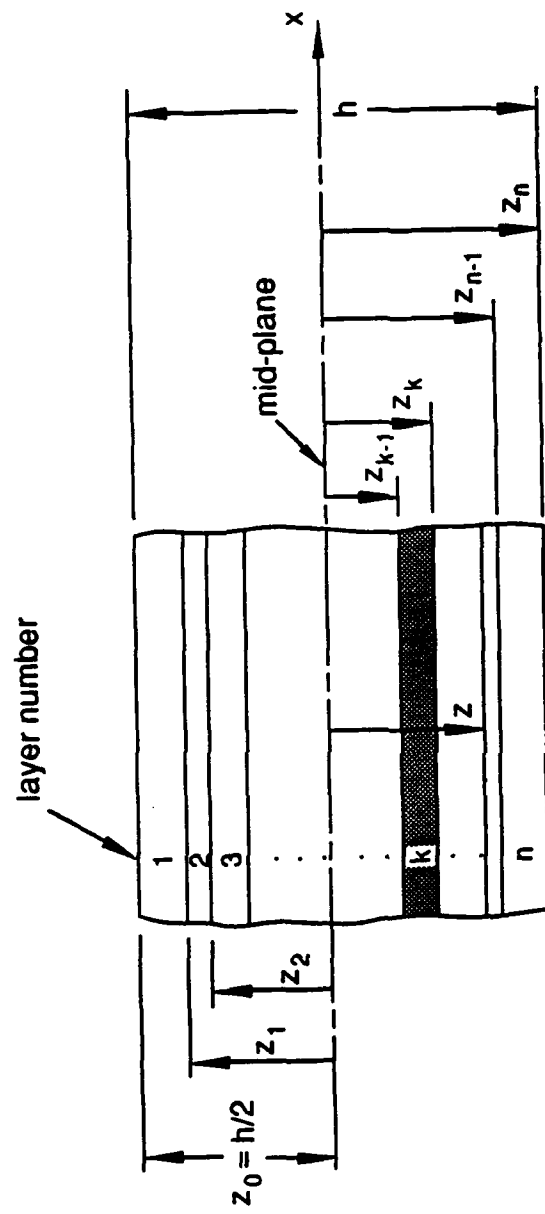


Figure 23
 Geometry and Layer Number of Multi-layered Laminate

RELIABILITY ANALYSIS OF COMPOSITE BEAMS AND PLATES

Reliability of Beams under Four Point Bending

Isotropic Beams

Unnotched Beams

As indicated in Fig. 24, only parts of the top and bottom portions of a beam experience stresses greater than the minimum strength R_{0C} or R_{0T} . Only those regions where the absolute values of the stresses are greater than the minimum strengths need be considered.

To include the contribution from the compressive stresses, the stressed-volume integral λ previously defined in Eq. 6 is written as

$$\lambda = \lambda_T + \lambda_C \quad (18)$$

where λ_T denotes the stressed-volume integral due to tensile stresses defined by

$$\lambda_T = \int_{|S| > R_{0T}} \left(\frac{S - R_{0T}}{R_{cT} - R_{0T}} \right)^{m_T} \frac{dV}{V} \quad (19)$$

where R_{cT} and R_{0T} are characteristic, and minimum tensile strengths, and m_T is the Weibull shape parameter for tensile strength. λ_C denotes the stressed-volume-integral due to compressive stresses defined by

$$\lambda_C = \int_{|S| > R_{0C}} \left(\frac{S - R_{0C}}{R_{cC} - R_{0C}} \right)^{m_C} \frac{dV}{V} \quad (20)$$

where R_{cC} and R_{0C} are characteristic, and minimum compressive strengths, and m_C is the Weibull shape parameter for compressive strength. In general, tensile strength and compressive strength of materials are different and so are the Weibull shape parameters. This is considered in the above equations.

Recognizing that

$$S_x = \frac{My}{I} \quad (21)$$

and

$$M = \begin{cases} Px & x < L_1 \\ P(x-L_1) & x_1 < x < L_2 \end{cases} \quad (22)$$

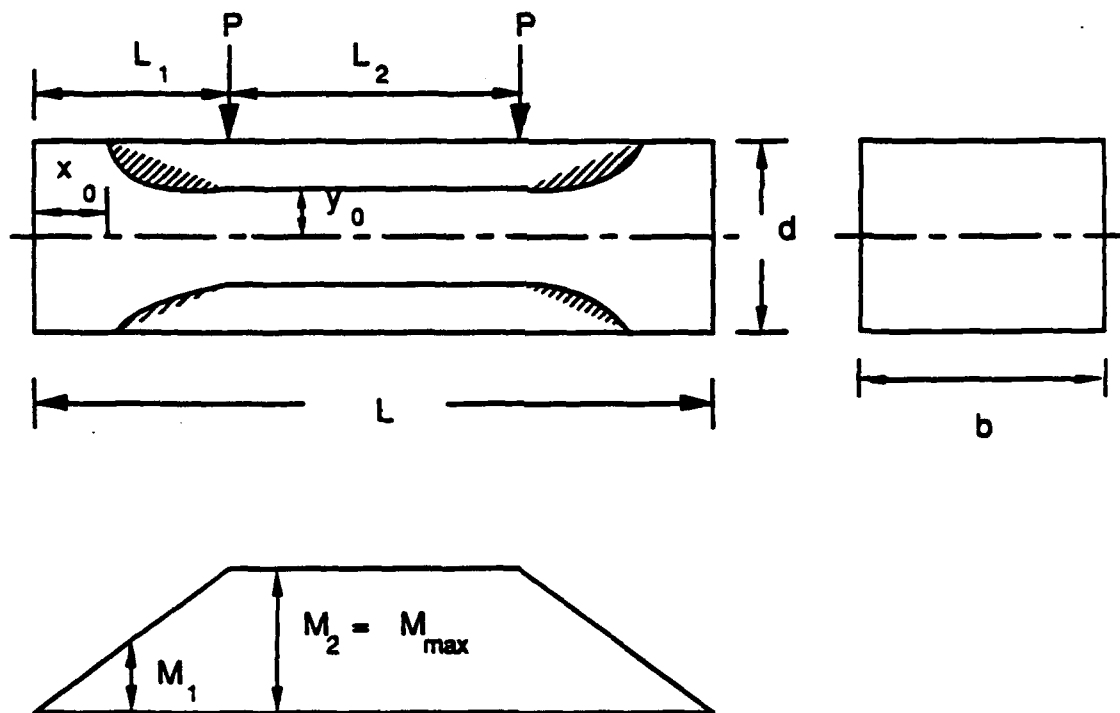


Figure 24

Four Point Bending Diagram on an Unnotched Isotropic Beam

with

$$S_{\max} = \frac{P L_1 h}{I} \quad (23)$$

the upper compressed region, where the absolute value of stresses is greater than the minimum compressive strength R_{0C} , is limited to values of $x > x_{0C}$ and $y > y_{0C}$ defined as

$$x_{0C} = \frac{R_{0C}}{S_{\max}} L_1 \quad (24)$$

$$y_{0C1} = \frac{R_{0C}}{S_{\max}} \frac{h L_1}{x} \quad x < L_1 \quad (25)$$

$$y_{0C} = \frac{R_{0C}}{S_{\max}} h \quad x_1 < x < L_2 \quad (26)$$

where h is the half depth of the beam. (i.e. $h=d/2$) and S_{\max} is the maximum stress in the beam.

For the lower tensile regions where stresses are greater than the minimum tensile strength R_{0T} ,

$$x_{0T} = \frac{R_{0T}}{S_{\max}} L_1 \quad (27)$$

$$y_{0T1} = \frac{R_{0T}}{S_{\max}} \frac{h L_1}{x} \quad x < L_1 \quad (28)$$

$$y_{0T} = \frac{R_{0T}}{S_{\max}} h \quad L_1 < x < L_2 \quad (29)$$

v_{0T} and v_{0C} are introduced for convenience, and they are defined as

$$v_{0T} = \frac{R_{0T}}{S_{\max}} = \frac{v_{cT}}{v_{T\max}} \quad (30)$$

$$v_{0C} = \frac{R_{0C}}{S_{\max}} = \frac{v_{cC}}{v_{C\max}} \quad (31)$$

with v_c and v_{\max} defined in Eq. 8.

Then, for the upper portions of the beam, substituting Eqs. 24 - 26 into Eq. 20 yields:

$$\lambda_C = \frac{2b}{(v_{cC} - v_{0C})^{mc}} \frac{1}{V} \left[\int_{x_{0C}}^{L_1} \int_{y_{0C1}}^h \left(\frac{xy}{hL_1} - \frac{v_{cC}}{v_{C\max}} \right)^{mc} dy dx \right]$$

$$+ \left[\int_{L_1}^{L_2} \int_{y_{0C}}^h \left(\frac{y}{h} - \frac{v_{0C}}{v_{Cmax}} \right)^{m_C} dy dx \right] \quad (32)$$

Denoting the first integral of Eq. 4.1.15 as I_{C1} and the second as I_{C2} and integrating for integer values of m_C

$$I_{C1} = \frac{h L_1}{(m_C+1)} \left\{ \sum_{k=0}^{m_C} (-1)^k C(m_C+1, k) v_{0C}^k \frac{1 - v_{0C}^{m_C+1-k}}{m_C+1-k} - (-1)^{m_C+1} v_{0C}^{m_C+1} \ln v_{0C} \right\} \quad (33)$$

and

$$I_{C2} = \frac{h L_2}{(m_C+1)} (1 - v_{0C})^{m_C+1} \quad (34)$$

result. $C(m_C+1, k)$ denotes the binomial coefficients defined by

$$C(m_C+1, k) = \frac{(m_C+1)!}{k! (m_C+1-k)!} \quad (35)$$

Substituting Eqs. 33 and 34 into Eq. 32

$$\lambda_C = \frac{2 b}{(v_{cC} - v_{0C})^{m_C}} \frac{1}{v} (I_{C1} + I_{C2}) \quad (36)$$

is obtained.

Similarly for the lower portions of the beam where the stresses are greater than the minimum tensile strength R_{0T} ,

$$\lambda_T = \frac{2 b}{(v_{cT} - v_{0T})^{m_T}} \frac{1}{v} (I_{T1} + I_{T2}) \quad (37)$$

where

$$I_{T1} = \frac{h L_1}{(m_T+1)} \left\{ \sum_{k=0}^{m_T} (-1)^k C(m_T+1, k) v_{0T}^k \frac{1 - v_{0T}^{m_T+1-k}}{m_T+1-k} - (-1)^{m_T+1} v_{0T}^{m_T+1} \ln v_{0T} \right\} \quad (38)$$

and

$$I_{T2} = \frac{hL_2}{(m_T + 1)} (1 - v_{0T})^{m_T+1} \quad (39)$$

Thus, the total stressed-volume integral, λ , becomes

$$\lambda = \frac{2b}{V} \left\{ \frac{1}{(v_{cT} - v_{0T})^{m_T}} (I_{T1} + I_{T2}) + \frac{1}{(v_{cC} - v_{0C})^{m_C}} (I_{C1} + I_{C2}) \right\} \quad (40)$$

where I_{T1} , I_{T2} , I_{C1} and I_{C2} are defined by the above equations. The foregoing reliability analysis for isotropic beams will, in the next section, be compared to one based on finite element methods.

Notched Beams

Finite Element Reliability Analysis for Notched Beams

To compare the results of unnotched and notched beam bending, both beams are analyzed with the aid of a finite element program that calculates the maximum principal stresses in each element. The stresses and the corresponding surface areas are stored. Once this has been accomplished, the largest maximum stress, S_{max} , in the beam is searched out; each stress is

divided by S_{max} ; the safety factors: $v_{cT} = \frac{R_{cT}}{S_{max}}$ for tensile stresses, and $v_{cC} = \frac{R_{cC}}{S_{max}}$ for compressive stresses are calculated and these are substituted into the finite element version of Eq. 7.

$$\ln \frac{1}{L} = \lambda = \frac{1}{(v_{cT} - v_{0T})^{m_T}} \frac{V}{V} \sum_{i=1}^n \left(\frac{S_{T_i}}{S_{max}} - v_{0T} \right)^{m_T} \frac{bA_i}{V} + \frac{1}{(v_{cC} - v_{0C})^{m_C}} \frac{V}{V} \sum_{i=1}^n \left(\frac{S_{C_i}}{S_{max}} - v_{0C} \right)^{m_C} \frac{bA_i}{V} \quad (41)$$

It is assumed that $m_C = m_T = m$.

The material properties used for the isotropic beam analysis are:

$$E = 2.14 \text{ (msi)} \quad \nu = 0.2$$

These were measured for the material in the warp direction [Part I]. The finite element results are compared to the closed form analysis in Fig. 25, where reliability is plotted as function of load carrying capacity. It is seen that the two methods produce very similar information.

To compare finite element results for unnotched and notched beams, they are analyzed with an identical mesh. The reliability of a solid (unnotched) beam due to tensile principal stresses alone and that due to tensile and compressive stresses combined as a function of load carrying capacity are also presented in Fig. 25 while those of a notched beam are shown in Fig. 26. In the

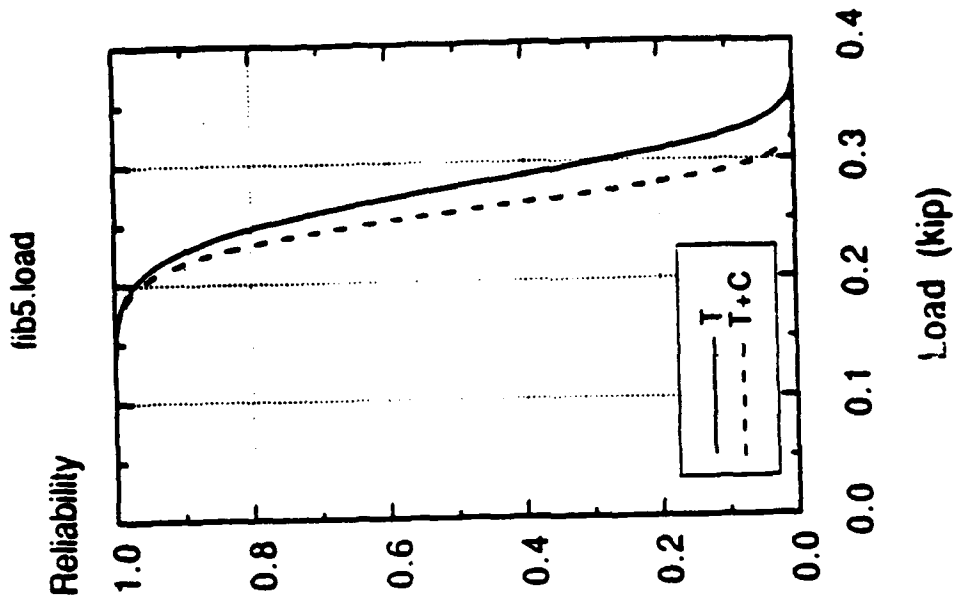


Figure 26
Reliability of an isotropic notched beam under 4-point bending as a function of load

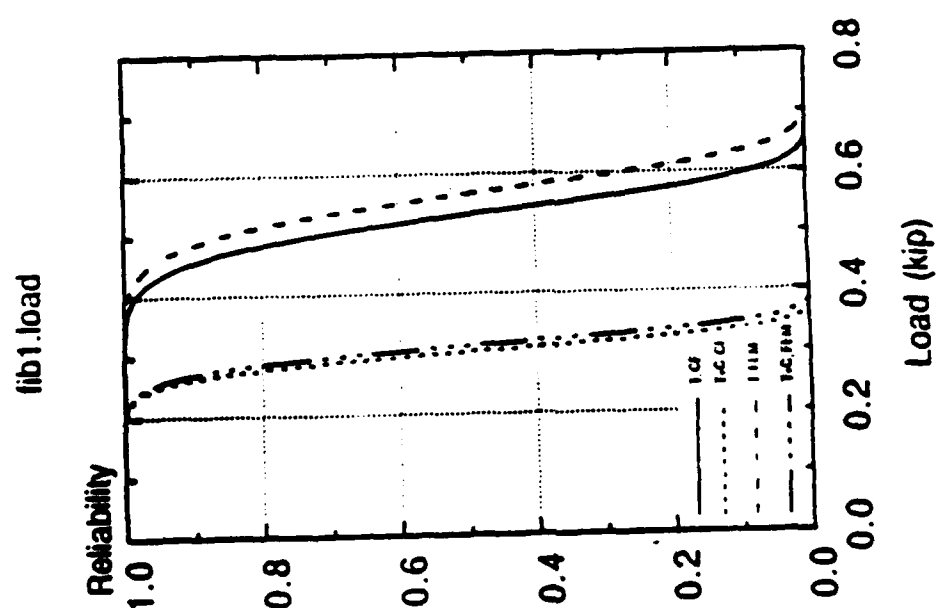


Figure 25
Comparison of reliabilities of an isotropic unnotched beam as a function of load carrying capacity (T: tensile stresses alone, T+C: tensile & compressive stresses combined, CF: closed-form)

figures, T denotes the reliability due to tensile stresses only, T+C the reliability due to tensile and compressive stresses combined and CF the reliability based on the closed-form solution.

For an unnotched beam, the compressive stresses have a significant effect on the total failure while for a notched beam, the contribution from these stresses is small. This may be interpreted as follows: Carbon-carbon has different mean strengths in tension (13.4 ksi) and in compression (8.3 ksi). In other words, the beam as a whole is much stronger in tension than in compression. As a result, for an unnotched beam, the elements in the top portion fail in compression before elements at the bottom start to fail in tension at higher a load. Thus, compressive stresses contribute much to the total failure. On the other hand, for a notched beam, tensile stresses near the notch tip are very high compared with those for an unnotched beam. (Maximum stress for an unnotched beam is about 33 (psi) and that for a notched beam is about 78 (psi) for 1 pound load.) Yet, stress distributions of both notched and unnotched beams away from the notch are quite similar. Hence, elements above the neutral surface in both beams undergo failure in compression at pretty much the same levels of load, while elements around the notch tip start to fail in tension at lower load levels than in the unnotched beam, thereby shifting the reliability graph to the left (to the lower side of load).

The comparison between the reliability of an unnotched beam and that of a notched beam due to tensile stresses alone as functions of load carrying capacity is presented in Fig. 27 and that due to tensile and compressive stresses combined in Fig. 28. The reliabilities of a solid (unnotched) beam due to tensile principal stresses only and those due to tensile and compressive stresses combined as functions of maximum principal stress are plotted in Fig. 29 and those of a notched beam are presented in Fig.30. Unnotched and notched beam reliabilities due to tensile stresses only as functions of maximum principal stress are compared in Fig. 31 while the effects of tensile and compressive stresses combined are presented in Fig. 32.

Specimen geometry and strength parameters used in the calculation are shown in Table 4 and load carrying capacities of unnotched and notched beams at 0.5 reliability level are compared with experimental failure loads in Table 5. Unnotched beams obviously carry more load (about twice as much) than notched beams. The analytical load carrying capacity of an unnotched beam (0.562 kip) is very close to that obtained by experiment (0.493 kip) when only tensile stresses are considered in the analysis. When both tensile & compressive stresses are included, the load carrying capacity predicted by analysis (0.313 kip) is a lot less than that obtained by experiment (0.493 kip). For a notched beam, both the analytical failure load due to tensile stresses alone (0.270 kip) and that due to tensile & compressive stresses combined (0.253 kip) coincide very well with experimental failure loads (0.250 kip).

It is also observed from Table 5 that the maximum principal stress at failure is greater for a notched beam than for an unnotched beam. The maximum principal stresses at failure for an unnotched beam are 19.944 (ksi) when only tensile stresses are considered and 10.437 (ksi) when both tensile & compressive stresses are involved. Those for a notched beam are 27.375 (ksi) for tensile stresses alone and 25.000 (ksi) when both tensile & compressive stresses are considered. The ratios of notched to unnotched theoretical strength are 1.41 for tensile stresses alone and 2.40 for both tensile & compressive stresses considered. These numbers can be applied in calculating the experimental failure strength for the notched beam. Because the experimental failure loads match the calculated loads (tension only) very well, it may be assumed that the calculated failure strength ratio of $1/0.710 = 1.41$ indicates the increased strength of the small volume of material at the notch tip. This increase in strength is an indication of the size effect.

The reliability contours for an unnotched beam due to tensile stresses only and those due to tensile and compressive stresses combined are presented in Figs. 33 and 34 at the 0.5 kip load level. Similar contours are plotted in Figs. 35 and 36 at the 0.25 kip load level for a notched beam.

fib1/5_I_load

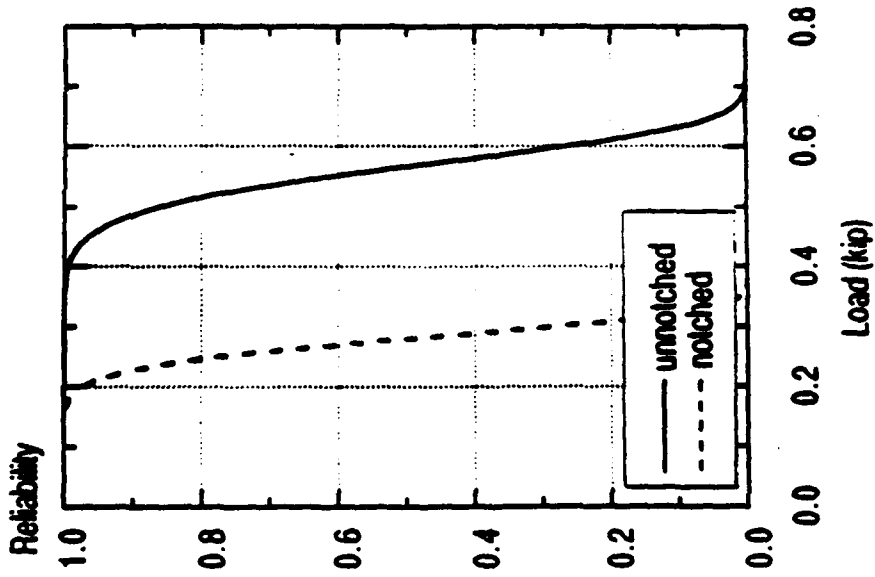


Figure 27

Comparison of reliabilities of an isotropic unnotched and notched beam due to tensile stresses alone as a function of load

fib1/5_I+C_load

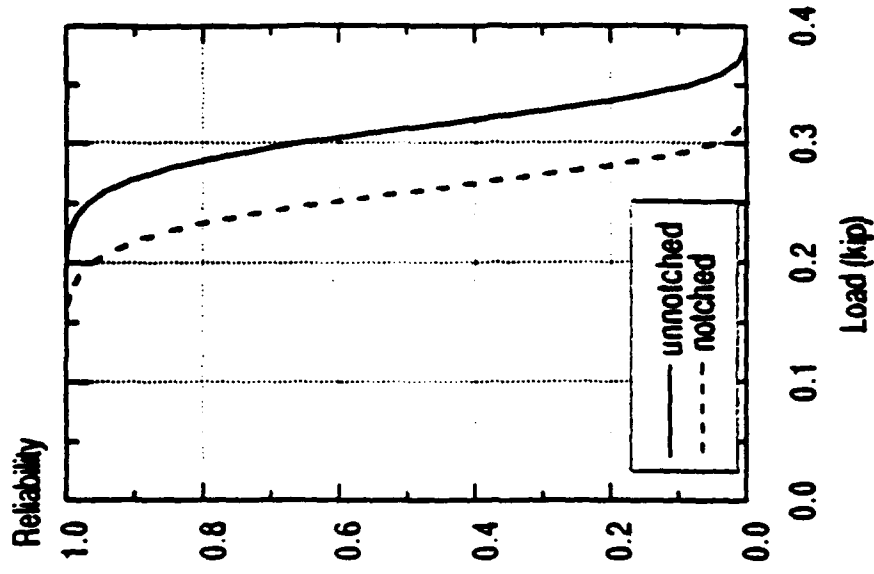


Figure 28

Comparison of reliabilities of an isotropic unnotched and notched beam due to tensile and compressive stresses combined as a function of load

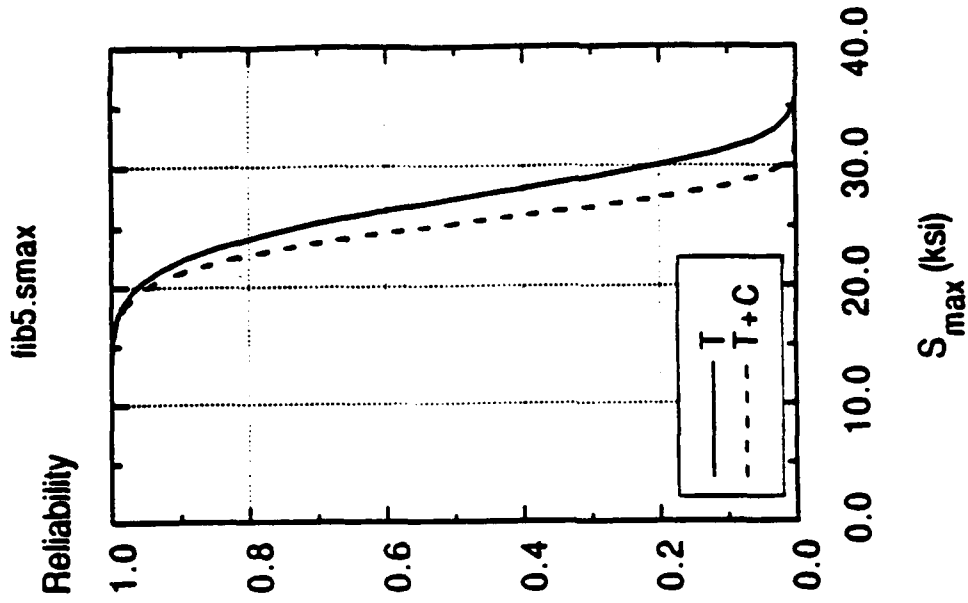


Figure 30

Reliability of an isotropic notched beam under 4-point bending as a function of maximum principal stress

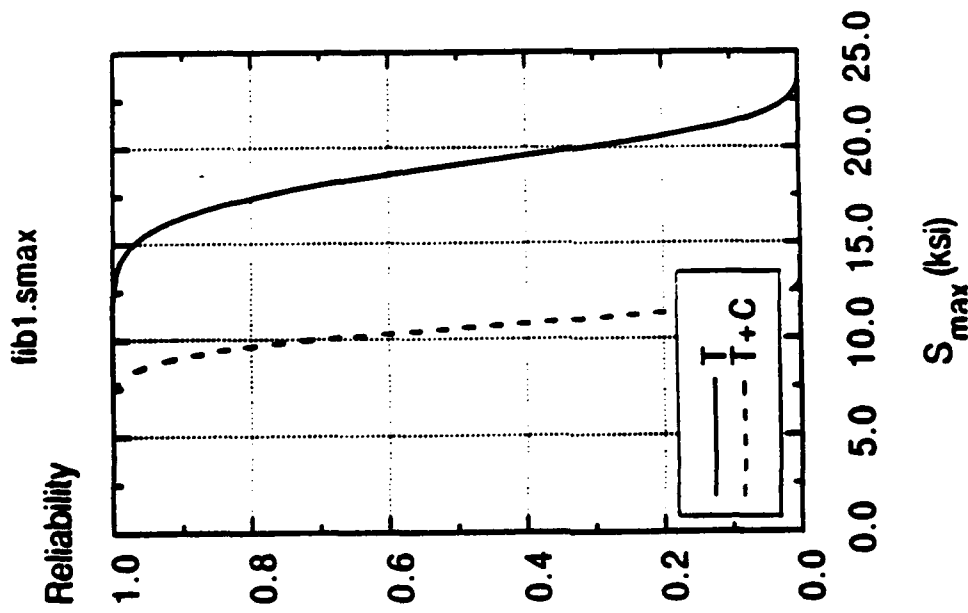


Figure 29

Reliability of an isotropic unnotched beam under 4-point bending as a function of maximum principal stress

fib15_I_Smax

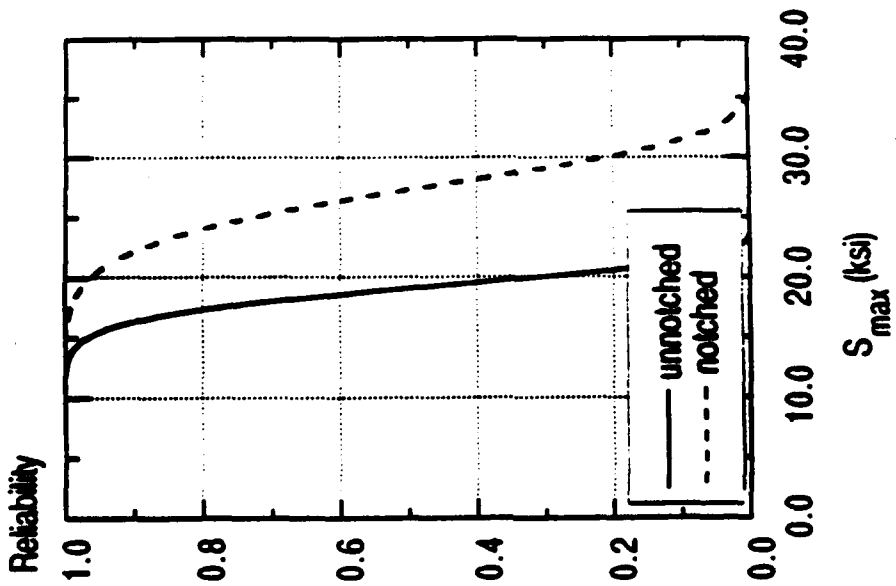


Figure 31

Comparison of reliabilities of an isotropic unnotched and notched beam due to tensile stresses alone as a function of maximum principal stress

fib15_I+C_Smax

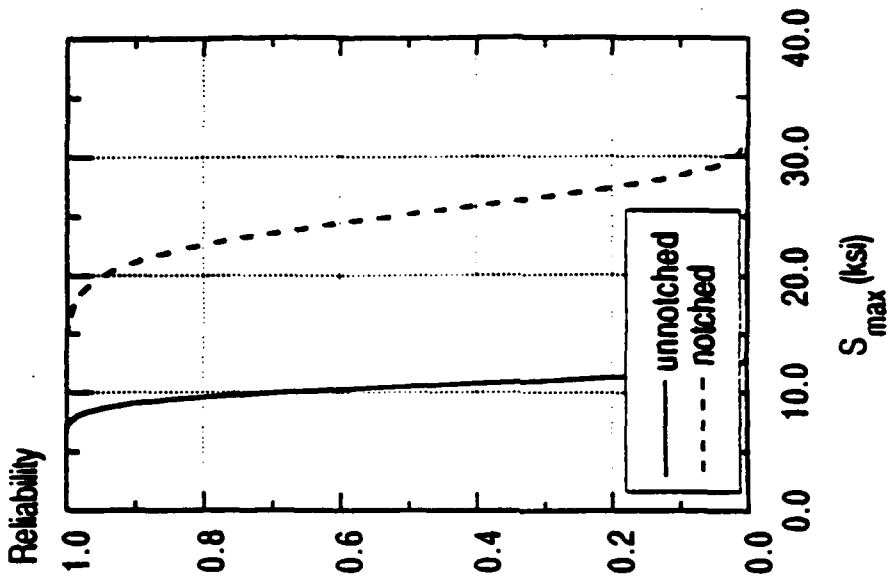


Figure 32

Comparison of reliabilities of an isotropic unnotched and notched beam due to tensile stresses alone as a function of maximum principal stress

Table 4. Dimensions and Weibull Parameters Used in the computation of Reliability of an Isotropic Beam

L_1	L_2	b	d	R_{cT}	R_{oT}	R_{cC}	R_{oC}	m_T	m_C
(in)									
0.8125	1.0	0.48	0.38	13.80	8.17	8.55	5.06	6	6

Table 5. Comparison of Experimental and Analytical Results for an Isotropic Beam

	Experimental		Ratio		Analytical		Ratio	
	U	N	U/N	N	U	N	U/N	T
Load (2p) kips	0.493	0.250	1.972	0.562	0.313	0.270	0.253	2.081
Strength ksi	19.71			19.444	10.437	27.375	25.000	0.710

(Note; U denotes unnotched beam, N denotes notched beam,

T denotes tensile, and T+C denotes tensile and compressive combined)

Reliability

- 1.00= A
- .999= B
- .998= C
- .998= D
- .997= E
- .996= F
- .995= G
- .995= H
- .994= I
- .993= J
- .993= K
- .992= L
- .991= M
- .991= N
- .990= O

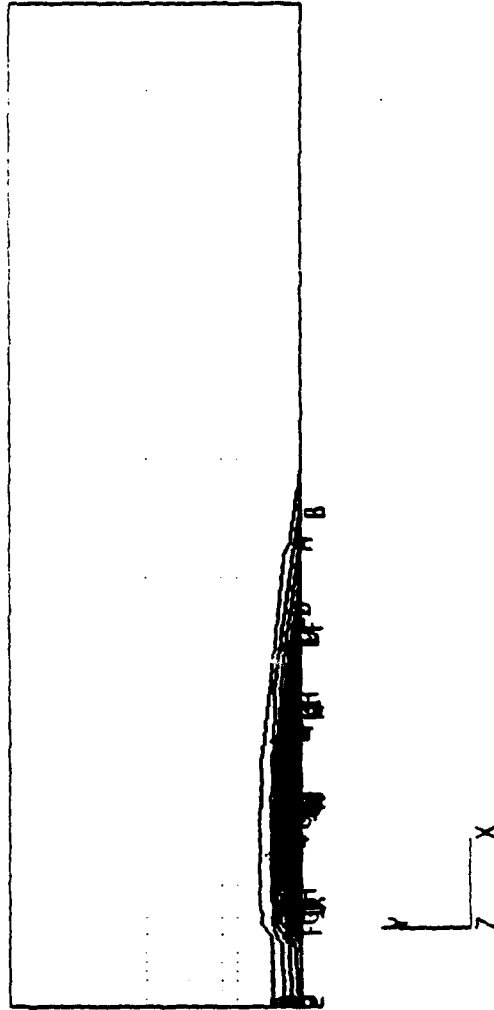


Figure 33

Reliability Contour of an Isotropic Unnotched Beam under 4-point Bending due to Tensile Stresses at 0.5 (kip) Load

Reliability	
.978=	A
.933=	B
.889=	C
.844=	D
.800=	E
.756=	F
.711=	G
.667=	H
.622=	I
.578=	J
.533=	K
.489=	L
.444=	M
.400=	N
.355=	O

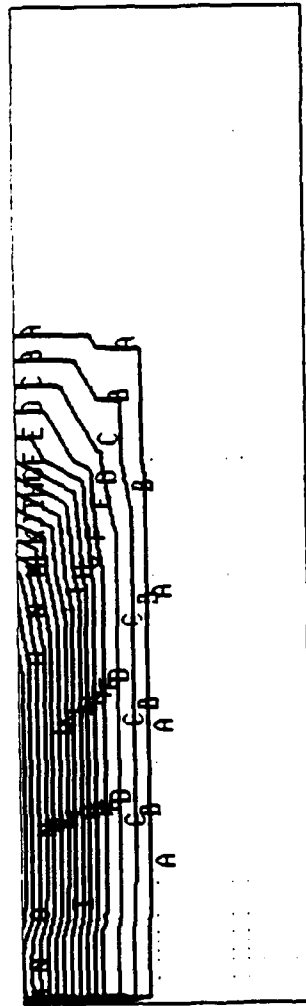


Figure 34

Reliability Contour of an Isotropic Unnotched Beam under 4-point Bending due to Tensile & Compressive Stresses Combined at 0.5 (kip) Load

Reliability

- .967= A
- .900= B
- .833= C
- .767= D
- .700= E
- .633= F
- .567= G
- .500= H
- .433= I
- .367= J
- .300= K
- .233= L
- .167= M
- .100= N
- .0333= O

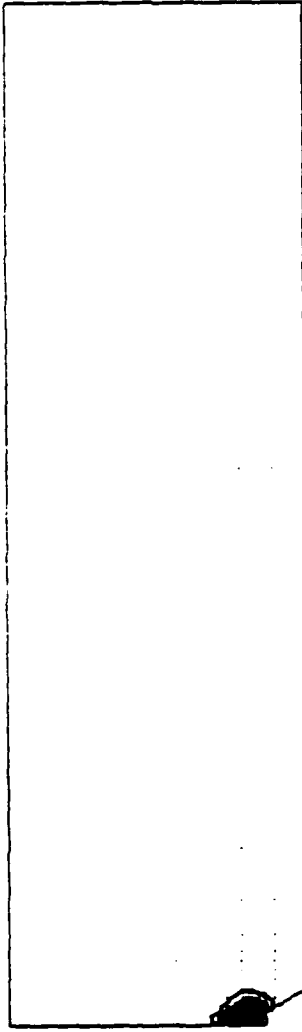


Figure 35

Reliability Contour of an Isotropic Notched Beam under 4-point Bending due to Tensile Stresses at 0.25 (kip) Load

Reliability

- .967 = H
- .900 = I
- .833 = J
- .767 = K
- .700 = L
- .633 = M
- .567 = N
- .500 = O
- .433 = P
- .367 = Q
- .300 = R
- .233 = S
- .167 = T
- .100 = U
- .033 = V

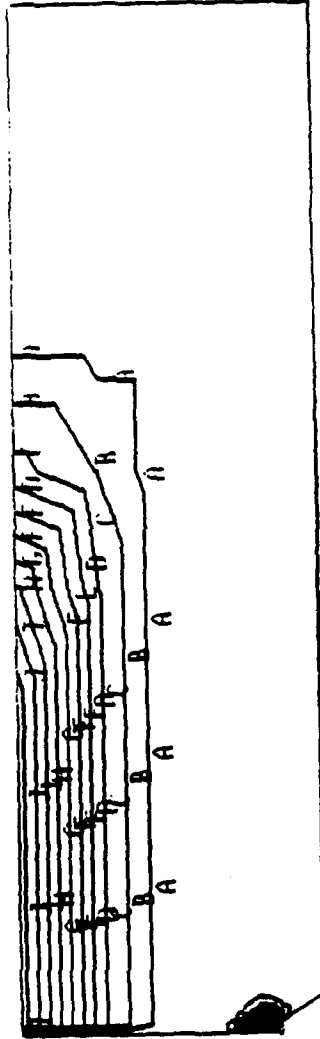


Figure 36

Reliability Contour of an Isotropic Notched Beam under 4-point Bending due to Tensile & Compressive Stresses Combined at 0.25 (kip) Load

Composite Beams

To preserve the effect of interlaminar shear stresses in the reliability analysis of laminated composite beams, Eq. 2.1.8 is modified so that the reliability is expressed in terms of cartesian stress components rather than principal stresses [Sun and Yamada, 1978]. Then the total reliability L becomes

$$L = L_{\sigma_x} \times L_{\sigma_z} \times L_{\tau_{zx}} \quad (42)$$

where σ_x , σ_z are longitudinal stress and transverse normal stress, τ_{zx} is the interlaminar shear stress, L_{σ_x} , L_{σ_z} , $L_{\tau_{zx}}$ are the reliabilities due to σ_x , σ_z and τ_{zx} , respectively, defined by the following :

$$\begin{aligned} L_{\sigma_x} &= \exp \left[- \int_V \left(\frac{\sigma_x - R_{01}}{R_{c1} - R_{01}} \right)^{m_1} \frac{dV}{V} \right] \\ L_{\sigma_z} &= \exp \left[- \int_V \left(\frac{\sigma_z - R_{03}}{R_{c3} - R_{03}} \right)^{m_3} \frac{dV}{V} \right] \\ L_{\tau_{zx}} &= \exp \left[- \int_V \left(\frac{\tau_{zx} - R_{05}}{R_{c5} - R_{05}} \right)^{m_5} \frac{dV}{V} \right] \end{aligned} \quad (43)$$

where R_{01} and R_{03} are minimum strengths in the x, z directions, respectively, R_{c1} and R_{c3} are characteristic strengths in the x, z directions, respectively, and R_{05} and R_{c5} are minimum and characteristic shear strengths in the xz plane, respectively.

The dimensions of composite beams are as follows:

$$L_1 = 0.8125 \text{ (in)}, L_2 = 1.0 \text{ (in)}, b = 0.485 \text{ (in)}, d = 0.38 \text{ (in)}$$

In all computations, a Weibull shape parameter of $m=6$ will be used. Material properties and strength parameters used in the analysis are presented in Table 6 and comparison between analysis and experiments is shown in Table 7.

The reliability of an unnotched composite beam due to tensile longitudinal stress alone, that due to tensile & compressive components combined and that due to all stresses, including interlaminar normal and shear stresses, as functions of load carrying capacity are plotted in Fig. 37. Those of a notched composite beam are shown in Fig. 38. In the figures, the designations: XT stands for the reliability due to tensile stress alone, XT + XC that due to tensile & compressive stress components combined, and XT + XC + SI that due to the interlaminar normal & shear stresses combined in addition to the longitudinal stress components.

As seen in the case of an isotropic beam, the compressive stresses contribute significantly to the total failure for an unnotched composite beam also while for a notched composite beam the contribution is small. Similar arguments can be applied to interpret this phenomenon: Fibers are the major load carrying mechanism, and therefore can resist a larger load

Table 6. Material Properties and Strength Parameters of a Composite Beam

Fiber		Matrix	
Material Properties (msi)	Strength Parameters (ksi)	Material Properties (msi)	Strength Parameters (ksi)
E_x	R_{cxT}	E	R_c
E_z	R_{cxC}		R_0
ν_{zx}	R_{czT}	ν	R_{cS}
G_{zx}	R_{czC}		R_{0S}
G_{xy}	R_{cS}		
G_{yz}	R_{0xT}		
	R_{0xC}		
	R_{0zT}		
	R_{0zC}		
	R_{0S}		

Table 7. Comparison of Experimental and Analytical Results for a Composite Beam

	Experimental		Ratio		Analytical		Ratio	
	U	N	U/N		U	N	U/N	
Load (2p) kips	0.506	0.289	1.752		0.345	0.167	2.066	
Strength ksi	15.238		20.140		32.200		0.625	

(Note; U denotes unnotched beam, N denotes notched beam,
Analytical results are due to tensile stresses only)

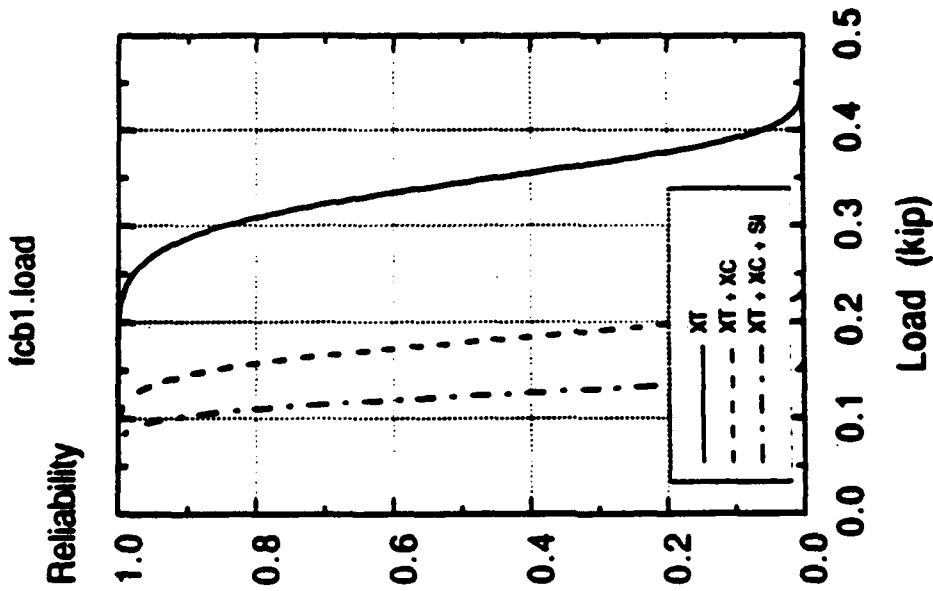


Figure 37

Reliability of an unnotched composite beam under 4-point bending as a function of load

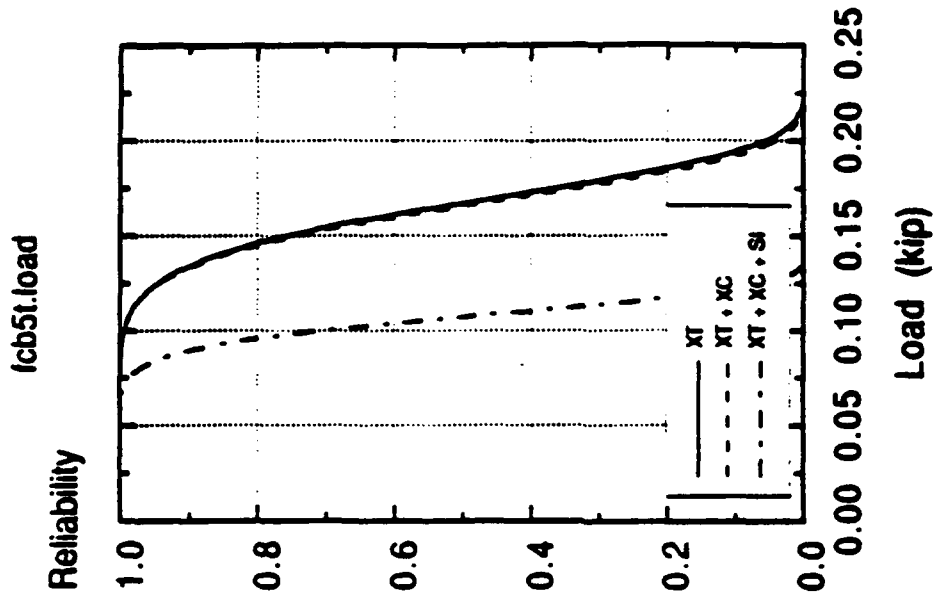


Figure 38

Reliability of a notched composite beam under 4-point bending as a function of load

(Mean fiber strengths are 24.8 (ksi) in tension and 14.0 (ksi) in compression whereas mean matrix strength is 2 (ksi) in both tension and compression). At an early stage of loading, most of the failures occur in matrix elements followed by failure of fibers. For an unnotched composite beam, as the fiber strength in compression is only about half as high as that in tension, the fibers fail first in compression and final failure takes place when fibers fail in tension at higher load. Thus the compressive stresses play a significant role in the total failure.

For a notched composite beam, however, the stresses at the notch tip are much higher than those of an unnotched composite beam whereas the stress distribution away from the notch is pretty much alike for both beams. Therefore, while the fibers fail in compression in the same fashion as they do in the unnotched beam, tensile stresses participate in the failure process earlier in a notched beam and fibers start to break in tension at a relatively low load level. Hence, the contribution of compressive stresses to the total failure is not as significant for notched beams as in the case of unnotched beams. This is the reason why compressive stresses contribute much to unnotched beam failures but not to those of notched beams. In contrast to isotropic beams interlaminar stresses are present in composite beams and as the interlaminar strengths are low (mean strength of 1.5 ksi), the failure due to interlaminar stresses starts at the very low load level followed by compressive and eventually tensile fiber failures.

The comparison between the reliability of an unnotched composite beam and that of a notched composite beam due to tensile stresses only as functions of load carrying capacity is presented in Fig. 39 while the effects of all stress components combined are shown in Fig. 40. At a reliability level of 0.5, the load carrying capacity of an unnotched beam and a notched beam are 0.345 (kips) and 0.167 (kips), respectively, whereas the experimental ultimate failure loads are 0.505 (kips) and 0.288 (kips), respectively. In view of the fact that ultimate failure occurs when all the fiber layers fail, the 0.345 kips load may be interpreted as first-fiber-ply-failure load for an unnotched composite beam, and the 0.167 kips for a notched beam. For an isotropic beam, there is no such thing as first-ply-failure. When an element breaks, the crack propagates very rapidly and this makes the reliability analysis for isotropic beams agree very well with experiments. On the other hand, for composite beams, there exists a so-called first-ply-failure, and the composite beam can sustain more load after first-ply-failure occurs. The experimental ultimate failure load is obtained after all the plies fail, and it is for this reason that progressive failure analysis is necessary.

The reliabilities of an unnotched composite beam due to tensile components of longitudinal stress alone, due to tensile & compressive components combined and due to interlaminar normal and shear stresses included as functions of maximum longitudinal stress are plotted in Fig. 41 and those of a notched beam are presented in Fig. 42. The comparison between the reliability of an unnotched beam and that of a notched beam due to tensile stresses only as a function of maximum longitudinal stress is shown in Fig. 43 and effects of all stress components combined are presented in Fig. 44.

It is interesting to note from Fig. 40 that the load carrying capacities for both beams when all the stress components are considered are close to each other (0.122 kips for unnotched beam and 0.117 kips for notched beam). The reason for this is that the stress distributions for both unnotched and notched beams are nearly identical away from the notched region. Furthermore, the fiber strength is so high that only a few elements near the notch tip region contribute to failure and that by the time fibers start to break in tension, other stress components have already reduced the total reliability to nearly zero. It is to be noted that as more stress components are considered in the analysis, the load carrying capacity at 0.5 reliability level approaches the first-ply-failure load. To demonstrate this, first-ply-failure analysis was performed on the composite beam using Brewer-Lagace's delamination criterion and the delamination part of the proposed criteria. Only three stress components, namely, σ_x , σ_z , and σ_{zx} , enter the calculation. The load carrying capacity of both beams at 0.5 reliability level when all the stress

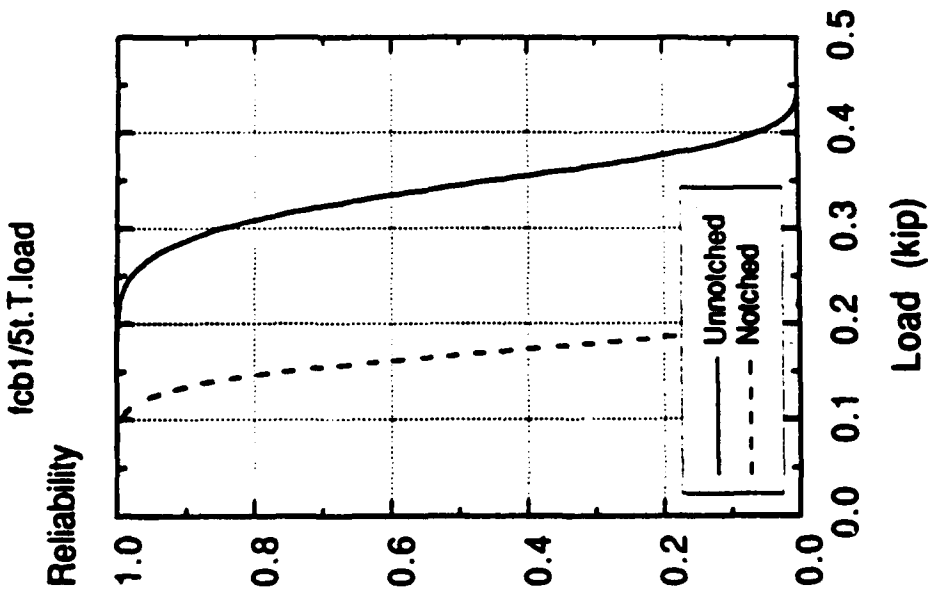


Figure 39

Comparison of reliabilities of an unnotched and notched composite beam due to tensile stresses alone as a function of load

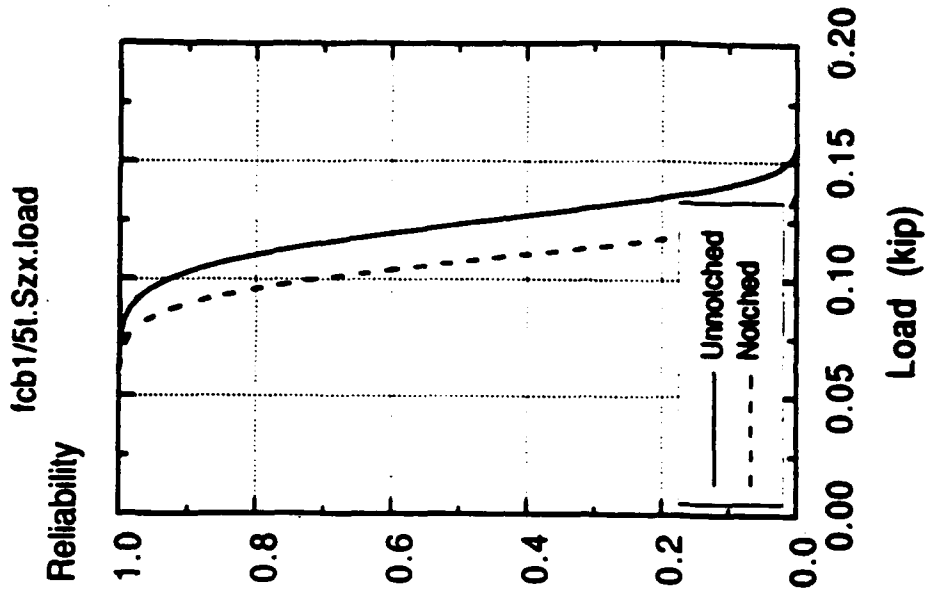


Figure 40

Comparison of reliabilities of an unnotched and notched composite beam due to tensile, compressive and interlaminar stresses combined as a function of load

components are considered is compared with first-ply-failure loads based on the two delamination criteria and also with experiment in Table 14.

To compare the reliability of unnotched and notched composite beams at the same load level, reliability contours are created for both unnotched and notched beams at 0.2 kips load level. The contours are shown in Fig. 45 and 46.

Reliability of Composite Plates under Transverse Loading

Reliability of square and rectangular plates with and without a hole is investigated in this section. The dimensions of the square plate are 6.5 x 6.5 (in) and the net loaded area is 6 x 6 (in). Those of the rectangular plates are 9.75 x 6.5 (in) and the net loaded area is 9.25 x 6.0 (in). The thickness of these plates is 0.485 (in) and the diameter of the hole is 0.64 (in). The aspect ratios (i.e. side-length-to-thickness ratio w/h) are 12.4 for both plates. Material properties and strength parameters used in the analysis are presented in Table 8.

Extension of "Weakest Link" Reliability to Account for Interlaminar Shear Stresses

τ_{zx} and τ_{zy}

For laminated plates under transverse loading, the stress field is no longer in a plane stress state. To account for the effect of interlaminar shear stresses to the total reliability, Eq. 42 should be extended to the following:

$$L = L_{2D} \times L_{3D} = (L_1 \times L_2 \times L_6) \times (L_4 \times L_5) \quad (44)$$

where $L_{2D} = L_1 \times L_2 \times L_6$ and $L_{3D} = L_4 \times L_5$ are the reliabilities due to a 2-D stress field and additional interlaminar stress field, respectively, defined by

$$\begin{aligned} L_1 &= \exp \left[- \int_V \left(\frac{\sigma_x - R_{01}}{R_{c1} - R_{01}} \right)^{m_1} \frac{dV}{V} \right] \\ L_2 &= \exp \left[- \int_V \left(\frac{\sigma_y - R_{02}}{R_{c2} - R_{02}} \right)^{m_2} \frac{dV}{V} \right] \\ L_6 &= \exp \left[- \int_V \left(\frac{\tau_{xy} - R_{06}}{R_{c6} - R_{06}} \right)^{m_6} \frac{dV}{V} \right] \\ L_4 &= \exp \left[- \int_V \left(\frac{\tau_{zy} - R_{04}}{R_{c4} - R_{04}} \right)^{m_4} \frac{dV}{V} \right] \\ L_5 &= \exp \left[- \int_V \left(\frac{\tau_{zx} - R_{05}}{R_{c5} - R_{05}} \right)^{m_5} \frac{dV}{V} \right] \end{aligned} \quad (45)$$

In this equation the transverse normal stress σ_z is neglected. By separating the total reliability into two parts, it is anticipated that the contribution from the interlaminar shear stresses to the total reliability can be clarified. It is assumed that $m_1=m_2=m_3=m_4=m_5=m_6$ in the analysis.

Square Plates under Transverse Loading

Square Plate without a Hole

The reliabilities of square plates without a hole as functions of uniform pressure, load, and maximum stress are presented in Figs. 47, 49, and 50. The contributions from tensile stress, compressive stress, in-plane shear stress σ_{12} , interlaminar shear stresses σ_{32} and σ_{31} are separated in the figures. The designations: T, C, 2-D stresses, 2-D + s_{23} , 2-D stresses + s_{23} + s_{13} in the figures, denote tensile stress, compressive stress, 2-D stress field which includes in-plane shear stress σ_{12} , interlaminar shear stress σ_{32} added to 2-D stress field, and interlaminar shear stresses σ_{31} and σ_{32} added to 2-D stress field, respectively.

Square Plate with a Hole

The reliabilities of square plates with a hole as functions of uniform pressure, load, and maximum stress are plotted in Figs. 48, 50, and 52.

4.2.3 Rectangular Plates under Transverse Loading

4.2.3.1. Rectangular Plate without a Hole

The reliabilities of rectangular plates without a hole as functions of uniform pressure, load, and maximum stress are presented in Figs. 53, 55, and 57.

4.2.3.2. Rectangular Plate with a Hole

The reliabilities of rectangular plates with a hole as functions of uniform pressure, load, and maximum stress are presented in Figs. 54, 56, and 58.

As presented in Figs. 47 - 48, analysis shows that for this particular type of woven carbon-carbon composite plate where the interlaminar shear moduli are low but strengths are relatively high, the contribution from the interlaminar shear stresses is little. This conclusion is supported by experimental results [Part I]. The comparison of reliabilities of both square and rectangular plates with and without a hole as functions of pressure is shown in Fig. 59, and as functions of total load in Fig. 60. In these figures, the designations: S,NH stand for a square plate without a hole, S,H a square plate with a hole, R,NH a rectangular plate without a hole, and R,H a rectangular plate with a hole.

From Fig. 59, it is seen that the intensities of uniform load at 0.5 reliability level are 0.15 (ksi) for a square plate without a hole and 0.125 (ksi) for a square plate with a hole while they are 0.09 (ksi) and 0.07 (ksi) for rectangular plates without a hole and with a hole, respectively. The failure loads at 0.5 reliability level are 5.6 (kips) for a square plate without a hole, 4.42 (kips) for a square plate with a hole, 4.90 (kips) for a rectangular plate without a hole, and 3.85 (kips) for a rectangular plate with a hole.

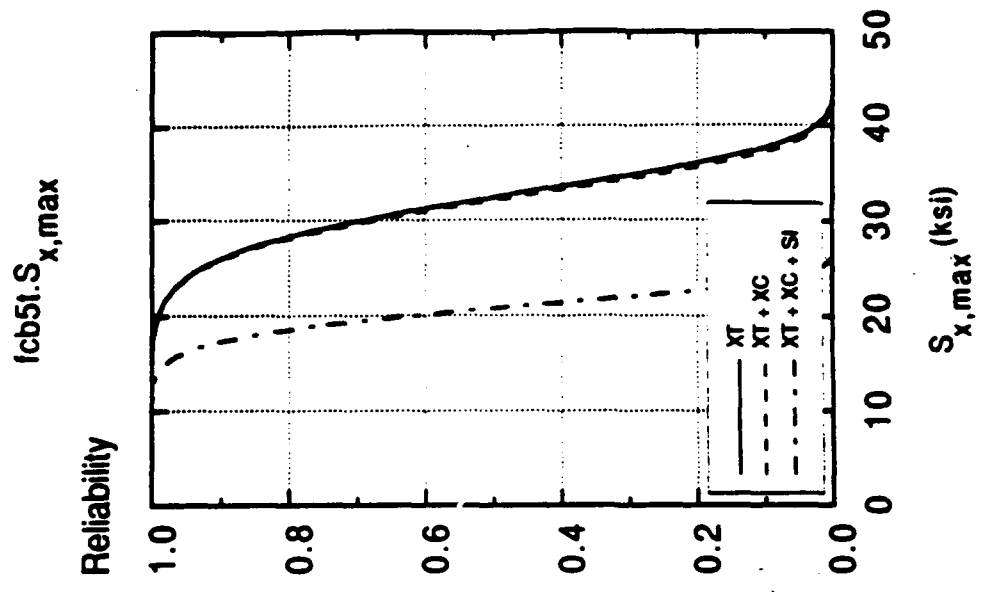


Figure 42
Reliability of a notched composite beam under 4-point bending as a function of maximum stress

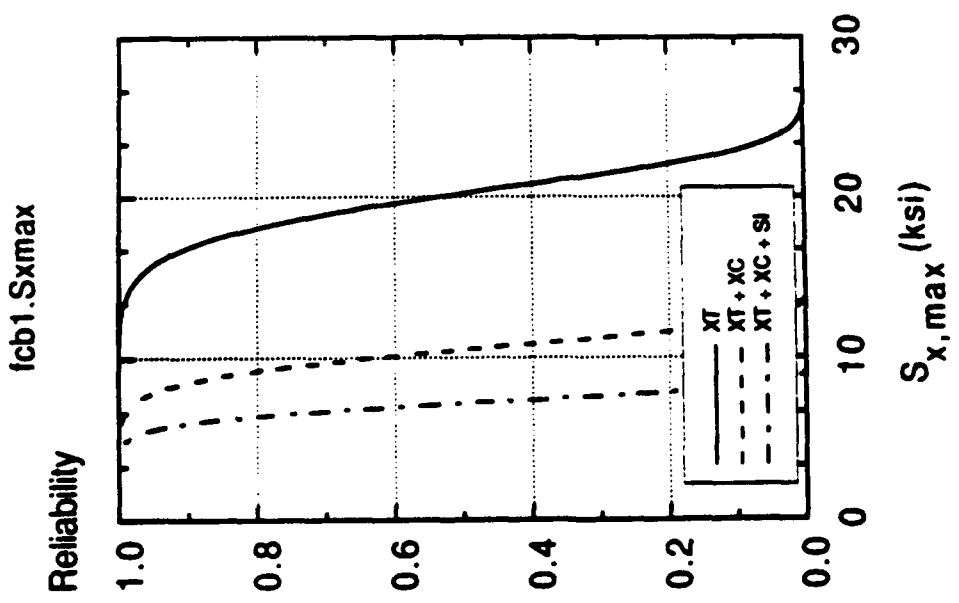


Figure 41
Reliability of an unnotched composite beam under 4-point bending as a function of maximum stress

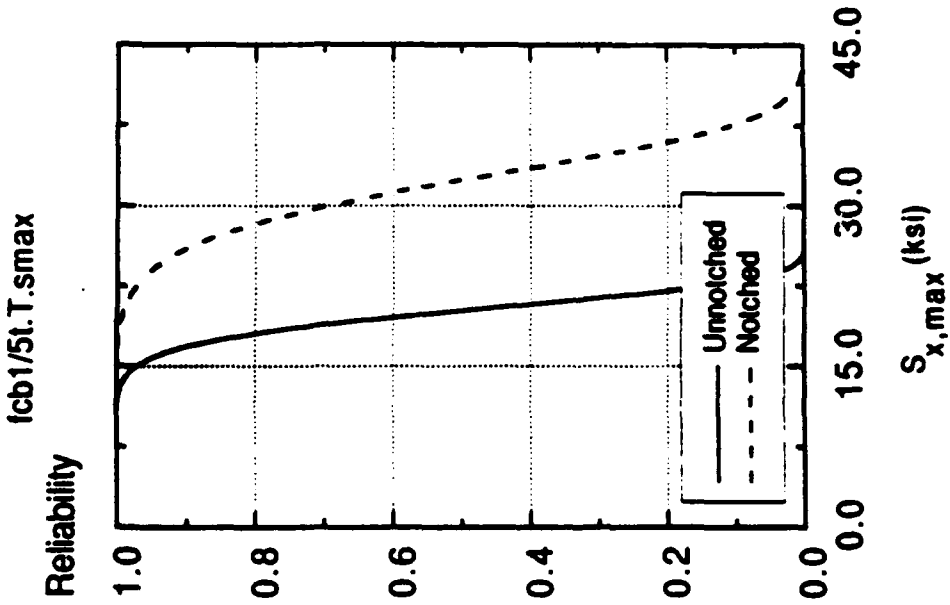


Figure 43

Comparison of reliabilities of an unnotched and notched composite beam due to tensile stresses alone as a function of maximum stress

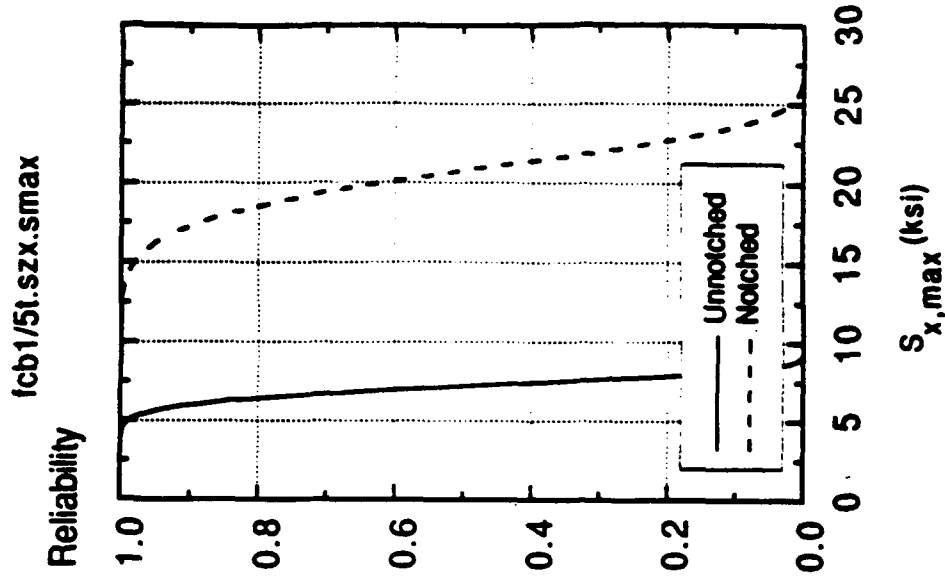


Figure 44

Comparison of reliabilities of an unnotched and notched composite beam due to tensile, compressive and interlaminar stresses combined as a function of maximum stress

.975= H
 .929= B
 .881= C
 .834= D
 .786= E
 .739= F
 .691= G
 .644= H
 .596= I
 .549= J
 .501= K
 .454= L
 .406= M
 .359= N
 .312= O

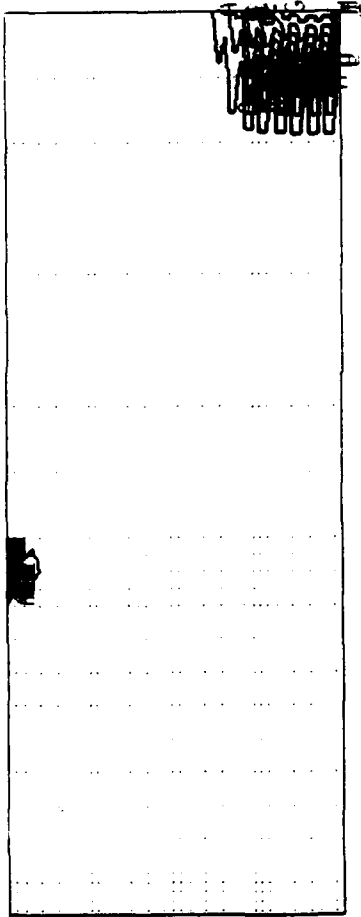


Figure 45

Reliability Contour of an Unnotched Composite Beam under 4-point Bending due to Tensile Stresses Alone at 0.2 (kip) Load

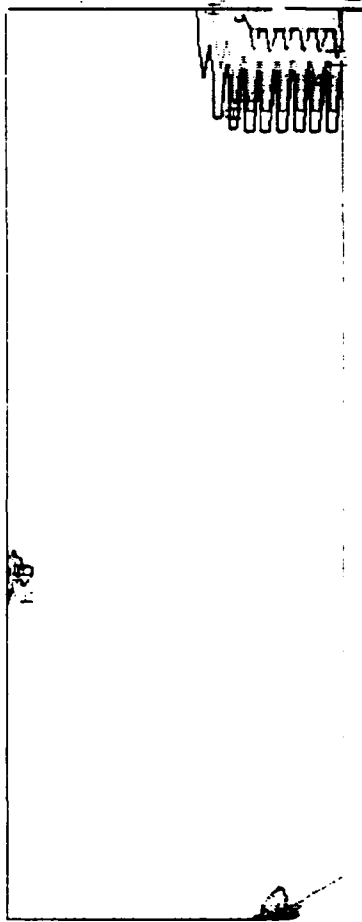
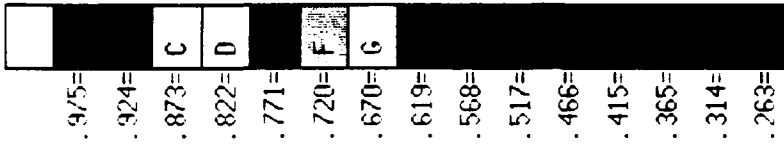


Figure 46

Reliability Contour of an Unnotched Composite Beam under 4-point Bending due to All Stress Components at 0.2 (kip) Load

Table 8. Material Properties and Strength Parameters of a Composite Plate

Fiber		Matrix	
Material Properties (msi)	Strength Parameters (ksi)	Material Properties (msi)	Strength Parameters (ksi)
E_x	3.780	R_{cxT}	25.544
E_y	2.790	R_{cxC}	14.420
ν_{xy}	0.048	R_{cyT}	12.360
G_{xy}	0.670	R_{cyC}	13.390
G_{zx}	0.025	R_{cxy}	10.197
G_{zy}	0.018	R_{czz}	2.060
		R_{czy}	1.648
		R_{0xT}	15.128
		R_{0xC}	8.540
		R_{0yT}	7.320
		R_{0yC}	7.930
		R_{0xy}	6.039
		R_{0zx}	1.220
		R_{0zy}	0.976
		E	0.5
		ν	0.25
		R_c	2.060
		R_0	1.220
		R_{cxy}	1.545
		R_{czz}	1.545
		R_{czy}	1.545
		R_{0xy}	0.915
		R_{0zx}	0.915
		R_{0zy}	0.915

The failure loads at 0.5 reliability level are compared with those predicted by first-ply-failure analysis and also with those obtained by experiment. As no experiment was performed on the square plate without a hole, the comparison is made with those 3 plates tested, namely square plate with a hole, rectangular plate without a hole, and with a hole. The comparison of reliabilities of square plates without a hole and with a hole as functions of $\sigma_{x,max}$ is shown in Fig. 61. The effects are presented in Fig. 62 for rectangular plates. As maximum stress occurs in different direction for square plate and rectangular plate, the reliability-maximum stress curves are separated for both cases.

The reliability contours at the top matrix layer and at the fiber layer second from the bottom are plotted in Figs. 63 - 67 at 100 psi pressure level for all plates considered. For this level of load intensity, no layer of the square plate without a hole shows failure. The fiber layers of the square plate with a hole do not show failure either. Only the matrix layers fail at that load level and the contour is presented in Fig. 63. The reliability contours of the rectangular plate without a hole at top matrix layer and at bottom fiber layer (above the bottom matrix layer) at 100 psi pressure are shown in Fig. 64 and 65, respectively. The reliability contours of the rectangular plate with a hole at top matrix layer and at bottom fiber layer at 100 psi pressure are shown in Fig. 66 and 67, respectively. As the reliability contours due to 2-D stress field and 3-D stress field are nearly identical, only the contours due to 3-D stress field are shown.

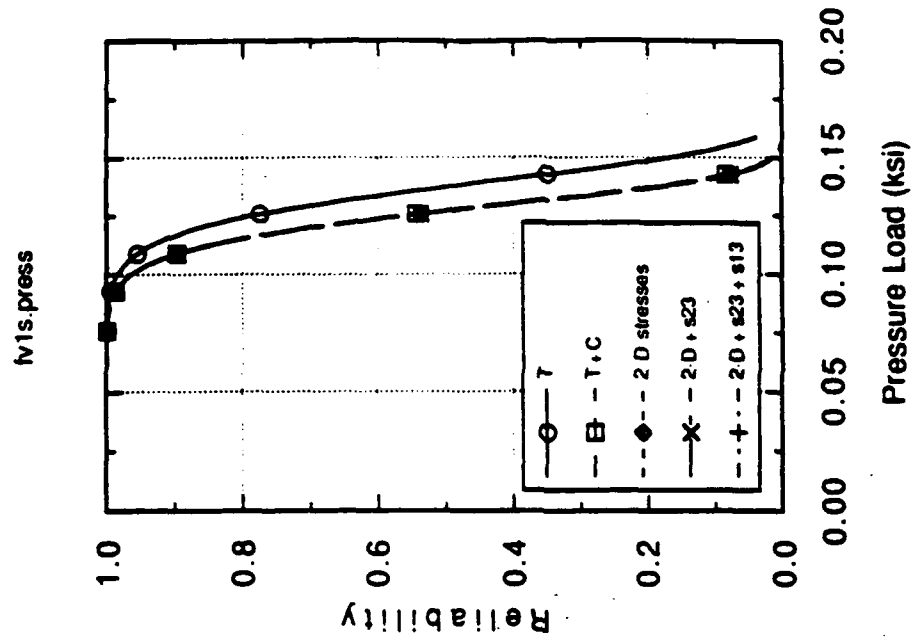


Figure 48
 Reliability of a carbon-carbon square plate with a hole under transverse loading as a function of pressure

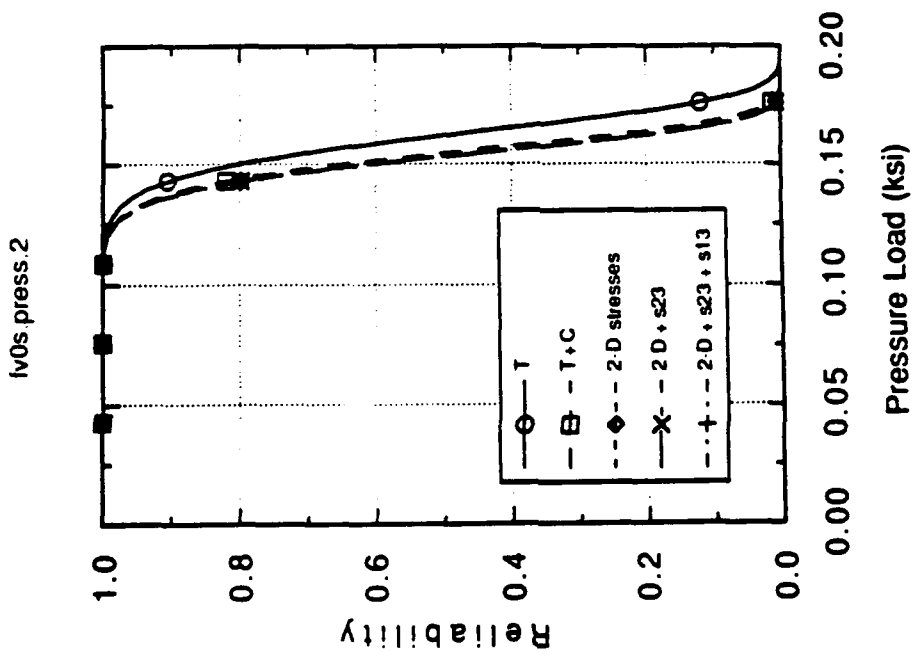


Figure 47
 Reliability of a carbon-carbon square plate without a hole under transverse loading as a function of pressure

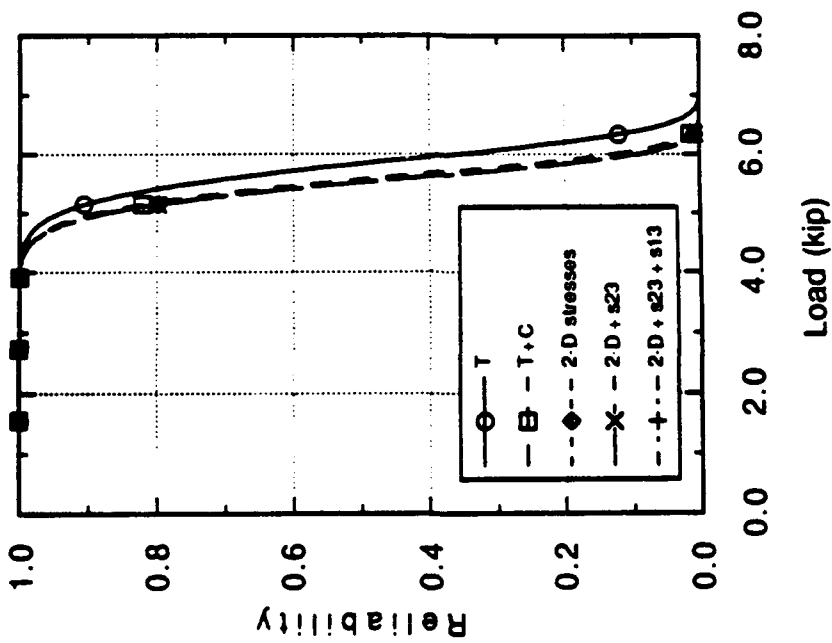


Figure 49

Reliability of a carbon-carbon square plate without a hole under transverse loading as a function of load

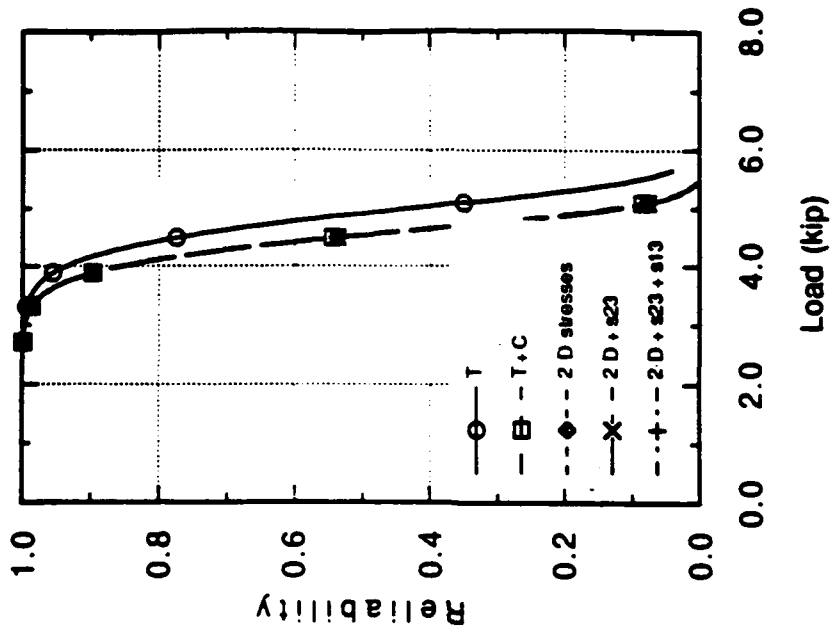


Figure 50

Reliability of a carbon-carbon square plate with a hole under transverse loading as a function of load

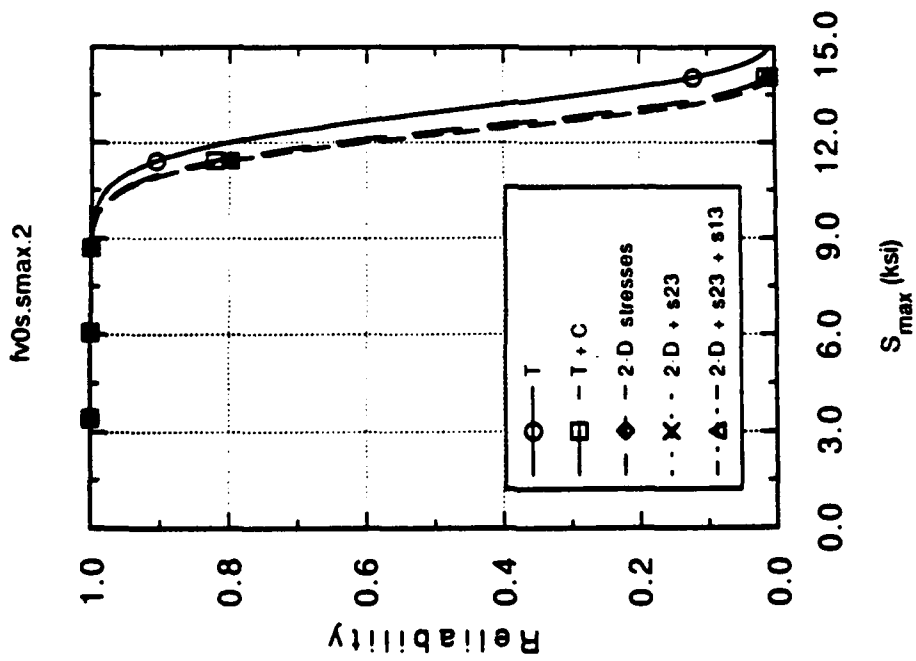


Figure 51

Reliability of a carbon-carbon square plate without a hole under transverse loading as a function of maximum stress

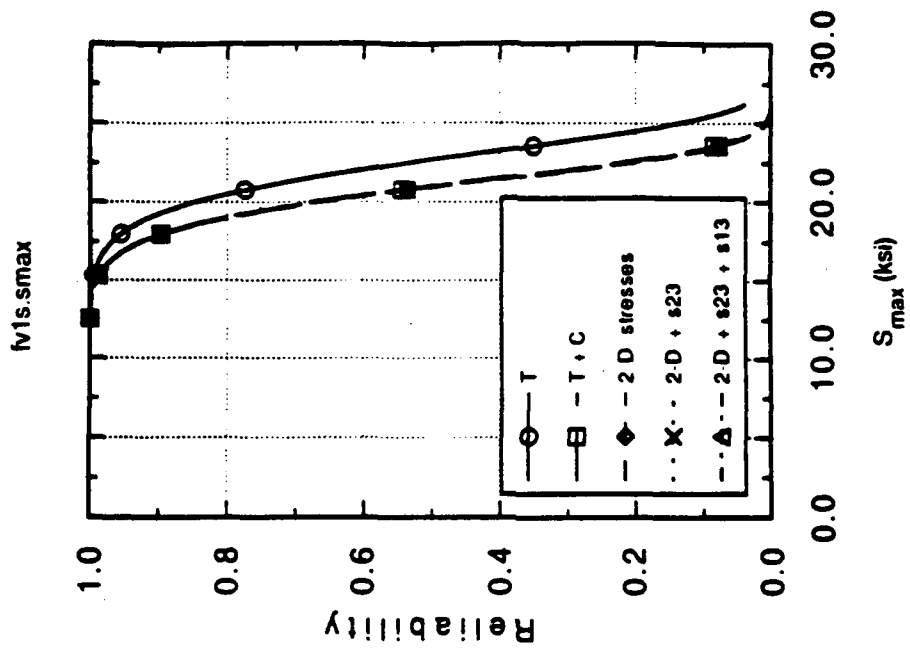


Figure 52

Reliability of a carbon-carbon square plate with a hole under transverse loading as a function of maximum stress

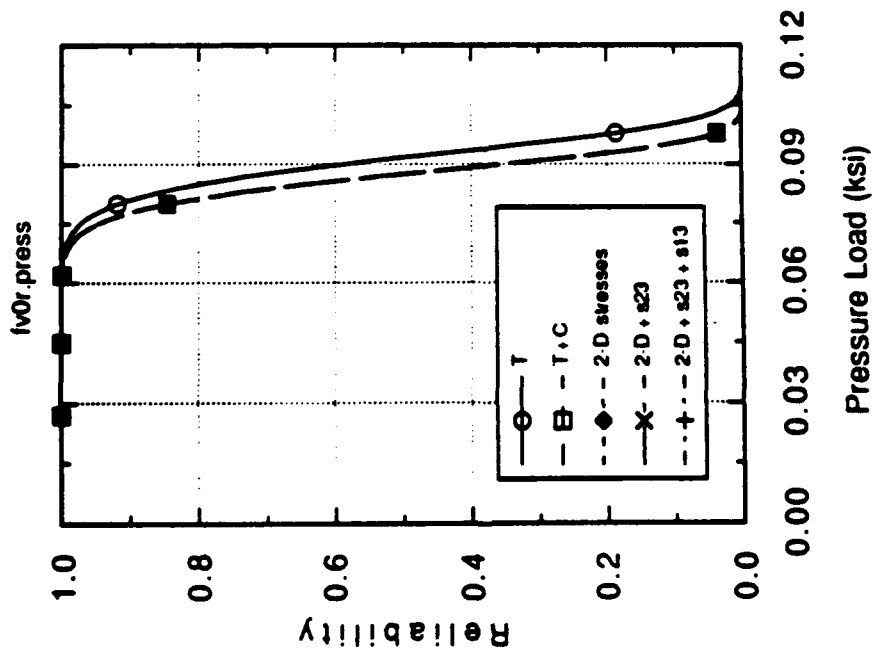


Figure 53

Reliability of a carbon-carbon rectangular plate without a hole under transverse loading as a function of pressure

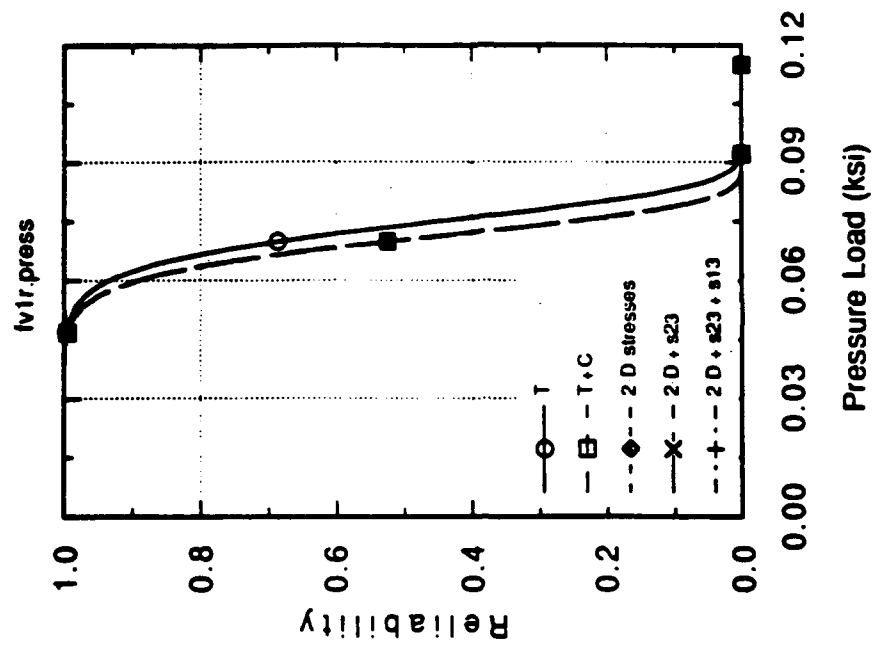


Figure 54

Reliability of a carbon-carbon rectangular plate with a hole under transverse loading as a function of pressure

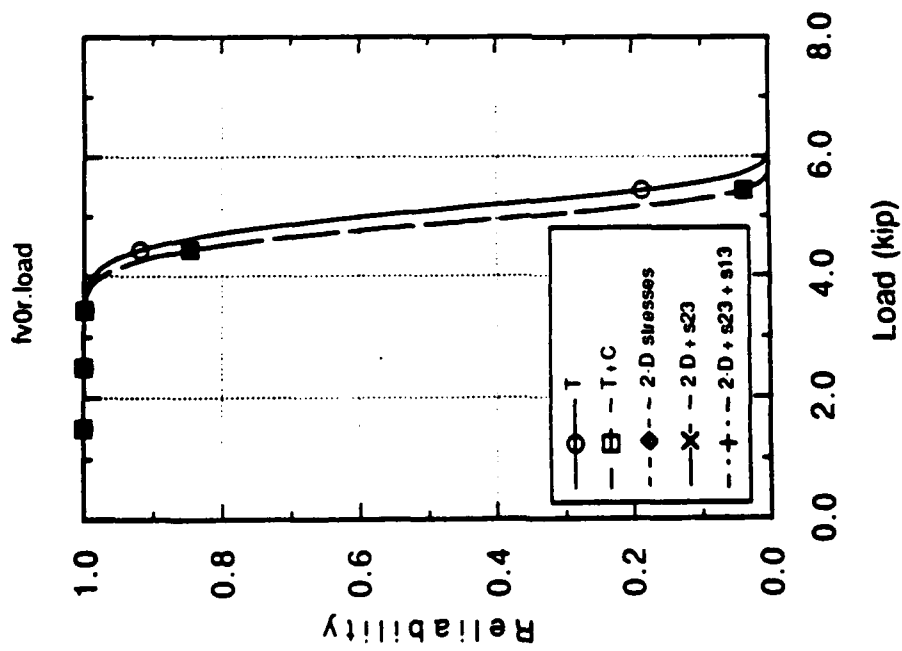


Figure 55

Reliability of a carbon-carbon rectangular plate without a hole under transverse loading as a function of load

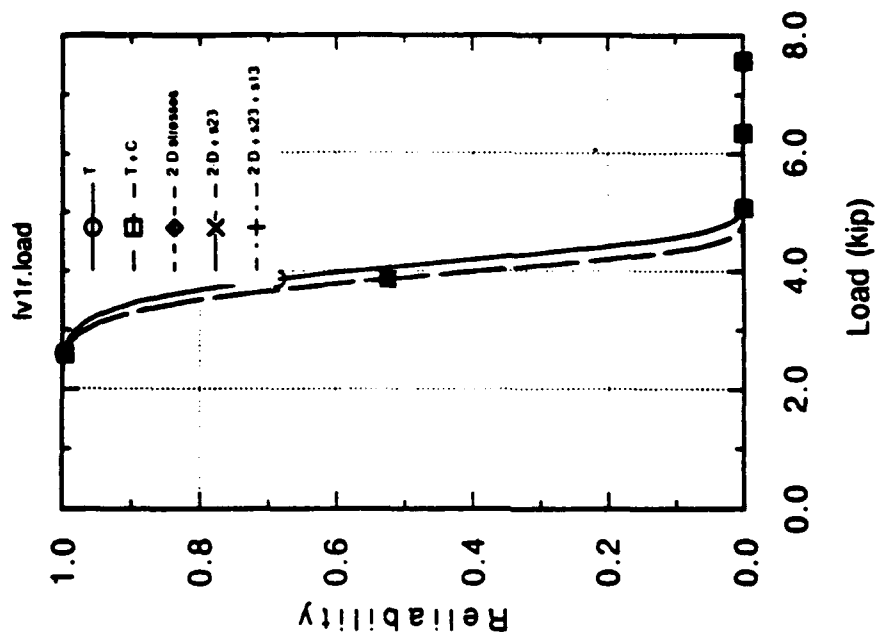


Figure 56

Reliability of a carbon-carbon rectangular plate with a hole under transverse loading as a function of load

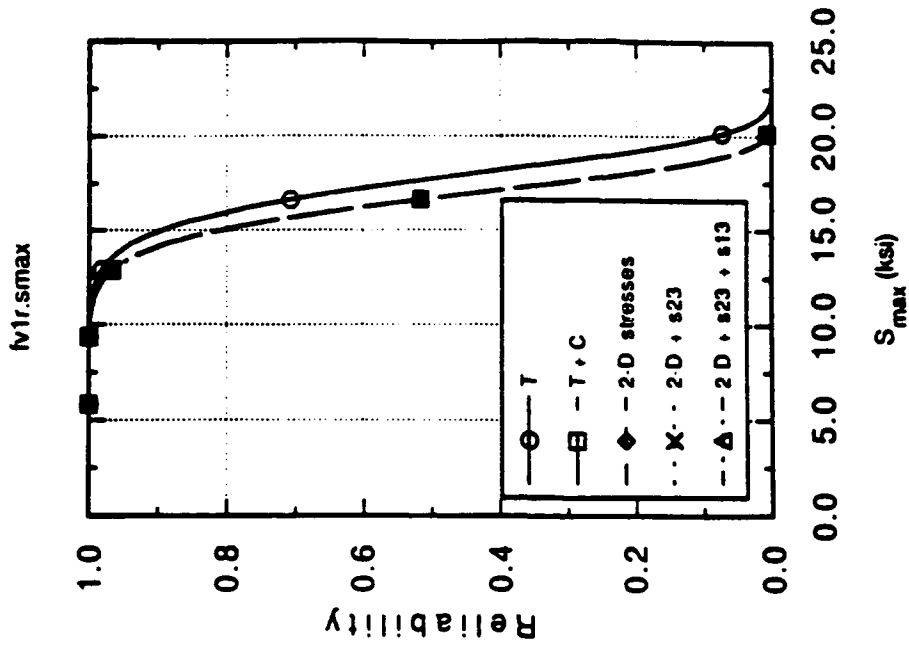


Figure 58

Reliability of a carbon-carbon rectangular plate with a hole under transverse loading as a function of maximum stress

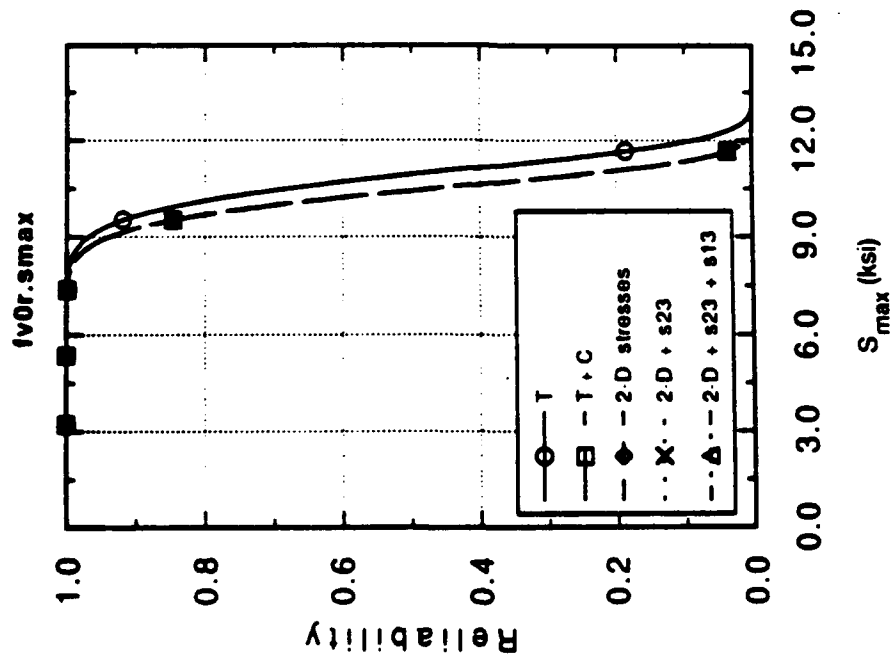


Figure 57

Reliability of a carbon-carbon rectangular plate without a hole under transverse loading as a function of maximum stress

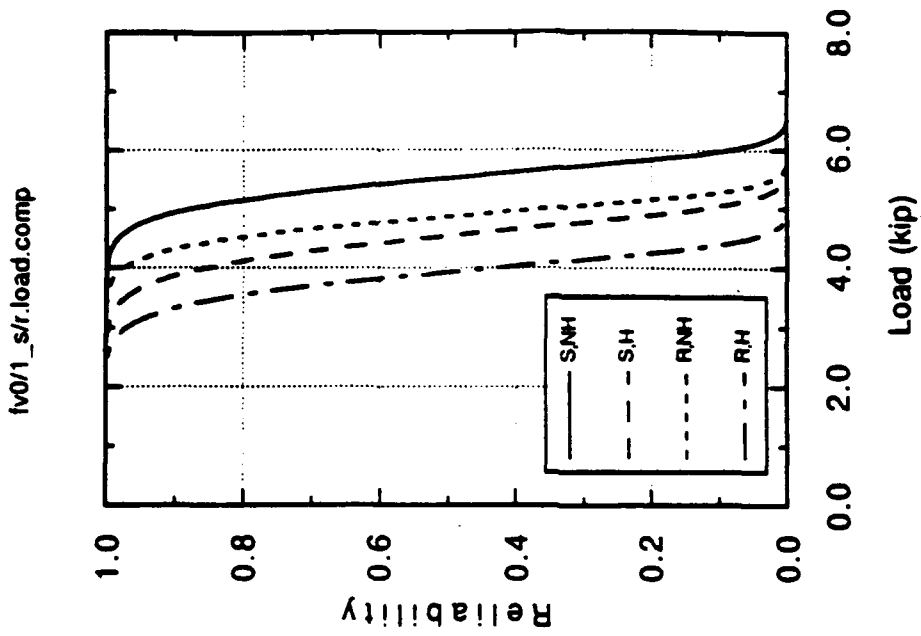


Figure 59

Comparison of reliabilities of carbon-carbon square and rectangular plates with and without a hole as a function of pressure

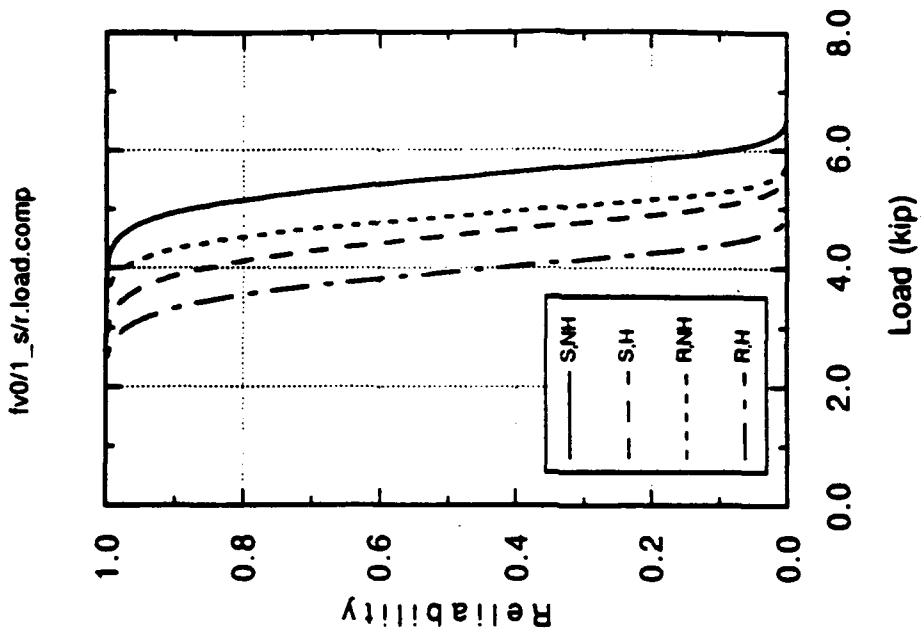


Figure 60

Comparison of reliabilities of carbon-carbon square and rectangular plates with and without a hole as a function of load

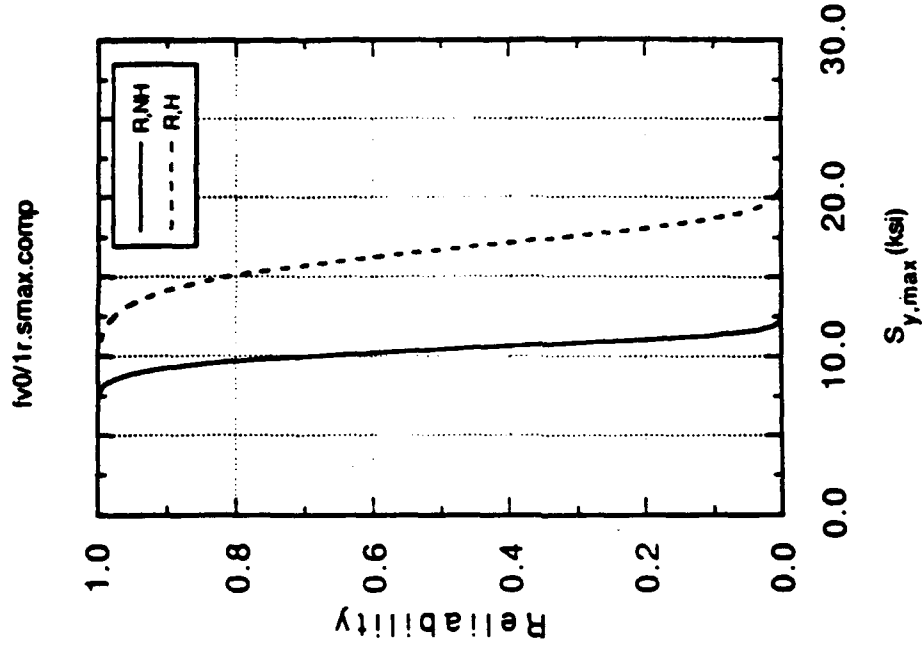


Figure 62
**Comparison of reliabilities of carbon-
 carbon rectangular plates with and
 without a hole as a function
 of maximum stress in y-direction**

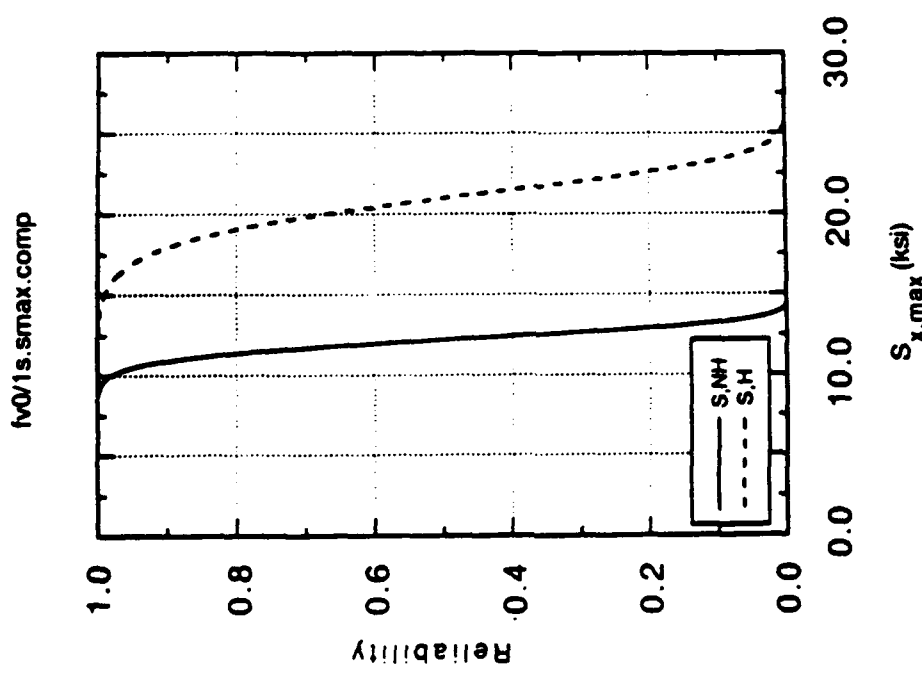
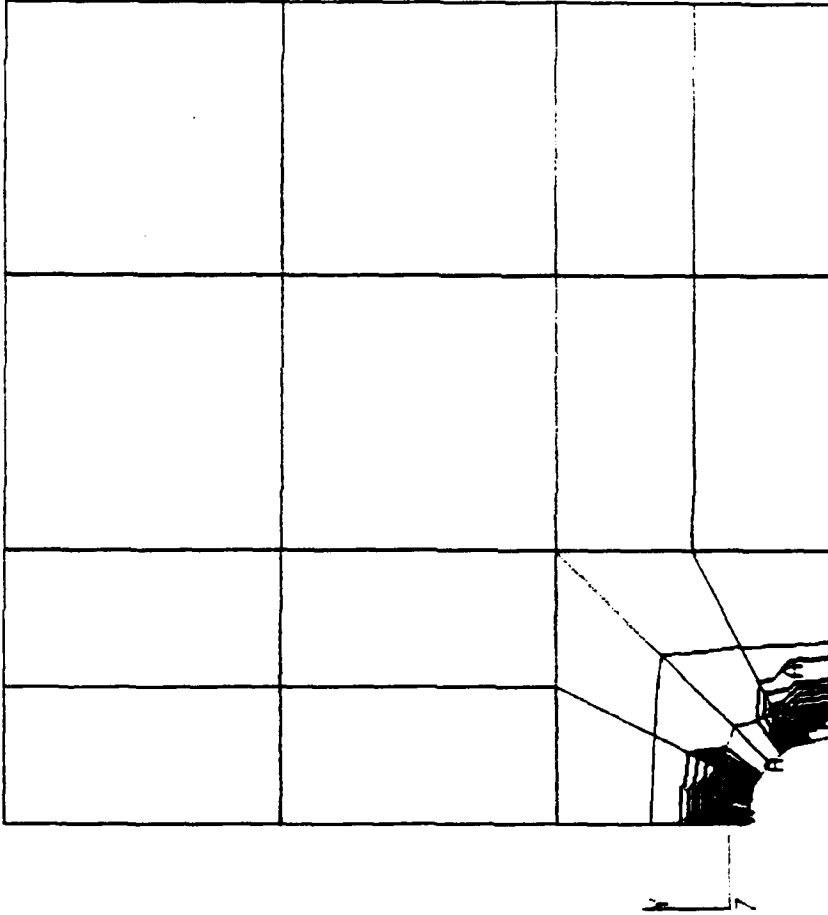


Figure 61
**Comparison of reliabilities of carbon-
 carbon square plates with and
 without a hole as a function
 of maximum stress in x-direction**

Reliability



.999 = 0
 .998 = 0
 .997 = 0
 .996 = 0
 .995 = 1
 .994 = 1
 .993 = 5
 .992 = 0
 .991 = 1
 .989 = 1
 .988 = 5
 .987 = 1
 .986 = M
 .985 = N
 .984 = 0

Figure 63

Reliability Contour at Top Matrix Layer of a Carbon-Carbon Square Plate with a Hole due to 3-D Stresses at 100 psi Uniform Transverse Loading

Reliability

- .978= A
- .935= B
- .891= C
- .848= D
- .804= E
- .761= F
- .717= G
- .674= H
- .630= I
- .587= J
- .544= K
- .500= L
- .457= M
- .413= N
- .370= O

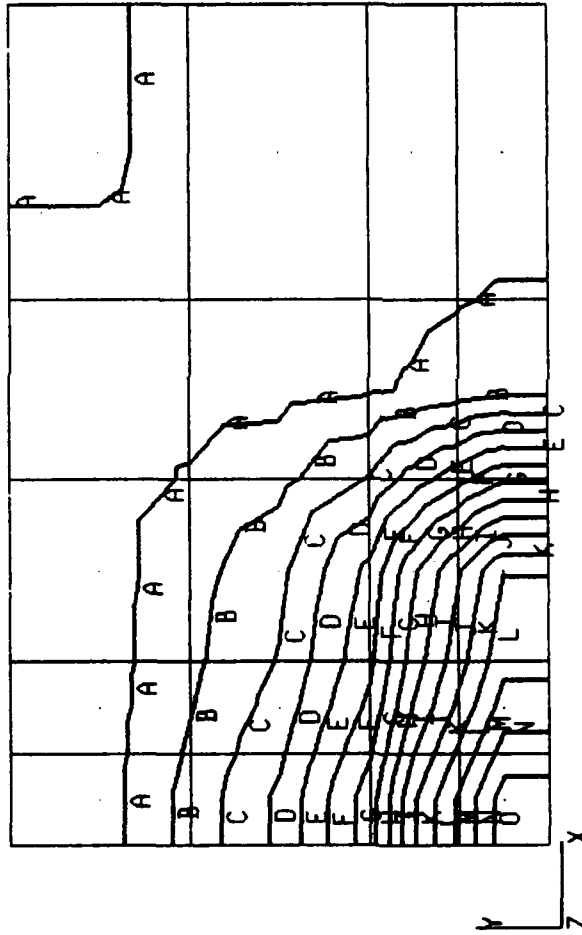


Figure 64

Reliability Contour at Bottom Matrix Layer of a Carbon-Carbon Rectangular Plate without a Hole due to 3-D Stresses at 100 psi Uniform Transverse Loading

Reliability

- .999= A
- .998= B
- .997= C
- .996= D
- .994= E
- .993= F
- .992= G
- .990= H
- .989= I
- .988= J
- .987= K
- .985= L
- .984= M
- .983= N
- .982= O

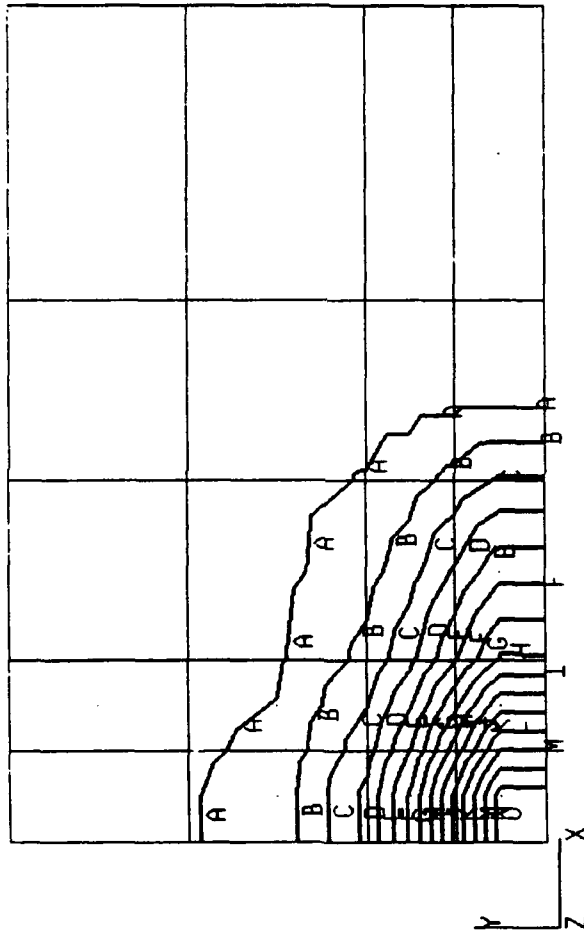


Figure 65

Reliability Contour at Bottom Fiber Layer of a Carbon-Carbon Rectangular Plate without a Hole due to 3-D Stresses at 100 psi Uniform Transverse Loading

Reliability

- .967= A .
- .900= B
- .833= C
- .767= D
- .700= E
- .633= F
- .567= G
- .500= H
- .434= I
- .367= J
- .300= K
- .234= L
- .167= M
- .100= N
- .0338= O

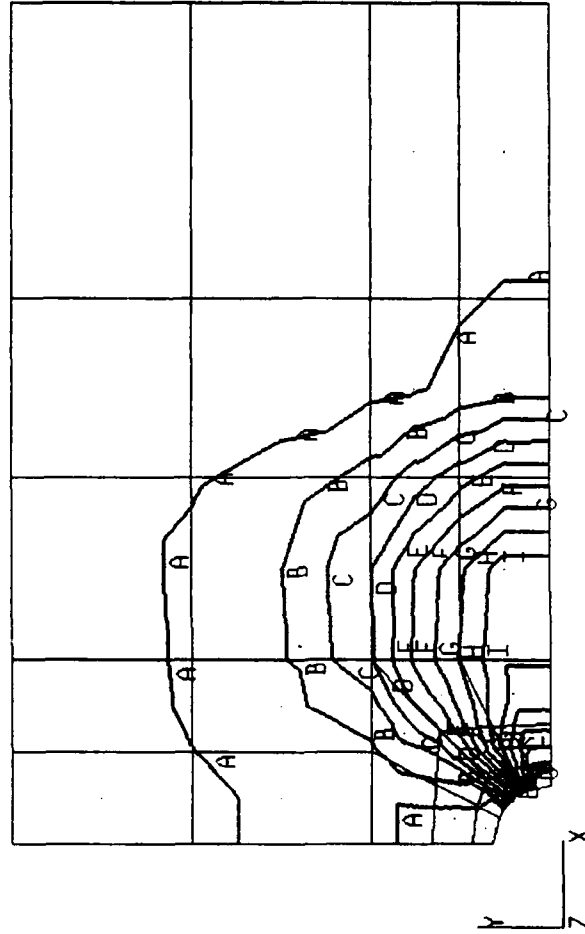


Figure 66

Reliability Contour at Bottom Matrix Layer of a Carbon-Carbon Rectangular Plate with a Hole due to 3-D Stresses at 100 psi Uniform Transverse Loading

Reliability

- .978= A
- .933= B
- .889= C
- .844= D
- .799= E
- .755= F
- .710= G
- .666= H
- .621= I
- .576= J
- .532= K
- .487= L
- .443= M
- .398= N
- .353= O

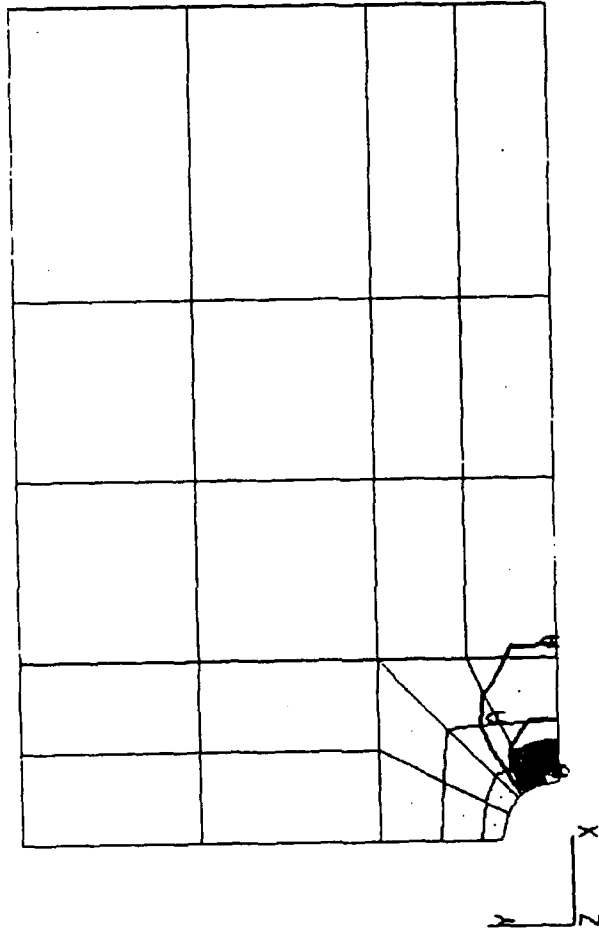


Figure 67

Reliability Contour at Bottom Fiber Layer of a Carbon-Carbon Rectangular Plate with a Hole due to 3-D Stresses at 100 psi Uniform Transverse Loading

FAILURE ANALYSIS

The reliability analysis does provide probability of failure on a certain layer of a composite structure, at some elements on a layer, but does not provide the mode of failure, the failure load or the location of failure, unless a probability level is pre-assigned. This information on the failure of composite structures is very important in design considerations. It is therefore necessary to supplement the reliability analysis with failure analysis.

Modeling of Failure in a Laminated Composite Plate

Although there are numerous failure criteria in the literature for a uni-directionally reinforced lamina, none are universally agreed upon and different criteria predict greatly different results [Soni, 1983]. Most of the criteria in the literature are of tensor polynomial type. The major shortcoming of the polynomial-type failure criteria is, however, that even though they can predict the initiation of failure, they do not say anything about the failure modes, failure locations, and so on. These are very important in the design and analysis of composite structures. Moreover, it is not evident that all of the distinct failure modes can be represented by a single failure criterion [Hashin, 1980].

There are various different failure modes that occur in the fiber, matrix and fiber-matrix interface as indicated by experimental observations [Pipes and Cole, 1973; Kim, 1981]. The various different failure modes may have their own failure criteria and further, these criteria may be of different form for tensile and compressive stresses. Failure criteria based on this notion have been proposed by Hashin [1980] and other authors [Lee, 1981; Brewer and Lagace, 1988; Hwang and Sun, 1989]. In these, the general three-dimensional stresses are considered, and each of the failure modes is modeled separately by a quadratic tensor polynomial containing the appropriate stress components.

Review of Failure Criteria

In this work, various failure criteria are grouped into two categories, namely, Category I, failure criteria that do not give information about the failure modes and Category II, those that do. Therefore, Tsai-Wu's and Hoffman's criteria belong to Category I, and maximum stress failure criteria, Hashin's criteria, Lee's criteria, Brewer and Lagace's criterion, and so on, belong to Category II. In the review that follows, the authors' symbols and nomenclatures are used, in general.

Category I Failure Criteria

Tsai-Wu's Failure Criterion

The most general failure criterion for composite materials is the quadratic tensor polynomial criterion of Tsai-Wu [1971]

$$F_i \sigma_i + F_{ij} \sigma_i \sigma_j = 1, \quad i, j = 1, 2, \dots, 6 \text{ (summation convention applies)} \quad (46)$$

Here, σ_i are the stress tensor components in the material coordinate system ($\sigma_1 = \sigma_{11}$, $\sigma_2 = \sigma_{22}$, $\sigma_3 = \sigma_{33}$, $\sigma_4 = \tau_{23}$, $\sigma_5 = \tau_{31}$, $\sigma_6 = \tau_{12}$) and F_i and F_{ij} are the components of the strength

tensors of the second and fourth order, respectively. All the failure criteria examined here are the degenerate cases of this tensor polynomial criterion. The Tsai-Wu failure criterion can be written in a long-hand form as

$$F_1 \sigma_1 + F_2 \sigma_2 + F_3 \sigma_3 + F_{11} \sigma_1^2 + F_{22} \sigma_2^2 + F_{33} \sigma_3^2 + F_{44} \sigma_4^2 + F_{55} \sigma_5^2 + F_{66} \sigma_6^2 + 2F_{12} \sigma_1 \sigma_2 + 2F_{13} \sigma_1 \sigma_3 + 2F_{23} \sigma_2 \sigma_3 = 1 \quad (47)$$

where

$$\begin{aligned} F_1 &= \frac{1}{X_T} - \frac{1}{X_C} & F_2 &= \frac{1}{Y_T} - \frac{1}{Y_C} & F_3 &= \frac{1}{Z_T} - \frac{1}{Z_C} \\ F_{11} &= \frac{1}{X_T X_C} & F_{22} &= \frac{1}{Y_T Y_C} & F_{33} &= \frac{1}{Z_T Z_C} \\ F_{44} &= \frac{1}{S_{23}^2} & F_{55} &= \frac{1}{S_{13}^2} & F_{66} &= \frac{1}{S_{12}^2} \\ F_{12} &= -\frac{1}{2} \frac{1}{\sqrt{X_T X_C Y_T Y_C}} & F_{13} &= -\frac{1}{2} \frac{1}{\sqrt{X_T X_C Z_T Z_C}} & F_{23} &= -\frac{1}{2} \frac{1}{\sqrt{Y_T Y_C Z_T Z_C}} \end{aligned} \quad (48)$$

where X_T, Y_T and Z_T are the uniaxial tensile strengths in the 1-, 2- and 3-directions, X_C, Y_C and Z_C are the uniaxial compressive strengths in the 1-, 2- and 3-directions, respectively and S_{23}, S_{13} , and S_{12} are the shearing strengths in the 23-, 13-, and 12-planes, respectively.

Hoffman's Failure Criterion

Hoffman's failure criterion [1967] has the same form as Tsai-Wu's. The coefficients $F_1, F_2, F_3, F_{11}, F_{22}, F_{33}, F_{44}, F_{55}, F_{66}$ are also the same as those for the Tsai-Wu failure criterion while

$$\begin{aligned} F_{12} &= -\frac{1}{2} \left(\frac{1}{X_T X_C} + \frac{1}{Y_T Y_C} - \frac{1}{Z_T Z_C} \right) \\ F_{13} &= -\frac{1}{2} \left(\frac{1}{X_T X_C} + \frac{1}{Z_T Z_C} - \frac{1}{Y_T Y_C} \right) \\ F_{23} &= -\frac{1}{2} \left(\frac{1}{Y_T Y_C} + \frac{1}{Z_T Z_C} - \frac{1}{X_T X_C} \right) \end{aligned} \quad (49)$$

Category II Failure Criteria

Maximum Stress Failure Criteria

In the maximum stress failure criteria the failure is said to occur if the stresses in the material coordinate system are larger than the respective strengths, that is, for tensile stresses,

$$\begin{aligned}
\sigma_1 &> X_T \\
\sigma_2 &> Y_T \\
\sigma_3 &> Z_T \\
|\tau_{12}| &> S_{12} \\
|\tau_{23}| &> S_{23} \\
|\tau_{13}| &> S_{13}
\end{aligned} \tag{50}$$

where X_T, Y_T and Z_T are the uni-axial tensile strengths in the 1-, 2- and 3-directions, respectively, and S_{23}, S_{13} , and S_{12} are the shearing strengths in the 23-, 13-, and 12-planes, respectively. When the stresses σ_1, σ_2 , and σ_3 are negative, they should be compared with corresponding compressive strengths (X_C, Y_C, Z_C). If any one of the foregoing inequalities is satisfied, then it is assumed that the material has failed by the failure mechanism associated with the stress component. There is no interaction between modes of failure in these criteria.

Hashin's Failure Criteria

Hashin [1980] proposed the following three-dimensional failure criteria of unidirectional fiber composites:

i) Tensile Fiber Mode, $\sigma_{11} > 0$

$$\left(\frac{\sigma_{11}}{\sigma_A^+}\right)^2 + \frac{1}{\tau_A^2} (\tau_{12}^2 + \tau_{13}^2) = 1 \tag{51}$$

where σ_A^+ is the tensile failure strength in the fiber direction and τ_A is the axial failure shear, or

$$\sigma_{11} = \sigma_A^+ \tag{52}$$

ii) Compressive Fiber Mode, $\sigma_{11} < 0$

$$\sigma_{11} = -\sigma_A^- \tag{53}$$

where σ_A^- is an absolute value of compressive failure strength in the fiber direction.

iii) Tensile Matrix Mode, $\sigma_{22} + \sigma_{33} > 0$

$$\frac{1}{\sigma_T^{+2}} (\sigma_{22} + \sigma_{33})^2 + \frac{1}{\tau_T^2} (\tau_{23}^2 - \sigma_{22} \sigma_{33})^2 + \frac{1}{\tau_A^2} (\tau_{12}^2 + \tau_{13}^2) = 1 \tag{54}$$

where σ_T^+, σ_T^- are the tensile and compressive failure strength in the transverse fiber direction, and τ_T is the transverse failure shear.

iv) Compressive Matrix Mode, $\sigma_{22} + \sigma_{33} < 0$

$$\frac{1}{\sigma_T^-} \left\{ \left(\frac{\sigma_T^-}{2\tau_T} \right)^2 - 1 \right\} (\sigma_{22} + \sigma_{33}) + \frac{1}{4\tau_T^2} (\sigma_{22} + \sigma_{33})^2 + \frac{1}{\tau_T^2} (\tau_{23}^2 - \sigma_{22}\sigma_{33}) + \frac{1}{\tau_A^2} (\tau_{12}^2 + \tau_{13}^2) = 1 \quad (55)$$

Lee's Failure Criteria

Lee [1981] proposed two failure criteria for two failure modes, i.e., fiber mode and matrix mode as follows:

i) Fiber Failure;

$$\frac{1}{\tau_A^2} (\tau_{12}^2 + \tau_{13}^2) = 1 \quad (56)$$

where τ_A is the axial shear strength associated with 1-2 and 1-3 planes, or

$$\sigma_{11} = X_T \quad (57)$$

where X_T is the tensile failure strength in the fiber direction.

ii) Matrix Failure;

$$\frac{1}{\tau_T^2} (\tau_{12}^2 + \tau_{23}^2) = 1 \quad (58)$$

where τ_T is the transverse shear strength in the 2-3 plane, or

$$\sigma_{22} = Y_T \quad (59)$$

where Y_T is the tensile strength in the 2 - direction.

Brewer and Lagace's Failure Criterion for Delamination

Brewer and Lagace [1988] proposed the following failure criterion for delamination:

$$\left(\frac{\sigma_{xz}}{Z^{sx}} \right)^2 + \left(\frac{\sigma_{yz}}{Z^{sy}} \right)^2 + \left(\frac{\sigma_{zz}^t}{Z^t} \right)^2 + \left(\frac{\sigma_{zz}^c}{Z^c} \right)^2 = 1 \quad (60)$$

where Z^t , Z^c are tensile and compressive interlaminar normal strength, Z^{sx} and Z^{sy} are interlaminar shear strength for σ_{xz} and σ_{yz} , respectively. "The superscript 't' and 'c' on σ_{zz} indicate that tensile values of interlaminar normal stress should be compared to the tensile interlaminar normal strength and compressive values of interlaminar normal stress should be compared to the compressive interlaminar normal strength."

Development of Three-Dimensional Failure Criteria for a Bi-Directional Composite Lamina

Proposed Failure Criteria for an Orthotropic Composite Lamina

Starting from the general three-dimensional tensor polynomial failure criterion, it is proposed that the following three separate criteria be used for identifying the failure in bi-directional orthotropic composite laminae. These separate failure modes have different criteria for tensile and compressive stresses.

1) fiber failure mode in 1-direction

i) tensile failure:

Experimental observation indicates that tensile failures are perpendicular to the longitudinal (fiber) direction and there is no evidence of shearing. Hence, fiber breakage in warp (1) direction is assumed to occur due to tensile stress in the fiber direction when the following inequality is satisfied:

$$\left(\frac{1}{X_T} - \frac{1}{X_C}\right) \sigma_1 + \frac{\sigma_1^2}{X_T X_C} \geq 1 \quad (61)$$

where X_T and X_C are the uni-axial tensile and compressive strengths in the 1-direction, respectively.

ii) compression/shear combined failure:

Compressive specimens fail along diagonal surfaces indicating influence of shear stresses, therefore, fiber micro-buckling/rupture in the warp direction is assumed to occur due to compressive stress in the fiber direction and interlaminar shear stress τ_{31} when the following inequality is satisfied:

$$\left(\frac{1}{X_T} - \frac{1}{X_C}\right) \sigma_1 + \frac{\sigma_1^2}{X_T X_C} + \left(\frac{\tau_{31}}{S_{31}}\right)^2 \geq 1 \quad (62)$$

where S_{31} is the interlaminar shear strength in the 1-3 plane.

2) fiber failure mode in 2-direction

i) tensile failure:

fiber breakage in the fill (2) direction is assumed to occur when the following inequality is satisfied:

$$\left(\frac{1}{Y_T} - \frac{1}{Y_C}\right) \sigma_2 + \frac{\sigma_2^2}{Y_T Y_C} \geq 1 \quad (63)$$

where Y_T and Y_C are the uni-axial tensile and compressive strengths in the 2-direction, respectively.

ii) compression/shear combined failure:

fiber micro-buckling/rupture in the fill direction is assumed to occur as a result of compressive stress in the 2- direction and interlaminar shear stress in the 2-3 plane when the following inequality is satisfied:

$$\left(\frac{1}{Y_T} - \frac{1}{Y_C}\right) \sigma_2 + \frac{\sigma_2^2}{Y_T Y_C} + \left(\frac{\tau_{32}}{S_{32}}\right)^2 \geq 1 \quad (64)$$

where Y_T and Y_C are tensile and compressive strengths in the fill direction, and S_{32} is interlaminar shear strength in the 2-3 plane.

3) delamination failure mode:

i) interlaminar normal failure:

it is assumed that fiber-matrix interface debonding occurs by positive interlaminar normal stress, σ_3 , when the following inequality is satisfied:

$$\frac{\sigma_3}{Z_1} \left(1 + \frac{\sigma_3}{Z_1}\right) \geq 1 \quad (65)$$

where Z_1 is interlaminar normal strength.

ii) interlaminar planar failure:

it is assumed that delamination occurs by interlaminar shear stresses τ_{31} and τ_{32} when the following inequality is satisfied:

$$\left(\frac{\tau_{31}}{S_{31}}\right)^2 + \left(\frac{\tau_{32}}{S_{32}}\right)^2 + \frac{\tau_{31} \tau_{32}}{S_{31} S_{32}} \geq 1 \quad (66)$$

where S_{31} and S_{32} are interlaminar shear strengths in the 1-3 plane and 2-3 plane, respectively.

Failure Analysis

In order to supplement the reliability analysis, failure analysis is carried out by making use of the above failure criteria. This provides the failure load, its mode and location from the various failure criteria's viewpoint.

First-Ply-Failure Analysis of Carbon-Carbon Composite Plates

First-ply-failure (abbreviated FPF) analysis is performed on carbon-carbon composite plates under uniform transverse load. The failure criteria used are those introduced previously and the failure criteria proposed in this work. The proposed failure criteria for an orthotropic lamina are applied to the carbon-carbon composite plates with varying aspect ratios to compute the FPF load, its mode and location. The results are compared with failure loads obtained by reliability analysis 0.5 reliability level and also with the ultimate failure loads obtained by experiments in Fig. 68. In the figure, S denotes a square plate, R a rectangular plate, H a plate with a hole and N a plate without a hole. The plates considered are a square plate with a hole, rectangular plates with and without holes. The geometry and the dimensions are the same as those considered earlier. The aspect ratios, b/h , applied are 5, 12.4, 20, 50 and 100 and to keep the layout of each plate the same, the thickness of the fiber and matrix layers is kept constant so that the corresponding numbers of layers are 101, 41, 25, 11 and 5, respectively. All plates considered are simply supported and subjected to uniform transverse load. The simply supported boundary condition used in the experiments and in the stress analysis is explained in the section on plate bending tests.

The matrix and fiber layers are alternating from the top of each plate so that the matrix layers cover the plate on top and bottom. As only plates with an aspect ratio of 12.4 were tested [Part I], there is one experimental ultimate failure load datum for each plate. The failure load, its mode and location predicted by the proposed criteria are tabulated in Table 9 for a square plate with a hole, in Table 10 and Table 11 for a rectangular plate without a hole and with a hole, respectively. For the particular plates considered, the predicted FPF loads are 3.033, 5.605 and 2.828 (kips) for a square plate with a hole, for a rectangular plate without a hole and with a hole, respectively, while the experimental ultimate failure loads are 20.479, 19.98 and 19.974 (kips), respectively. The ratios of the experimental ultimate failure loads to the FPF loads predicted by the proposed failure criteria are 6.75, 3.565 and 7.063. It is reported [Hwang and Sun, 1989] that for a graphite-epoxy plate with a hole under in-plane loading, the ratio of experimental failure load to the FPF load is 6.6. The layup considered there is $[\pm\theta]_S$ where θ equals 0.

To compare predicted FPF loads further with experimental failure loads as a function of aspect ratio, relatively small (6.5" x 5") rectangular plates without a hole were chosen. In order to produce several aspect ratios, one thick plate was sliced into 3 thin pieces. The thickness of the plates thus machined are 0.1825 (in), 0.059 (in), and 0.0445 (in) and, therefore, the aspect ratios are 24.66, 76.27, and 101.12, respectively. The plates were simply supported on all 4 edges (for simple-support boundary condition used in the analysis, see Fig. 8) and a uniform transverse load was applied. The actual loaded area was 6" x 4.5". The FPF analysis was performed on the same rectangular plates with 6 different aspect ratios ranging from about 20 to 135. Again, matrix layers and fiber layers are alternating from the top of each plate and the plates considered have 21, 15, 11, 7, 5, and 3 layers. Their thicknesses are 0.247, 0.200, 0.128, 0.081, 0.057, and 0.033 (in), respectively, with corresponding aspect ratios: 18.20, 22.53, 35.05, 55.67, 78.86 and 135.20. The same 5 by 4 finite element mesh with 9 - node elements that was used for rectangular plates without a hole was adopted to compute stresses. Only a quarter plate was modeled in the analysis.

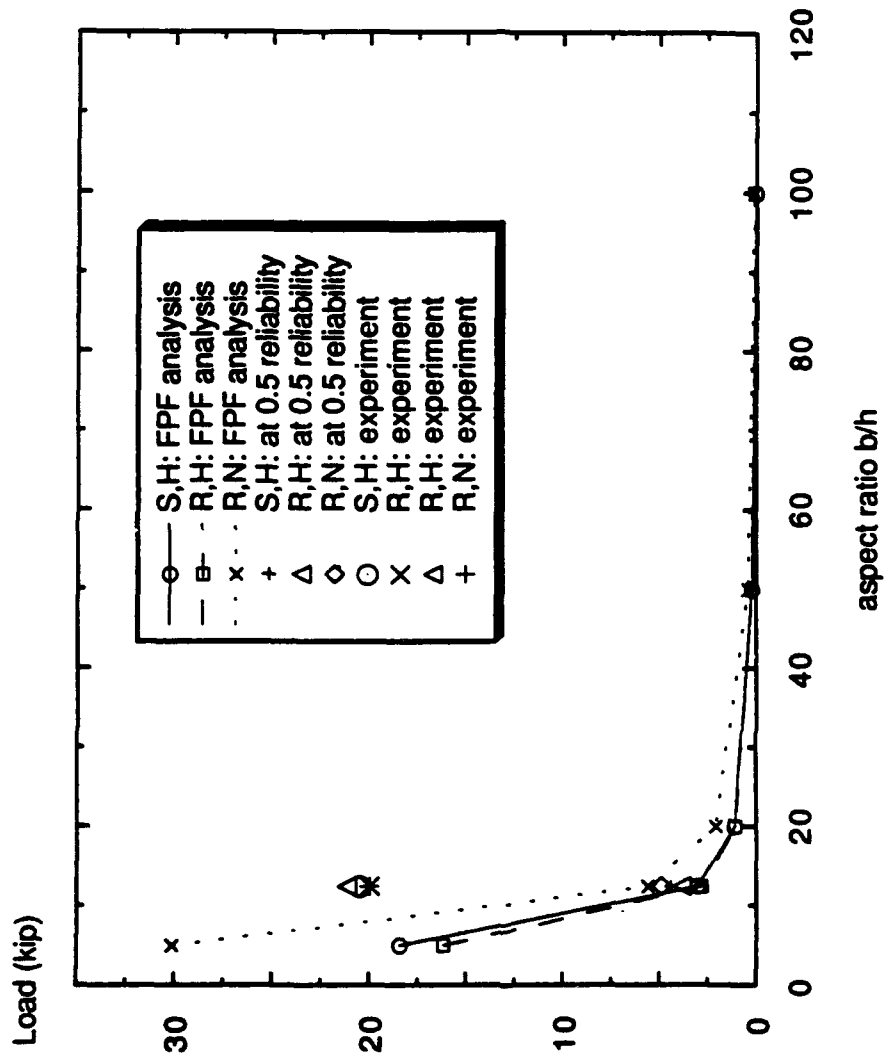


Figure 68

Comparison of FPF Loads Predicted by the Proposed Criteria and Failure Loads at 0.5 Reliability with Experimental Failure Loads for Carbon-Carbon Square and Rectangular Plates Under Uniform Transverse Load

Table 9. First-Ply-Failure Load Mode and Location of a Carbon-Carbon Square Plate with a Hole Under Uniform Transverse Load Predicted by the Proposed Failure Criteria

aspect ratio	failure load		failure mode	failure location		
	intensity (psi)	load (kip)		layer	element	Gauss point
5	516.5	18.428	compression/shear	2	1	1
12.4	85.00	3.033		2	1	1
20	32.05	1.144	combined mode in fiber	2	1	1
50	6.58	0.235		2	1	1
100	1.77	0.0632	in 1 - direction	2	1	1

Table 10. First-PLY-Failure Load Mode and Location of a Carbon-Carbon Rectangular Plate without a Hole Under Uniform Transverse Load Predicted by the Proposed Failure Criteria

aspect ratio	failure load		failure mode	failure location		
	intensity (psi)	load (kip)		layer	element	Gauss point
5	543.0	30.136	compression/shear in fiber in 2 - direction	2	16	2
12.4	101.0	5.605	tension in fiber in 2 - direction	40	1	1
20	38.00	2.109	tension in fiber in 2 - direction	24	1	1
50	7.860	0.436	tension in fiber in 2 - direction	10	1	1
100	2.136	0.119	tension in fiber in 2 - direction	4	1	1

Table 11. First-Ply-Failure Load Mode and Location of a Carbon-Carbon Rectangular Plate with a Hole Under Uniform Transverse Load Predicted by the Proposed Failure Criteria

aspect ratio	failure load		failure mode	failure location		
	intensity (psi)	load (kip)		layer	element	Gauss point
5	293.1	16.173		100	4	3
12.4	51.25	2.828	tension	40	4	3
20	19.82	1.094	in fiber	24	4	3
50	4.200	0.232		10	4	3
100	1.153	0.064	in 2 - direction	4	4	3

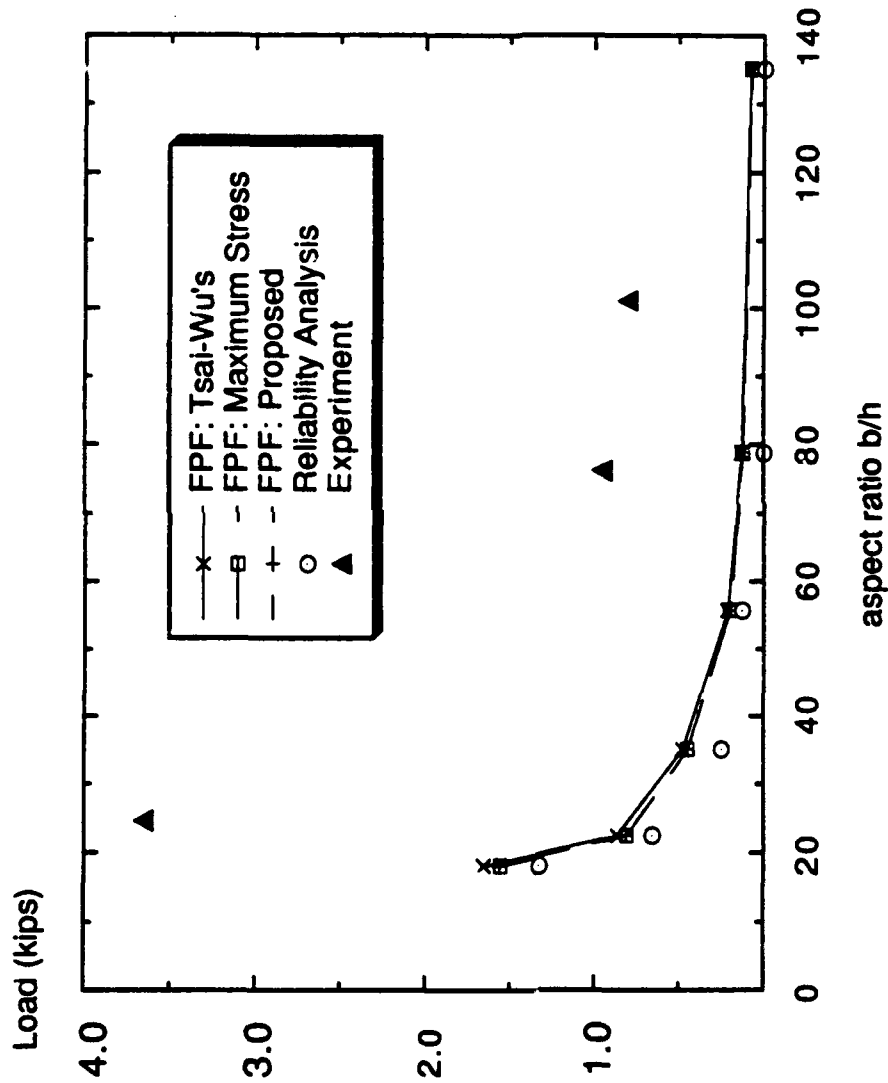


Figure 69

Comparison of FPF Loads Predicted by Various Criteria with Those Obtained by Reliability Analysis and Experiment for Carbon-Carbon Rectangular Plates Without a Hole Under Uniform Transverse Loading

The Tsai-Wu criterion, maximum stress criteria and the proposed criteria are chosen for comparison with experimental failure loads. The proposed criteria give nearly identical failure loads with maximum stress criteria whereas Tsai-Wu's criterion gives slightly higher failure loads. The comparison of failure loads produced by FPF analysis and by experiments is shown in Fig. 69. The 3 plates failed at 3.66 (kips), 0.95 (kip) and 0.81 (kip) and the predicted FPF loads on those plates are about 0.8 (kip), 0.14 (kip) and 0.11 (kip), respectively. The ratios of the experimental ultimate failure loads to the FPF loads predicted by the proposed criteria are 4.58 for a rectangular plate with aspect ratio 24.66, 6.79 with aspect ratio 76.27 and 7.36 with aspect ratio 101.12, respectively.

Reliability analysis was also performed on those carbon-carbon rectangular plates with various aspect ratios and the failure loads are plotted in the same figure. It is seen in the Fig. 69 that the FPF loads are very close to those predicted by reliability analysis.

When the FPF occurs, the ply is considered to have effectively no stiffness (very low value for computation purposes) and the load is re-distributed among other load carrying members so that the plate can sustain more loads. As the experimental failure loads are obtained after all major load carrying mechanisms (i.e. fiber layers) break, they are naturally much higher than the FPF loads. To properly address this problem, a progressive failure analysis would have to be performed. Such an analysis is beyond the scope of the present work.

Comparison of the Proposed Criteria with Other Criteria

The proposed failure criteria are compared with other criteria. Even though the proposed failure criteria are for bi-directional orthotropic lamina, they are applied to uni-directional graphite-epoxy lamina to compare with the existing criteria. In such a case, the fiber failure in the 2-direction is considered as matrix failure in 2-direction, and all other failure modes remain unchanged.

To compare the FPF loads (pressures) predicted by the proposed criteria with those predicted by various other failure criteria, typical laminated composite plates made of graphite-epoxy under transverse loading are considered. The material properties of graphite-epoxy plates used are as follows [Reddy, 1984]:

$E_1 = 25.0$ msi, $E_2 = 1.0$ msi, $\nu_{12} = 0.25$, $G_{12} = G_{13} = 0.5$ msi, $G_{23} = 0.2$ msi
 $X_T = 210$, $X_C = 250$, $Y_T = 7$, $Y_C = 25$, $S_{12} = S_{13} = 9$, $S_{23} = 4$ (ksi)
 thickness of each layer = 0.005 inch

The laminates considered have a stacking sequence of $[0/90]_s$. The length of the square plates, a , is 2 inches and the aspect ratios are 5, 10, 20, 50 and 100. The laminates are simply supported and subjected to a sinusoidally distributed transverse load of the following form:

$$p = p_0 \sin \frac{\pi x}{a} \sin \frac{\pi y}{a} \quad (67)$$

where p_0 is the maximum pressure and a is the dimension of the plates.

As the experimental data are not available, the first-ply-failure pressures are compared with each other. The FPF pressures predicted by various failure criteria are plotted in Fig. 70. The FPF pressures are normalized as

$$\overline{\text{FPF}} = \frac{\text{FPF} \times s^2}{100} \quad (68)$$

where \overline{FPF} is the normalized pressure and s is the aspect ratio, a/h , and are plotted in Fig. 71. For plates with aspect ratios equal to 10 and 100, the FPF pressures, modes and the locations in terms of layer number, element number and Gauss point number are tabulated in Table12 and Table13, respectively.

For a moderately thick plate (i.e. aspect ratio equal to 10), different failure modes are predicted even though the failure loads are similar. For instance, the failure mode based on Hashin's criteria is matrix cracking and that based on Lee's is fiber breakage, while maximum stress criteria, Brewer and Lagace's criterion and the proposed criteria predict failure due to interlaminar shear stresses.

For a very thin plate with aspect ratio equal to 100, FPF loads are almost the same except for Lee's criteria and the failure is due to matrix cracking.

Brewer and Lagace's criterion is a delamination criterion and as can be seen in Fig. 70 and Fig. 72, it is suitable for the moderately thick to thick plate whose aspect ratio is less than 10 suggesting that delamination is also an important failure mechanism to moderately thick plates.

Lee's criteria gave the most conservative failure loads for plates with aspect ratios greater than 10. The proposed criteria showed good agreement with Hashin's criteria and maximum stress criteria.

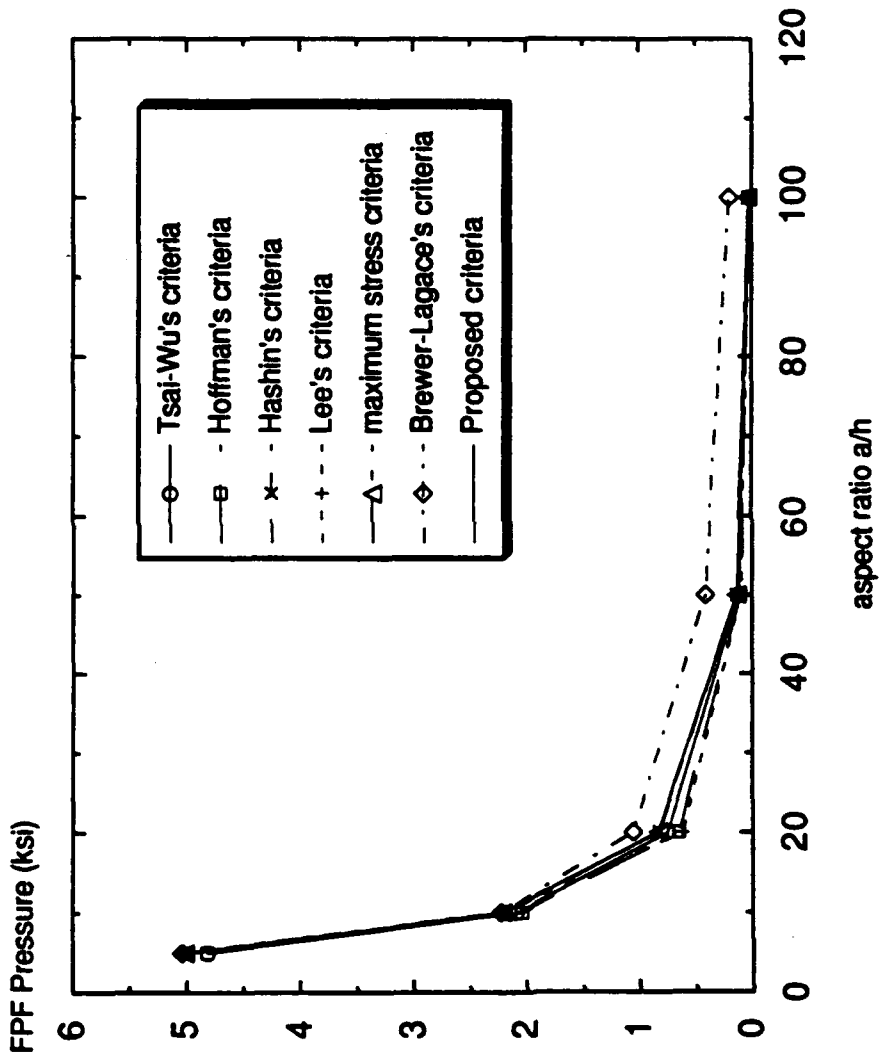


Figure 70
 Comparison of FPF Pressures Predicted by Various Failure Criteria for a Graphite-Epoxy Square Plate Under Sinusoidal Transverse Loading

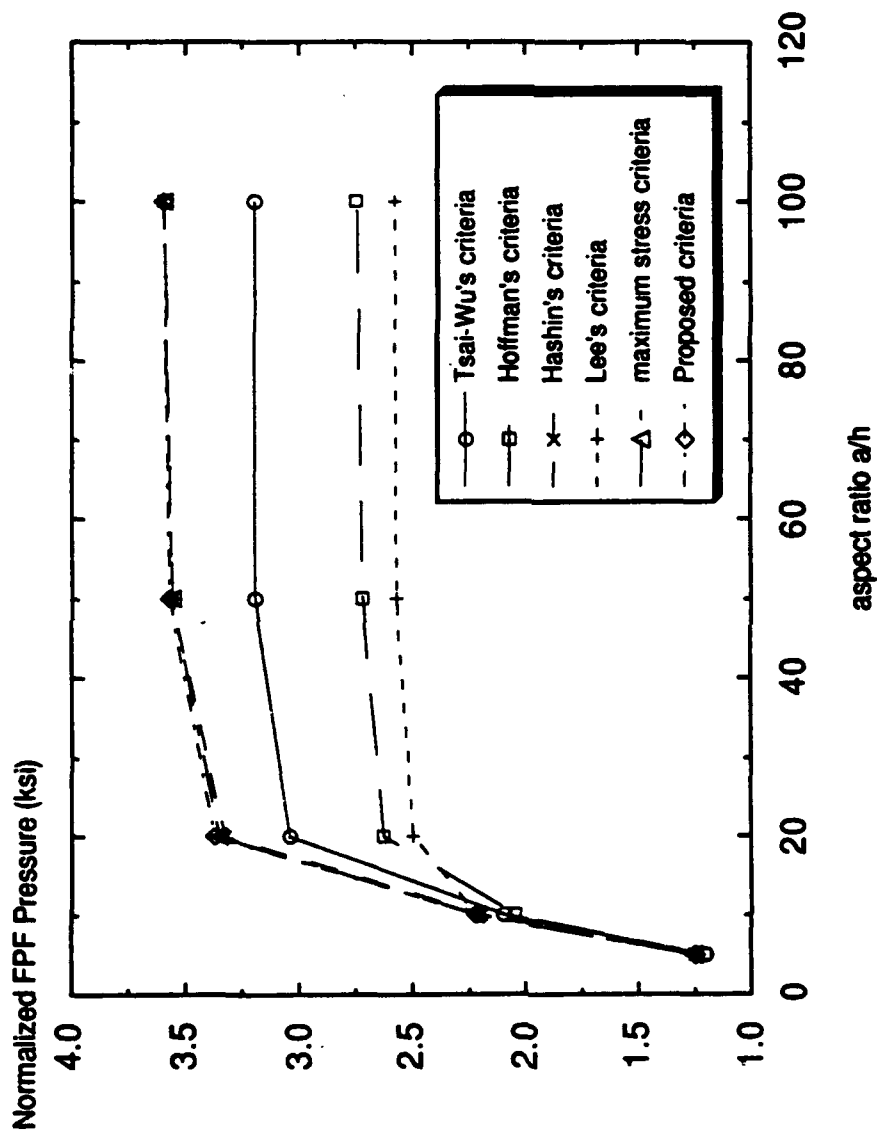


Figure 71

Comparison of Normalized FPF Pressures Predicted by Various Failure Criteria for Graphite-Epoxy Square Plate Under Sinusoidal Transverse Loading

Table 12. Comparison of Normalized First-Ply-Failure Pressure, Mode and Location Predicted by the Proposed Failure Criteria with those of Criteria for a [0/90]s Graphite -Epoxy Square Plate with Aspect Ratio 10 Under Sinusoidal Load

	normalized failure pressure (ksi)	mode	location		
			layer	element	Gauss point
Tsai - Wu	2.10	---	4	2	1
Hoffman	2.05	---	4	2	1
Hashin	2.20	matrix cracking	4	2	3
Lee	2.222	fiber breakage	1	2	3
Max. Stress	2.226	interl. shear σ_{13}	1	2	3
Brewer - Lagace (delamination)	2.230	delamination	1st interface from top	2	3
Proposed	2.222	delamination	1st interface from top	2	3

Table 13. Comparison of Normalized First-Ply-Failure Pressure, Mode and Location Predicted by the Proposed Failure Criteria with those of Criteria for a [0/90]s Graphite -Epoxy Square Plate with Aspect Ratio 100 Under Sinusoidal Load

	normalized failure pressure (ksi)	mode	location		
			layer	element	Gauss point
Tsai - Wu	3.21	---	4	1	1
Hoffman	2.75	---	4	1	1
Hashin	3.60	matrix cracking	4	1	1
Lee	2.58	matrix cracking	1	4	4
Max. Stress	3.60	matrix cracking	4	1	1
Brewer - Lagace (delamination)	20.9	delamination	1st interface from top	2	3
Proposed	3.60	matrix cracking	4	1	1

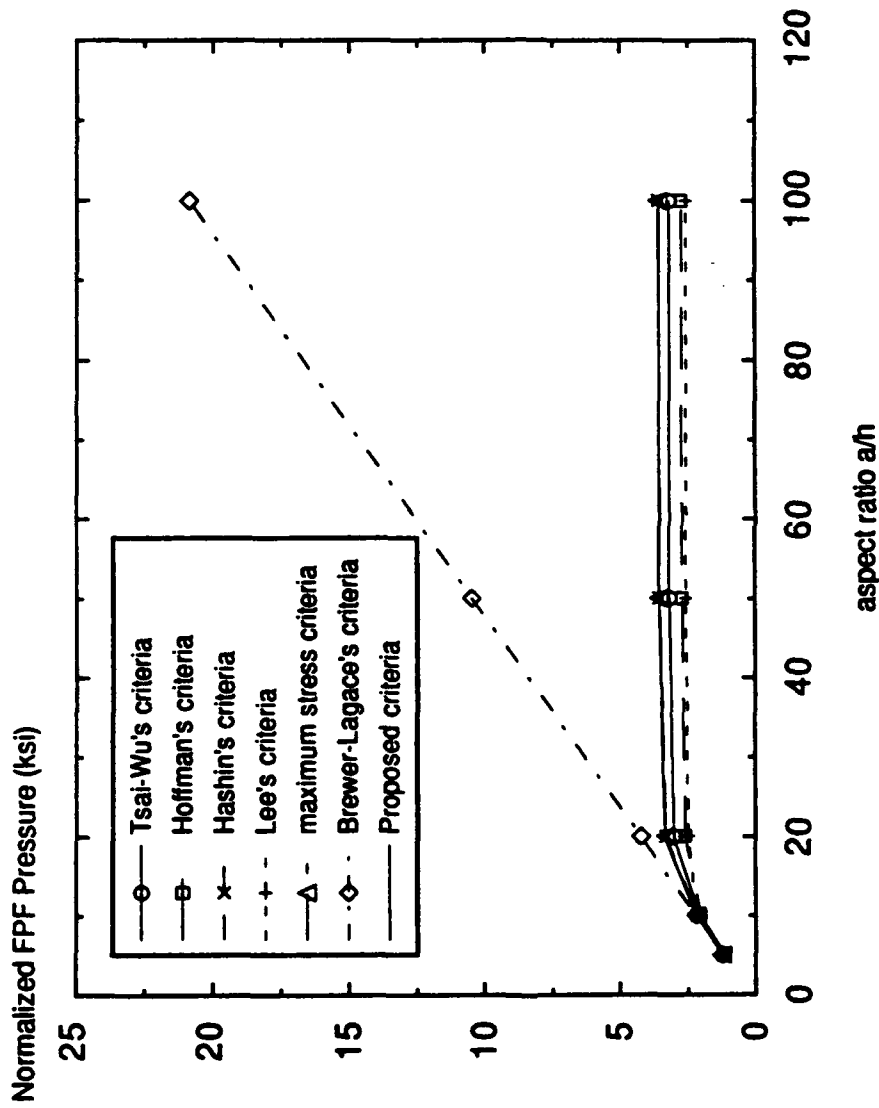


Figure 72

Comparison of Normalized FPF Pressures Predicted by Various Failure Criteria Including Brewer-Lagace's Delamination Criteria for Graphite-Epoxy Square Plate Under Sinusoidal Transverse Loading

Comparison of Reliability Analysis with First-ply-failure Analysis and Experiments

As the reliability analysis based on the *weakest link* theory assumes that the whole component fails if one element fails, it is also a first-ply-failure type analysis. It is for this reason that the reliability analysis is compared with FPF analysis in this section. As the median value is close to the mean value, failure loads at 0.5 reliability level are compared with those obtained by FPF analysis, which uses mean properties.

Composite Beams

In an attempt to relate the probabilistic failure analysis (i.e. reliability analysis) to the FPF analysis, the failure loads for carbon-carbon composite beams predicted by reliability analysis at 0.5 reliability level are compared with those predicted by FPF analysis which employs the Brewer-Lagace's delamination criteria and the proposed criteria. Comparison is also made with experimental ultimate failure loads. The comparison is presented in Table 14.

For an unnotched composite beam, the failure load at 0.5 reliability level is about 70 % of the experimental value (0.506 kip from experiment and 0.345 from analysis) while for a notched composite beam, it is about 60 % (0.289 kip from experiment and 0.167 from analysis) when only tensile stresses are considered. However, the ratio of unnotched to notched failure loads obtained by reliability analysis (2.066) is close to the experimental ratio of 1.752. When all stress components including interlaminar stresses are considered, the failure loads predicted by reliability analysis are much more conservative. The ratios of experimental failure load to that predicted by reliability analysis at 0.5 reliability level are about 4 for an unnotched composite beam (0.506 kip from experiment and 0.122 from analysis) and 2.5 for a notched composite beam (0.289 kip from experiment and 0.117 from analysis).

Composite Plates

The failure loads for carbon-carbon composite plates under transverse load predicted by reliability analysis at 0.5 reliability level are compared with those predicted by FPF analysis which employs the proposed criteria. The comparison is made also with the experimental ultimate failure loads. The comparison is presented in Table 15.

The ratios of experimental failure load to that predicted by reliability analysis at 0.5 reliability level are about 4.6 for a square laminate with a hole (20.479 kip from experiment and 4.42 from analysis), 4.1 for a rectangular laminate without a hole (19.980 kip from experiment and 4.90 from analysis) and 5.2 for a rectangular laminate with a hole (19.974 kip from experiment and 3.85 from analysis).

It is also shown in Fig. 69 that the failure loads predicted by reliability analysis are very close to FPF loads.

Table 14. Comparison of Failure Loads Predicted by Reliability Analysis, FPF Analysis Based on the Proposed Criteria and Experiment for a Carbon-Carbon Composite Beam Under Four Point Bending

	Unnotched Beam		Notched Beam	
	Load (kip)	Delamination Location	Load (kip)	Delamination Location
Reliability Analysis* (at 0.5 reliability level)	0.122	---	0.117	---
First-ply-failure Analysis	0.063	A	0.062	B
Proposed	0.077	A	0.030	B

(Note: Reliability analysis when all stress components are considered.

First-ply-failure analysis is based on delamination criteria)

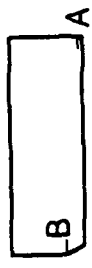


Table 15. Comparison of Failure Loads Predicted by Reliability Analysis, FPF Analysis Based on the Proposed Criteria and Experiment for Carbon-Carbon Composite Plate with Aspect Ratio 12.4 Under Uniform Transverse Load (Unit: Kips)

	Reliability Analysis (at 0.5 level)	FPF Analysis* (Proposed Criteria)	Experiment (ultimate failure loads)
square plate with a hole	4.42	3.033	20.479
rectangular plate without a hole	4.90	5.605	19.980
rectangular plate with a hole	3.85	2.828	19.974

(* All stress components are considered)

CLOSURE

Discussions

One of the main objectives of this work is to verify size effects present in a brittle material. To verify size effect experimentally, specimens with widely differing volumes would have to be tested. Such tests are, however, impractical both from a material cost point of view and due to the unavailability of large capacity test equipment. To avoid this difficulty and to simulate specimens of widely varying sizes, an approach was devised: Specimens with and without stress concentrations were tested. Specimens with stress raisers have only a "small" volume highly stressed while specimens without such concentrations have a "larger" volume stressed, thereby simulating specimens with small and large size, respectively. In this manner stressed volume ratios of the order of 1:1000 may be achieved in the laboratory. Extensive experiments have been performed on carbon-carbon composite beams and plates with and without stress concentrations and size effect was confirmed on small notched and unnotched beam specimens, which validates the approach. Reliability analysis based on Weibull's weakest link hypothesis has also been applied to composite structural components such as composite beams with and without notches and composite plates with and without a hole using the experimental data to validate the analysis.

The failure loads obtained from reliability analysis at 0.5 reliability level for notched and unnotched isotropic beams under 4-point bending agree very well with those obtained by experiments. This essentially proves the applicability of reliability analysis to brittle structural components. For an unnotched isotropic beam agreement with experimental data is better when tensile stresses alone are considered. On the other hand, for a notched isotropic beam, the agreement was excellent for both cases (i.e. when tensile stresses alone are considered and when both tensile and compressive stresses combined are considered). The ratios of notched to unnotched failure stresses range from 1.4 for the case when only tensile stresses are considered to 2.4 for the case when both tensile and compressive stresses are included. These numbers represent the degree of size effect present in the material and can be used for the calculation of experimental failure stresses.

For composite beams under 4-point bending, the agreement is not as good as that for the isotropic case. For an unnotched composite beam, the failure load at 0.5 reliability level is about 70 % of the experimental value while for a notched composite beam, it is about 60 % when only tensile stresses are considered. However, the ratio of unnotched to notched failure loads obtained by reliability analysis (2.066) is close to the experimental ratio of 1.752. When all stress components including interlaminar stresses are considered, the failure loads predicted by reliability analysis are much more conservative. The ratios of experimental failure load to that predicted by reliability analysis at 0.5 reliability level are about 4 for an unnotched composite beam and 2.5 for a notched composite beam.

For composite plates under transverse loading, the reliability formulation was extended to account for 3-D stress fields including interlaminar stresses. The reliability analysis showed that for this particular type of material the contribution from interlaminar stresses to total failure was small and this was confirmed by experiment [Heller et al. 1991]. The ratios of experimental failure load to that predicted by reliability analysis at 0.5 reliability level are about 4.6 for a square laminate with a hole, 4.1 for a rectangular laminate without a hole and 5.2 for a rectangular laminate with a hole.

In general, the reliability analysis predicted failure loads very well for isotropic beams. For composite beams and plates, however, the failure loads predicted were very conservative (25 % to 40 % for composite beams under 4-point bending and 20 % to 25 % for composite plates with and/or without a hole under transverse loading). The difference is attributed to the progressive failure mechanisms, stress redistribution after failure at the most sensitive region and with gradual stiffness reduction inherent in the composite structures.

Through careful examination of experimental results on carbon-carbon materials, new failure criteria were proposed. The criteria are intended for bi-directional composite laminae, however, as there are no failure criteria for bi-directional composite laminae appearing in the literature, the proposed criteria were applied to uni-directional composite laminae and the first-ply-failure loads were compared with those predicted by other criteria. Very good agreement between proposed and existing criteria was observed.

In an effort to relate the reliability analysis to FPF analysis, FPF analysis has been performed on the same composite beams and plates considered in the reliability analysis. The FPF analysis is based on the proposed criteria and Brewer-Lagace's criteria for composite beams and on the proposed criteria for composite plates. The agreement between the failure loads obtained by the two approaches was fairly good.

Future Work

By definition, first-ply-failure criteria are point stress criteria. In other words, FPF only detects the first element where a certain failure condition is met. Consequently, the FPF loads are on the conservative side and FPF does not necessarily mean the structure will fail. As explained earlier, when FPF takes place, the load is re-distributed among other remaining layers and the stiffness of the structure is reduced. This process is repeated each time a layer fails and the whole structure fails in a gradual manner layer after layer. The analysis based on this gradual stiffness reduction mechanism of composite structures is known as a progressive failure analysis and is recommended as a future research work.

REFERENCES

ABAQUS User's Manual, Ver. 4.8, Hibbitt, Karlsson & Sorensen, Inc., 1989

Brewer, J. C., Lagace, P. A., "Quadratic Stress Criterion for Initiation of Delamination," *Journal of Composite Materials*, Vol. 22, Dec., 1988

Christensen, R. M., "Tensor Transformations and Failure Criteria for the Analysis of Fiber Composite Materials," *Journal of Composite Materials*, Vol. 22, Sep., 1988

Cook, R. D., "Concepts and Applications of Finite Element Analysis," John Wiley & sons

George, K. P., "Statistical Theory of Size Effect on Material Strength - A Review"

Goldenblat, I., Kopnov, V. A., "Strength of Glass-Reinforced Plastics in the Complex Stress State," *Polymer Mechanics* 1(2), 1965, pp 54-59

Hahn, H. T., "On Approximations for Strength of Random Fiber Composites," *Journal of Composite Materials*, Vol. 9, Oct., 1975

Hashin, Z., Rotem, A., "A Fatigue Failure Criterion for Anisotropic Materials," *Journal of Composite Materials*, Vol. 7, 1971

Hashin, Z., "Failure Criteria for Unidirectional Fiber Composites," vol. 47, *Journal of Applied Mechanics*, June, 1980

Heller, R. A., "Tensile and Bend Strength of Graphite," HRB-Bericht Nr. BF 0843, Feb. 17, 1982

Heller, R. A., "Reliability Analysis of Brittle Components," HRB-Bericht, Nr. BF 0687, Dec. 12, 1981

Heller, R. A., "Guide of the Use of the Weibull Distribution," HRB-Bericht Nr. BF 0684, Dec. 1, 1981

Heller, R. A., Schmidt, A., Deninghoff, R., "The 'Weakest link' Concept after Proof Testing," *Proceedings of the IUTAM Symposium on Probabilistic Methods in the Mechanics of Solids & Structures*, S. Eggwertz Ed., Springer, Berlin, June, 1984, pp. 241-251.

Heller, R. A., Thangjitham, S., Wall, L. L., "Probability of failure of a Proof-Loaded Composite Plate with a Circular Hole," *Proceedings of International Symposium on Composite Materials and Structures*, T. T. Loo and C. T. Sun, eds., Beijing, China, June 10-13, 1986, pp. 764-769.

Heller, R. A., Thangjitham, S., Yeo, I., "Size Effects in Brittle Ceramics," *AIAA/ASME/ASCE/AHS 31st Structures, Structural Dynamics and Materials Conference*, Long Beach, CA, April 2-4, 1990

Heller, R. A., Thangjitham, S., Rantis T., Heller, T. G., "Experimental Determination of Mechanical Properties for a Carbon-Carbon Composite", Air Force Phillips Lab Technical Report PL - TR - 91 - 3068 - 4G (1) Edwards AFB, California. June 1991

Hill, R., "A Theory of the Yielding and Plastic Flow of Anisotropic Materials," *Proceedings of Royal Society, Series A*, Vol. 193, 1948, p. 281

- Hill, R., "The Mathematical Theory of Plasticity," Oxford University Press, London, 1950
- Hoffman, O., "The Brittle Strength of Orthotropic Materials," *Journal of Composite Materials*, Vol. 1, 1967, p. 200
- Hong, C. S., Crews, Jr., J. H., "Stress Concentration Factors for Finite Orthotropic Laminates with a Circular Hole and Uniaxial Loading," NASA Technical Paper 1469, 1979
- Hwang, W. C., Sun, C.T., "Failure Analysis of Laminated Composites by Using Iterative Three-Dimensional Finite Element Method," vol. 33, No. 1, *Computers & Structures*, 1989, pp 41-47
- I-DEAS User's Manual
- Jones, R. M., "Mechanics of Composite Materials," MacGraw-Hill
- Kim, R. Y., "On the Off-axis and Angle-ply Strength of Composites," Test Methods & Design Allowables for Fibrous Composites, ASTM STP 734, 1981, pp 281 - 337
- Kim, R. Y., Soni, S. R., "Experimental and Analytical Studies On the Onset of Delamination in Laminated Composites," *Journal of Composite Materials*, Vol. 18, Jan., 1984, pp. 70-80
- Kim, R. Y., Soni, S. R., "Failure of Composite Laminates due to Combined Interlaminar Normal and Shear Stresses," *Composites '86: Recent Advances in Japan and the United States*, 1986, pp 341-350
- Lee, J. D., "Three Dimensional Finite Element Analysis of Damage Accumulation in Composite Laminate," *Fracture of Composite Materials*, Ed. G. C. Sih, V. P. Tamuzs, Martinus Nijhoff Publishers, Mar. 9-12, 1981
- Margetson, J., "A Statistical Theory of Brittle Failure for an Anisotropic Structure Subjected to a Multi-axial Stress State," *AIAA 12th Propulsion Conference*, Paper No. 76-632, Palo Alto, CA., July 26-29, 1976.
- Margetson, J., "Failure Probability Evaluation of an Anisotropic Brittle Structure Derived from a Thermal Stress Solution," in Thermal Stresses in Severe Environment, D. P. H. Hasselman and R. A. Heller Eds., Plenum Press, New York, 1980, pp. 503-519
- PATRAN Plus User's Manual, PDA Engineering, 1988
- Pagano, N. J., Hatfield, S. J., "Elastic Behavior of Multilayered Bi-directional Composites," *AIAA Journal* Vol. 10, July 1972, pp 931-933
- Pipes, R. B., Cole, B. W., "On the Off-axis Strength Test for Anisotropic Materials," *Journal of Composite Materials*, Vol. 7, 1973
- Pollock, P. B., Private Communication, 1990
- Pollock, P. B., "Tensile Failure in 2-D Carbon-Carbon Composites," *Carbon*, Vol. 28, No. 5, 1990, pp 717-732
- Putchu, N. S., Reddy, J. N., "A Penalty Plate-Bending Element for the Analysis of Laminated Anisotropic Composite Plate," *International Journal for Numerical Method in Engineering*, vol. 15, 1980, pp 1187- 1206

Reddy, J. N., Chao, W. C., "A Comparison of Closed-Form and Finite Element Solutions of Thick Laminated Anisotropic Rectangular Plates," *Nuclear Engineering and Design* 64, 1981, pp 153-167

Reddy, J. N., "A simple Higher-Order Theory for Laminated Composite Plates," *Journal of Applied Mechanics*, Vol. 51, 1984, pp 745-752

Reddy, J. N., "A Mixed Shear Flexible Finite Element for the Analysis of Laminated Plates," *Computer Methods in Applied Mechanics and Engineering* 44, 1984, pp 213-227

Reddy, J. N., "An Introduction to the Finite Element Method," McGregor, 1984

Reddy, J. N., *Energy and Variational Methods in Applied Mechanics*, Wiley Interscience, 1984

Reddy, J. N., and Pandey, A. K., "A First-Ply Failure Analysis of Composite Laminates," *Computers and Structures*, Vol. 25, No. 3, 1987, pp 371-393

Rickman, D. K., Davis, H. O., and Wood, G., "Nozzle Material Evaluation", Final Report, Air Force Rocket Propulsion Laboratory, AFRPL TR-84-052, August, 1984

Rowlands, R. E., "Strength(Failure) Theories and Their Experimental Correlation," Handbook of Composites, Vol. 3, Failure Mechanics of Composites, Ed. G. C. Sih, A. M., Skudra, North-Holland, 1985

Sandhu, R. S., Sendeckyj, G. P., Gallo, R. L., "Modeling of the Failure Process in Notched Laminates," *Mechanics of Composite Materials, Recent Advances*, Ed. Z. Hashin, C. T. Herakovich, Proceedings of IUTAM Symposium on Mechanics of Composite Materials, Aug. 16-19, 1982

Soni, S. R., "A Comparative Study of Failure Envelopes in Composite Laminates," *Journal of Reinforced Plastics and Composites*, Vol. 2, Jan. 1983

Stanley, P. and Margetson, S., "Failure Probability Analysis of an Elastic Orthotropic Brittle Cylinder Subjected to Axi-symmetric Thermal and Pressure Loading," *International Journal of Fracture*, Vol. 13, No. 6, 1977, pp. 787-806.

Stanley, P., Sivill, A. D., and Fessler, H., "The Application and Confirmation of a Predictive Technique for Fracture of Brittle Components," *Proceedings of the 5th International Conference on Experimental Stress Analysis*, Paper No. 22, Udine, Italy, 1974.

Sun, C. T., Yamada, S. E., "Strength Distribution of a Uni-directional Fiber Composites," Vol. 12, *Journal of Composite Materials*, April 1978, p. 169

Thangjitham, S., Heller, R. A., "Reliability of a Proof-Loaded Fiber-Composite Plate under Randomly Oriented Loads," *AIAA/ASME/ASCE/AHS 28th Structures, Structural Dynamics and Materials Conference*, Part 1, April 6-8, 1987, pp 275-281

Toison, S, Zabarar, N, "Finite Element Analysis of Progressive Failure in Laminated Composite Plates," *Computers and Structures*, Vol. 38, No. 3, , 1991, pp 361 - 376

Tsai, S. W., "Fundamental Aspects of Fiber Reinforced Plastic Composites," Eds., R. T. Schwartz, H. S. Schwartz, in *Strength Theories of Filamentary Structures*, Wiley Interscience, New York, 1968, pp 3-11

- Tsai, S. W., and Wu, E. M., "A General Theory of Strength for Anisotropic Materials," *Journal of Composite Materials*, Vol. 5, 1971, p. 58
- Weibull, W., "Investigation into Strength Properties of Brittle Materials," *Proceedings of the Royal Swedish Institute for Engineering Research*, No. 149, 1938, pp. 1-27.
- Weibull, W., "The phenomenon of Rupture in Solids," *Ingeniors-vetenskapakademiens, Handlingar*, No. 153, 1939
- Weibull, W., "A Statistical Distribution Function of Wide Applicability," *Journal of Applied Mechanics*, Vol.18(3), 1951, pp. 293-297
- Wetherhold, R. C., "Reliability Calculation for Strength of a Fibrous Composites under Multi-axial Loading," *Journal of Composite Materials*, Vol. 15, 1981, p. 240
- Wetherhold, R. C., "The Effect of Stress Concentration on the Reliability of Composite Materials," *Journal of Composite Materials*, Vol 19, Jan. 1985
- Whitney, J. M., "Structural Analysis of Laminated Anisotropic Plates," Technomic Publishing Co. Inc., 1987
- Wu, E. M., "Failure Analysis of Composites with Stress Gradient," *Fracture of Composite Material*, G. Sih, V. Tamuzs Eds., Sijthoff & Noordoff, 1979, pp. 63-76.
- Yamada, S. E., Sun, C. T., "Analysis of Laminate Strength and Its Distribution," *Journal of Composite Materials*, Vol. 12, July 1978, pp. 275
- Yeo, J. C., "Reliability and Failure Analysis of Composite Beams and Plates Containing Stress Concentrations" PhD Dissertation, Virginia Polytechnic Inst. and State Univ. Blacksburg, VA. August 1991
- Zaghloul, S. A., Kennedy, J. B., "Nonlinear Behavior of Symmetrically Laminated Plates," *Journal of Applied Mechanics*, 42, , 1975, pp 234 - 236

Appendix-A

Table A.1 Average Tension and Compression Data

No. of specimens tested	Test direction	Type of test	E ksi = 10^3	σ_E ksi = 10^3	S_{max} ksi	σ_S ksi	ϵ_{max} in/in = 10^{-3}	σ_C in/in = 10^{-3}	ν_{12}	ν_{31}	ν_{21}	ν_{32}
18	W	T	2.140	149	13.416	926	8.500	1.710	.426	.093		
6	F	T	1.188	277	5.638	219	9.000	2.959	.048			203
6	W	C	2.125	247	8.298	628	4.366	1.152				
14	F	C	1.501	260	5.652	686	6.399	3.212				

Table A.2 In-plane Shear Data

No. of specimens tested	Specimen Type	Test direction	Modulus G_c , ksi - 10^3	σ_c , ksi - 10^3	Shear Strength $R = \gamma_{max}$, ksi	σ_R , ksi	Shear Strain γ_{symax} , in/in - 10^{-3}	σ_{γ} in/in - 10^{-3}
2	A	FA	237	--	2.494	--	15.682	--
3	B	WA	356	017	3.251	451	22.907	11.803
3	C	WF	305	101	4.328	261	43.11	13.928
5	D	FW	246	130	3.947	745	37.24	10.681

Table A.3 Interlaminar Shear Data

Test Direction	Shear Modulus $G \cdot 10^4$ psi	Shear Strength $R \cdot 10^3$ ksi
W	$G_{CW} = 2.5$	$R_{CW} = 2.00$
F	$G_{CF} = 1.3$	$R_{CF} = 1.58$

Formulation of Finite Element Program F2DELAST

Equilibrium Equations(without body forces)

The equilibrium equations are:

$$\frac{\partial \sigma_x}{\partial x} + \frac{\partial \tau_{xy}}{\partial y} = 0 \quad (69)$$

$$\frac{\partial \tau_{xy}}{\partial x} + \frac{\partial \sigma_y}{\partial y} = 0 \quad (70)$$

where σ_x , σ_y and τ_{xy} are normal stresses in the x- and y- directions and in-plane shear stress, respectively

Strain-Displacement Equations

The strain-displacement equations for two-dimensional elasticity are

$$\epsilon_x = \frac{\partial u}{\partial x} \quad (71)$$

$$\epsilon_y = \frac{\partial v}{\partial y} \quad (72)$$

$$\gamma_{xy} = \frac{\partial u}{\partial y} + \frac{\partial v}{\partial x} \quad (73)$$

where ϵ_x , ϵ_y , and γ_{xy} are normal strains in the x-, y-directions and in-plane shear strain, respectively.

Constitutive Equations

The constitutive equations that represent the behavior of two-dimensional elastic materials are:

$$\begin{Bmatrix} \sigma_x \\ \sigma_y \\ \tau_{xy} \end{Bmatrix} = \begin{bmatrix} C_{11} & C_{12} & 0 \\ C_{12} & C_{22} & 0 \\ 0 & 0 & C_{33} \end{bmatrix} \begin{Bmatrix} \epsilon_x \\ \epsilon_y \\ \gamma_{xy} \end{Bmatrix} \quad (74)$$

where C_{ij} are the elastic constants. For an isotropic elastic body, these can be written in terms of Young's modulus E and Poisson's ratio ν .

Boundary Conditions

Natural Boundary Conditions:

$$t_x = \sigma_x n_x + \tau_{xy} n_y = \hat{t}_x$$

and

$$t_y = \tau_{xy} n_x + \sigma_y n_y = \hat{t}_y, \text{ on } \Gamma_1 \quad (75)$$

Essential Boundary conditions:

$$u = \hat{u}$$

and

$$v = \hat{v}, \text{ on } \Gamma_2 \quad (76)$$

where $\hat{n} = (n_x, n_y)$ denotes the unit normal vector to the boundary Γ , Γ_1 and Γ_2 are disjoint portions of the boundary, \hat{t}_x and \hat{t}_y are the specified boundary traction forces in x- and y- directions, and \hat{u} and \hat{v} are the specified displacements in x- and y- directions.

Displacement Finite Element Formulation

In deriving displacement-based algebraic equations for a typical finite element, the stress components are expressed in terms of displacements by substituting strain-displacement equations (Eqs. 71-73) into the equilibrium equations as follows:

$$\begin{aligned} \sigma_x &= C_{11} \frac{\partial u}{\partial x} + C_{12} \frac{\partial v}{\partial y} \\ \sigma_y &= C_{12} \frac{\partial u}{\partial x} + C_{22} \frac{\partial v}{\partial y} \\ \tau_{xy} &= C_{33} \left(\frac{\partial u}{\partial y} + \frac{\partial v}{\partial x} \right) \end{aligned} \quad (77)$$

Variational Formulation

The original differential equilibrium equations are recast in the equivalent integral equation form (weak formulation). Then the following variational equations for a typical element can be obtained by multiplying the equilibrium equations by weighting functions w_i ($i=1,2$) and integrating over the domain of the element Ω^e . The typical element is shown in Fig.19. The variational form of equilibrium equations (Eqs.69– 70) over a typical element Ω^e is given by the following:

Weak Statements:

$$\begin{aligned}
(1) \quad 0 &= \int_{\Omega^e} w_1 \left(\frac{\partial \sigma_x}{\partial x} + \frac{\partial \tau_{xy}}{\partial y} \right) dx dy \\
&= \int_{\Omega^e} \left\{ \frac{\partial w_1}{\partial x} \left(C_{11} \frac{\partial u}{\partial x} + C_{12} \frac{\partial v}{\partial y} \right) + C_{33} \frac{\partial w_1}{\partial y} \left(\frac{\partial u}{\partial y} + \frac{\partial v}{\partial x} \right) \right\} dx dy - \int_{\Gamma^e} w_1 t_x ds \quad (78)
\end{aligned}$$

$$\begin{aligned}
(2) \quad 0 &= \int_{\Omega^e} w_2 \left(\frac{\partial \tau_{xy}}{\partial x} + \frac{\partial \sigma_y}{\partial y} \right) dx dy \\
&= \int_{\Omega^e} \left\{ C_{33} \frac{\partial w_2}{\partial x} \left(\frac{\partial u}{\partial y} + \frac{\partial v}{\partial x} \right) + \frac{\partial w_2}{\partial y} \left(C_{12} \frac{\partial u}{\partial x} + C_{22} \frac{\partial v}{\partial y} \right) \right\} dx dy - \int_{\Gamma^e} w_2 t_y ds \quad (79)
\end{aligned}$$

Finite Element Model

The two primary degrees of freedom u and v are approximated by the following scheme in terms of nodal displacements u_j^e and interpolation functions Ψ_i as follows:

$$\begin{aligned}
u &= \sum_{j=1}^n u_j^e \psi_j^1(x,y) \\
v &= \sum_{j=1}^n v_j^e \psi_j^2(x,y) \quad (80)
\end{aligned}$$

where u_j^e, v_j^e are the nodal values of the primary degrees of freedom u and v at node j , ψ_j^1, ψ_j^2 are the interpolation functions for u and v at node j , and n is the number of nodes in the element. For simplicity, the same interpolation function is used for both u and v , i.e. $\psi_i^1 = \psi_i^2 = \psi_i$.

Using the above interpolation scheme for u and v , and substituting Eq. 80 into Eqs. B178-79, the following are obtain:

$$(1) \quad w_1 = \psi_i^1 = \psi_i$$

$$\sum_{j=1}^n (K_{ij}^{11} u_j^e + K_{ij}^{12} v_j^e) = t_i^1 \quad (81)$$

$$(2) \quad w_2 = \psi_i^2 = \psi_i$$

$$\sum_{j=1}^n (K_{ij}^{21} u_j^e + K_{ij}^{22} v_j^e) = t_i^2 \quad (82)$$

where $[K^e]$ is the element stiffness matrix, $\{\Delta^e\}$ is the nodal displacement vector $\{u^e, v^e\}^T$ and $\{t^e\}$ is the boundary 'force' vector defined as follows:

$$K_{ij}^{11} = \int_{\Omega^e} \left(C_{11} \frac{\partial \psi_i}{\partial x} \frac{\partial \psi_j}{\partial x} + C_{33} \frac{\partial \psi_i}{\partial y} \frac{\partial \psi_j}{\partial y} \right) dx dy \quad (83)$$

$$K_{ij}^{12} = \int_{\Omega^e} \left(C_{12} \frac{\partial \psi_i}{\partial x} \frac{\partial \psi_j}{\partial y} + C_{33} \frac{\partial \psi_i}{\partial y} \frac{\partial \psi_j}{\partial x} \right) dx dy \quad (84)$$

$$t_i^1 = \int_{\Gamma^e} t_x \psi_i ds \quad (85)$$

$$K_{ij}^{21} = \int_{\Omega^e} \left(C_{33} \frac{\partial \psi_i}{\partial x} \frac{\partial \psi_j}{\partial y} + C_{12} \frac{\partial \psi_i}{\partial y} \frac{\partial \psi_j}{\partial x} \right) dx dy \quad (86)$$

$$K_{ij}^{22} = \int_{\Omega^e} \left(C_{33} \frac{\partial \psi_i}{\partial x} \frac{\partial \psi_j}{\partial x} + C_{22} \frac{\partial \psi_i}{\partial y} \frac{\partial \psi_j}{\partial y} \right) dx dy \quad (87)$$

$$t_i^2 = \int_{\Gamma^e} t_y \psi_i ds \quad (88)$$

Combining the system of equations above results in the following matrix equation for a typical element:

$$\begin{bmatrix} [K^{11}] & [K^{12}] \\ [K^{21}] & [K^{22}] \end{bmatrix}^e \begin{Bmatrix} \{u\} \\ \{v\} \end{Bmatrix}^e = \begin{Bmatrix} \{t^1\} \\ \{t^2\} \end{Bmatrix}^e \quad (89)$$

or in a compact form

$$[K^e(\Delta^e)] \{\Delta^e\} = \{t^e\} \quad (90)$$

Note that t_x and t_y are boundary traction terms defined by

$$\begin{aligned} t_x &= \sigma_x n_x + \tau_{xy} n_y \\ t_y &= \tau_{xy} n_x + \sigma_y n_y \end{aligned} \quad (91)$$

Finite Element Formulation for Nonlinear Bending of a Laminated Composite Plate with Shear Deformation

Equilibrium Equations

The equations for the first order shear-deformable plate theory used in the formulation of the finite element program FNCOMPLT are

$$\frac{\partial N_x}{\partial x} + \frac{\partial N_{xy}}{\partial y} = 0 \quad (92)$$

$$\frac{\partial N_{xy}}{\partial x} + \frac{\partial N_y}{\partial y} = 0 \quad (83)$$

$$\frac{\partial Q_x}{\partial x} + \frac{\partial Q_y}{\partial y} + \Phi(w, N_i) = -q_z \quad (94)$$

$$\frac{\partial M_x}{\partial x} + \frac{\partial M_{xy}}{\partial y} - Q_x = 0 \quad (95)$$

$$\frac{\partial M_{xy}}{\partial x} + \frac{\partial M_y}{\partial y} - Q_y = 0 \quad (96)$$

where $\Phi(w, N_i) = \frac{\partial}{\partial x} \left(\frac{\partial w}{\partial x} N_x + \frac{\partial w}{\partial y} N_{xy} \right) + \frac{\partial}{\partial y} \left(\frac{\partial w}{\partial x} N_{xy} + \frac{\partial w}{\partial y} N_y \right)$, $\{N_x, N_y, N_{xy}\}$ denote the in-plane stress resultants, $\{M_x, M_y, M_{xy}\}$ are the moment resultants, $\{Q_x, Q_y\}$ are the transverse shear stress resultants, respectively, defined by

$$\begin{Bmatrix} N_x \\ N_y \\ N_{xy} \end{Bmatrix} = \int_{-\frac{h}{2}}^{\frac{h}{2}} \begin{Bmatrix} \sigma_x \\ \sigma_x \\ \tau_{xy} \end{Bmatrix} dz \quad (97)$$

$$\begin{Bmatrix} M_x \\ M_y \\ M_{xy} \end{Bmatrix} = \int_{-\frac{h}{2}}^{\frac{h}{2}} \begin{Bmatrix} \sigma_x \\ \sigma_x \\ \tau_{xy} \end{Bmatrix} z dz \quad (98)$$

$$\begin{Bmatrix} Q_x \\ Q_y \end{Bmatrix} = \int_{-\frac{h}{2}}^{\frac{h}{2}} \begin{Bmatrix} \tau_{zx} \\ \tau_{yz} \end{Bmatrix} dz \quad (99)$$

and q_z is the transverse distributed load .

Laminate Constitutive Equations

The constitutive equations for a shear-deformable anisotropic laminated composite plate are

$$\begin{Bmatrix} \{N\} \\ \{M\} \end{Bmatrix} = \begin{bmatrix} [A] & [B] \\ [B] & [D] \end{bmatrix} \begin{Bmatrix} \{\epsilon^0\} \\ \{\kappa\} \end{Bmatrix} \quad (100)$$

$$\begin{Bmatrix} Q_y \\ Q_x \end{Bmatrix} = \begin{bmatrix} \bar{A}_{44} & \bar{A}_{45} \\ \bar{A}_{45} & \bar{A}_{55} \end{bmatrix} \begin{Bmatrix} \gamma_{yz} \\ \gamma_{xz} \end{Bmatrix} \quad (101)$$

where [A] is the extensional stiffness, [B] is the coupling stiffness, [D] is the bending stiffness, respectively, defined by

$$A_{ij} = \sum_{k=1}^n \bar{Q}_{ij}^k (z_k - z_{k-1}) \quad (102)$$

$$B_{ij} = \frac{1}{2} \sum_{k=1}^n \bar{Q}_{ij}^k (z_k^2 - z_{k-1}^2) \quad (103)$$

$$D_{ij} = \frac{1}{3} \sum_{k=1}^n \bar{Q}_{ij}^k (z_k^3 - z_{k-1}^3), \text{ for } i,j = 1,2,6 \quad (104)$$

\bar{A} is the transverse shear stiffness defined by

$$\bar{A}_{ij} = k_s^2 \sum_{k=1}^n \bar{Q}_{ij} (z_k - z_{k-1}), \text{ for } i,j = 4,5, \quad (105)$$

\bar{Q} is the transformed reduced stiffness matrix, and k_s^2 is the transverse shear correction factor(5/6 used here).

Strain-Displacement Equations

It is assumed that for first order shear-deformable plate theory, the displacement field is of the form

$$u(x,y,z) = u^0(x,y) + z \phi_x(x,y) \quad (106)$$

$$v(x,y,z) = v^0(x,y) + z \phi_y(x,y) \quad (107)$$

$$w(x,y,z) = w^0(x,y) \quad (108)$$

where $u(x,y,z)$, $v(x,y,z)$, $w(x,y,z)$ are the displacements in the x , y , and z directions, respectively, u^0 , v^0 , w^0 the mid-plane displacements, ϕ_x , ϕ_y are the rotations of the transverse normals about the y - and x -axis, respectively.

Then the nonlinear strain-displacement relations for the shear-deformable plate theory with geometrical nonlinearity in the sense of von Karman are

$$\epsilon_x = \epsilon_x^0 + z\kappa_x \quad (109)$$

$$\epsilon_y = \epsilon_y^0 + z\kappa_y \quad (110)$$

$$\gamma_{xy} = \gamma_{xy}^0 + z\kappa_{xy} \quad (111)$$

$$\gamma_{yz} = \gamma_{yz}^0 = \frac{\partial w}{\partial y} + \phi_y \quad (112)$$

$$\gamma_{zx} = \gamma_{zx}^0 = \frac{\partial w}{\partial x} + \phi_x \quad (113)$$

where ϵ_x^0 , ϵ_y^0 , γ_{xy}^0 are mid-plane strains, γ_{zx}^0 , γ_{yz}^0 are transverse shear strains, respectively, defined by

$$\epsilon_x^0 = \frac{\partial u^0}{\partial x} + \frac{1}{2} \left(\frac{\partial w}{\partial x} \right)^2 \quad (114)$$

$$\epsilon_y^0 = \frac{\partial v^0}{\partial y} + \frac{1}{2} \left(\frac{\partial w}{\partial y} \right)^2 \quad (115)$$

$$\gamma_{xy}^0 = \frac{\partial u^0}{\partial y} + \frac{\partial v^0}{\partial x} + \frac{\partial w}{\partial x} \frac{\partial w}{\partial y} \quad (116)$$

$$\gamma_{yz} = \gamma_{yz}^0 = \frac{\partial w}{\partial y} + \phi_y \quad (117)$$

$$\gamma_{zx} = \gamma_{zx}^0 = \frac{\partial w}{\partial x} + \phi_x \quad (118)$$

and κ_x , κ_y , κ_{xy} are bending curvatures defined by

$$\kappa_x = \frac{\partial \phi_x}{\partial x} \quad (119)$$

$$\kappa_y = \frac{\partial \phi_y}{\partial y} \quad (120)$$

$$\kappa_{xy} = \frac{\partial \phi_x}{\partial y} + \frac{\partial \phi_y}{\partial x} \quad (121)$$

Variational Formulation

Following the same weak formulation used for two-dimensional elasticity problems, the following variational equations for a typical element can be obtained. The typical element is shown in Fig. 19. It should be noted that w_i ($i=1,2,\dots,5$) are weighting functions, while w is a transverse displacement of the plate.

Weak statements:

$$(1): \quad 0 = \int_{\Omega^e} \left(\frac{\partial w_1}{\partial x} N_x + \frac{\partial w_1}{\partial y} N_{xy} \right) dx dy - \int_{\Gamma^e} w_1 (N_x n_x + N_{xy} n_y) ds \quad (122)$$

$$(2): \quad 0 = \int_{\Omega^e} \left(\frac{\partial w_2}{\partial x} N_{xy} + \frac{\partial w_2}{\partial y} N_y \right) dx dy - \int_{\Gamma^e} w_2 (N_{xy} n_x + N_y n_y) ds \quad (123)$$

$$(3): \quad 0 = \int_{\Omega^e} \left\{ \frac{\partial w_3}{\partial x} Q_x + \frac{\partial w_3}{\partial y} Q_y + \frac{\partial w_3}{\partial x} \left(\frac{\partial w}{\partial x} N_x + \frac{\partial w}{\partial y} N_{xy} \right) + \frac{\partial w_3}{\partial y} \left(\frac{\partial w}{\partial x} N_{xy} + \frac{\partial w}{\partial y} N_y \right) - w_3 q_z \right\} dx dy - \int_{\Gamma^e} w_3 \left\{ Q_x n_x + Q_y n_y + \left(N_x \frac{\partial w}{\partial x} + N_{xy} \frac{\partial w}{\partial y} \right) n_x + \left(N_{xy} \frac{\partial w}{\partial x} + N_y \frac{\partial w}{\partial y} \right) n_y \right\} ds \quad (124)$$

$$(4): 0 = \int_{\Omega^e} \left\{ \frac{\partial w_4}{\partial x} M_x + \frac{\partial w_4}{\partial y} M_{xy} + w_4 Q_x \right\} dx dy - \int_{\Gamma^e} w_4 (M_x n_x + M_{xy} n_y) ds \quad (125)$$

$$(5): 0 = \int_{\Omega^e} \left\{ \frac{\partial w_5}{\partial x} M_{xy} + \frac{\partial w_5}{\partial y} M_y + w_5 Q_y \right\} dx dy - \int_{\Gamma^e} w_5 (M_{xy} n_x + M_y n_y) ds \quad (126)$$

where w_i are the weighting functions, and from Eqs. 3.4.6 – 3.4.7, N_x , N_y , N_{xy} , M_x , M_y , M_{xy} are defined as follows:

$$N_x = A_{11} \left\{ \frac{\partial u^0}{\partial x} + \frac{1}{2} \left(\frac{\partial w}{\partial x} \right)^2 \right\} + A_{12} \left\{ \frac{\partial v^0}{\partial y} + \frac{1}{2} \left(\frac{\partial w}{\partial y} \right)^2 \right\} + A_{16} \left\{ \frac{\partial u^0}{\partial y} + \frac{\partial v^0}{\partial x} + \frac{\partial w}{\partial x} \frac{\partial w}{\partial y} \right\} \\ + B_{11} \frac{\partial \phi_x}{\partial x} + B_{12} \frac{\partial \phi_y}{\partial y} + B_{16} \left\{ \frac{\partial \phi_x}{\partial y} + \frac{\partial \phi_y}{\partial x} \right\} \quad (127)$$

$$N_y = A_{12} \left\{ \frac{\partial u^0}{\partial x} + \frac{1}{2} \left(\frac{\partial w}{\partial x} \right)^2 \right\} + A_{22} \left\{ \frac{\partial v^0}{\partial y} + \frac{1}{2} \left(\frac{\partial w}{\partial y} \right)^2 \right\} + A_{26} \left\{ \frac{\partial u^0}{\partial y} + \frac{\partial v^0}{\partial x} + \frac{\partial w}{\partial x} \frac{\partial w}{\partial y} \right\} \\ + B_{12} \frac{\partial \phi_x}{\partial x} + B_{22} \frac{\partial \phi_y}{\partial y} + B_{26} \left\{ \frac{\partial \phi_x}{\partial y} + \frac{\partial \phi_y}{\partial x} \right\} \quad (128)$$

$$N_{xy} = A_{16} \left\{ \frac{\partial u^0}{\partial x} + \frac{1}{2} \left(\frac{\partial w}{\partial x} \right)^2 \right\} + A_{26} \left\{ \frac{\partial v^0}{\partial y} + \frac{1}{2} \left(\frac{\partial w}{\partial y} \right)^2 \right\} + A_{66} \left\{ \frac{\partial u^0}{\partial y} + \frac{\partial v^0}{\partial x} + \frac{\partial w}{\partial x} \frac{\partial w}{\partial y} \right\} \\ + B_{16} \frac{\partial \phi_x}{\partial x} + B_{26} \frac{\partial \phi_y}{\partial y} + B_{66} \left\{ \frac{\partial \phi_x}{\partial y} + \frac{\partial \phi_y}{\partial x} \right\} \quad (129)$$

$$M_x = B_{11} \left\{ \frac{\partial u^0}{\partial x} + \frac{1}{2} \left(\frac{\partial w}{\partial x} \right)^2 \right\} + B_{12} \left\{ \frac{\partial v^0}{\partial y} + \frac{1}{2} \left(\frac{\partial w}{\partial y} \right)^2 \right\} + B_{16} \left\{ \frac{\partial u^0}{\partial y} + \frac{\partial v^0}{\partial x} + \frac{\partial w}{\partial x} \frac{\partial w}{\partial y} \right\} \\ + D_{11} \frac{\partial \phi_x}{\partial x} + D_{12} \frac{\partial \phi_y}{\partial y} + D_{16} \left\{ \frac{\partial \phi_x}{\partial y} + \frac{\partial \phi_y}{\partial x} \right\} \quad (130)$$

$$M_y = B_{12} \left\{ \frac{\partial u^0}{\partial x} + \frac{1}{2} \left(\frac{\partial w}{\partial x} \right)^2 \right\} + B_{22} \left\{ \frac{\partial v^0}{\partial y} + \frac{1}{2} \left(\frac{\partial w}{\partial y} \right)^2 \right\} + B_{26} \left\{ \frac{\partial u^0}{\partial y} + \frac{\partial v^0}{\partial x} + \frac{\partial w}{\partial x} \frac{\partial w}{\partial y} \right\} \\ + D_{12} \frac{\partial \phi_x}{\partial x} + D_{22} \frac{\partial \phi_y}{\partial y} + D_{26} \left\{ \frac{\partial \phi_x}{\partial y} + \frac{\partial \phi_y}{\partial x} \right\} \quad (131)$$

$$M_{xy} = B_{16} \left\{ \frac{\partial u^0}{\partial x} + \frac{1}{2} \left(\frac{\partial w}{\partial x} \right)^2 \right\} + B_{26} \left\{ \frac{\partial v^0}{\partial y} + \frac{1}{2} \left(\frac{\partial w}{\partial y} \right)^2 \right\} + B_{66} \left\{ \frac{\partial u^0}{\partial y} + \frac{\partial v^0}{\partial x} + \frac{\partial w}{\partial x} \frac{\partial w}{\partial y} \right\} \\ + D_{16} \frac{\partial \phi_x}{\partial x} + D_{26} \frac{\partial \phi_y}{\partial y} + D_{66} \left\{ \frac{\partial \phi_x}{\partial y} + \frac{\partial \phi_y}{\partial x} \right\} \quad (132)$$

$$Q_x = A_{55} \left(\frac{\partial w}{\partial x} + \phi_x \right) + A_{45} \left(\frac{\partial w}{\partial y} + \phi_y \right) \quad (133)$$

$$Q_y = A_{45} \left(\frac{\partial w}{\partial x} + \phi_x \right) + A_{44} \left(\frac{\partial w}{\partial y} + \phi_y \right) \quad (134)$$

Finite Element Model

The 5 primary degrees of freedom are approximated by the following scheme in terms of nodal displacements and interpolation functions:

$$u^0 = \sum_{j=1}^m u_j^0 \psi_j^{(1)} \\ v^0 = \sum_{j=1}^m v_j^0 \psi_j^{(1)} \\ w = \sum_{j=1}^n w_j \psi_j^{(2)} \\ \phi_x = \sum_{j=1}^p s_j^1 \psi_j^{(3)} \\ \phi_y = \sum_{j=1}^p s_j^2 \psi_j^{(3)} \quad (135)$$

where $u_j^0, v_j^0, w_j, s_j^1, s_j^2$ denote the nodal values of the primary degrees of freedom at node j , ψ_j is the interpolation function at node j , and m, n , and p are the number of nodes in a typical finite element, respectively. For simplicity, the same interpolation function and the same number of nodes are used for each of the 5 primary degrees of freedom, i.e. $\psi_j^{(1)} = \psi_j^{(2)} = \psi_j^{(3)} = \psi_j$, and $m=n=p$.

Using the definitions above and replacing the weighting functions w_i ($i=1,2,3,4,5$) by the interpolation functions ψ_i , the variational statements (Eqs.122 – 126) can be rewritten in terms of the element stiffness matrices, nodal displacements, and force vectors as

$$(1) w_1 = \psi_i^{(1)} = \psi_i$$

$$[K^{11}] \{u^0\} + [K^{12}] \{v^0\} + [K^{13}] \{w\} + [K^{14}] \{s^1\} + [K^{15}] \{s^2\} = \{F^1\} \quad (137)$$

$$(2) w_2 = \psi_i^{(1)} = \psi_i$$

$$[K^{21}] \{u^0\} + [K^{22}] \{v^0\} + [K^{23}] \{w\} + [K^{24}] \{s^1\} + [K^{25}] \{s^2\} = \{F^2\} \quad (138)$$

$$(3) w_3 = \psi_i^{(2)} = \psi_i$$

$$[K^{31}] \{u^0\} + [K^{32}] \{v^0\} + [K^{33}] \{w\} + [K^{34}] \{s^1\} + [K^{35}] \{s^2\} = \{F^3\} \quad (139)$$

$$(4) w_4 = \psi_i^{(3)} = \psi_i$$

$$[K^{41}] \{u^0\} + [K^{42}] \{v^0\} + [K^{43}] \{w\} + [K^{44}] \{s^1\} + [K^{45}] \{s^2\} = \{F^4\} \quad (140)$$

$$(5) w_5 = \psi_i^{(3)} = \psi_i$$

$$[K^{51}] \{u^0\} + [K^{52}] \{v^0\} + [K^{53}] \{w\} + [K^{54}] \{s^1\} + [K^{55}] \{s^2\} = \{F^5\} \quad (141)$$

Combining the system of equations above results in the following matrix equation for a typical element:

$$\begin{bmatrix} [K^{11}] & [K^{12}] & [K^{13}] & [K^{14}] & [K^{15}] \\ & [K^{22}] & [K^{23}] & [K^{24}] & [K^{25}] \\ & & [K^{33}] & [K^{34}] & [K^{35}] \\ & & & [K^{44}] & [K^{45}] \\ sym. & & & & [K^{55}] \end{bmatrix} \begin{bmatrix} \{u^0\} \\ \{v^0\} \\ \{w\} \\ \{s^1\} \\ \{s^2\} \end{bmatrix} = \begin{bmatrix} \{F^1\} \\ \{F^2\} \\ \{F^3\} \\ \{F^4\} \\ \{F^5\} \end{bmatrix} \quad (142)$$

or in a compact form

$$[K^e(\Delta)] \{\Delta^e\} = \{F^e\} \quad (143)$$

where $[K^e(\Delta)]$ is the element stiffness matrix, $\{\Delta^e\}$ is the nodal displacement vector $\{\Delta^e\} = \{\{u^0\}, \{v^0\}, \{w\}, \{s^1\}, \{s^2\}\}^T$ and $\{F^e\}$ is the 'force' vector containing boundary and the transverse force terms. The element stiffness matrix $[K^e(\Delta)]$ is a function of nodal displacements and the nodal displacements contain geometrically nonlinear terms which indicates that the nonlinear algebraic equations have to be solved iteratively.

The element stiffness matrix K_{ij}^{kl} and force vector F_i are presented later.

Assembly of Element Stiffness Matrix

The element stiffness matrices are assembled for all elements in the finite element mesh to give the following set of global algebraic equations:

$$[K(\Delta)]\{\Delta\} = \{F\} \quad (144)$$

where $[K(\Delta)]$ is the assembled global stiffness matrix, $\{\Delta\}$ is the 'solution' vector and $\{F\}$ is the assembled 'force' vector.

Solution Procedure (Newton-Raphson Iterative Method)

In the Newton-Raphson iteration method, the algebraic equation is rewritten in the form

$$\{R(\Delta)\} = [K(\Delta)]\{\Delta\} - \{F\} \quad (145)$$

where the residual $\{R(\Delta)\}$ is defined as the vector of unbalanced nodal forces at any given deformed state $\{\Delta\}^r$. The nonlinear solution procedure consists of searching for a vector $\{\Delta\}$ that renders the residual as small as possible. The deformed state $\{\Delta\}$ is an exact solution of the discretized equations if, and only if, the unbalanced nodal forces vanish.

Assuming that the solution is known at the r -th iteration for any given load step, the residual vector $\{R(\Delta)\}$ is expanded in Taylor series about $\{\Delta\}^r$:

$$\{R\} = \{R\}_{(\Delta) = \{\Delta\}^r} + \left[\frac{\partial \{R\}}{\partial \{\Delta\}} \right]_{(\Delta) = \{\Delta\}^r} (\{\Delta\}^{r+1} - \{\Delta\}^r) + \dots \quad (146)$$

If the higher order terms are neglected, the equation above can be written as

$$\{R\}_r + [K^T(\{\Delta\}^r)]\{\delta\Delta^r\} = \{0\} \quad (147)$$

where $[K^T(\{\Delta\}^r)]$ is the tangent stiffness matrix defined by

$$[K^T(\{\Delta\}^r)] = \left[\frac{\partial \{R\}}{\partial \{\Delta\}} \right]_{(\Delta) = \{\Delta\}^r} \quad (148)$$

or

$$K_{ij}^{T\alpha\beta} = K_{ij}^{\alpha\beta} + \sum_p \sum_\gamma \frac{\partial K_{ip}^{\alpha\gamma}}{\partial \Delta_j^\beta} \Delta_p^\gamma \quad (149)$$

and $\{\delta\Delta^r\}$ is the incremental solution defined by

$$\{\delta\Delta^r\} = \{\Delta\}^{r+1} - \{\Delta\}^r \quad (150)$$

From Eq. 3.4.56

$$\begin{aligned} \{\delta\Delta^r\} &= -[K^T(\{\Delta\}^r)]^{-1} \{R\}_r \\ &= [K^T(\{\Delta\}^r)]^{-1} (\{F\} - [K]^r \{\Delta\}^r) \end{aligned} \quad (151)$$

The residual vector or imbalance force $\{R(\{\Delta\}^r)\}$ is gradually reduced to zero if the procedure converges. The iteration continues until the following convergence criterion is satisfied:

$$\sqrt{\frac{\sum_{i=1}^n |\Delta_i^{r+1} - \Delta_i^r|^2}{\sum_{i=1}^n (\Delta_i^r)^2}} \leq \epsilon_{tol} \quad (152)$$

where n is the total number of degrees of freedom and ϵ_{tol} is the convergence tolerance.

Coefficients of Symmetric Tangent Stiffness Matrices $[K^T]$

$$\begin{aligned} K_{ij}^{T11} &= K_{ij}^{11}, K_{ij}^{T12} = K_{ij}^{12}, K_{ij}^{T13} = 2K_{ij}^{13}, K_{ij}^{T14} = K_{ij}^{14}, K_{ij}^{T15} = K_{ij}^{15} \\ K_{ij}^{T21} &= K_{ij}^{21}, K_{ij}^{T22} = K_{ij}^{22}, K_{ij}^{T23} = 2K_{ij}^{23}, K_{ij}^{T24} = K_{ij}^{24}, K_{ij}^{T25} = K_{ij}^{25} \\ K_{ij}^{T31} &= K_{ij}^{31}, K_{ij}^{T32} = K_{ij}^{32}, K_{ij}^{T34} = K_{ij}^{34}, K_{ij}^{T35} = K_{ij}^{35} \end{aligned} \quad (153)$$

$$\begin{aligned} K_{ij}^{T41} &= K_{ij}^{41}, K_{ij}^{T42} = K_{ij}^{42}, K_{ij}^{T43} = 2K_{ij}^{43}, K_{ij}^{T44} = K_{ij}^{44}, K_{ij}^{T45} = K_{ij}^{45} \\ K_{ij}^{T51} &= K_{ij}^{51}, K_{ij}^{T52} = K_{ij}^{52}, K_{ij}^{T53} = 2K_{ij}^{53}, K_{ij}^{T54} = K_{ij}^{54}, K_{ij}^{T55} = K_{ij}^{55} \\ K_{ij}^{T33} &= \int_{\Omega^e} \left\{ C^{T331} \frac{\partial \psi_i}{\partial x} \frac{\partial \psi_j}{\partial x} + C^{T332} \left(\frac{\partial \psi_i}{\partial x} \frac{\partial \psi_j}{\partial y} + \frac{\partial \psi_i}{\partial y} \frac{\partial \psi_j}{\partial x} \right) + C^{T333} \frac{\partial \psi_i}{\partial y} \frac{\partial \psi_j}{\partial y} \right\} dx dy \end{aligned} \quad (154)$$

where

$$\begin{aligned}
 C^{T331} = & A_{11} \frac{\partial u}{\partial x} + A_{16} \left(\frac{\partial u}{\partial y} + \frac{\partial v}{\partial x} \right) + A_{12} \frac{\partial v}{\partial y} + \frac{3}{2} A_{11} \left(\frac{\partial w}{\partial x} \right)^2 + 3 A_{16} \frac{\partial w}{\partial x} \frac{\partial w}{\partial y} \\
 & + \left(\frac{A_{12}}{2} + A_{66} \right) \left(\frac{\partial w}{\partial y} \right)^2 + A_{55} + B_{11} \frac{\partial \phi_x}{\partial x} + B_{16} \left(\frac{\partial \phi_x}{\partial y} + \frac{\partial \phi_y}{\partial x} \right) + B_{12} \frac{\partial \phi_y}{\partial y} \quad (155)
 \end{aligned}$$

$$\begin{aligned}
 C^{T332} = & A_{16} \frac{\partial u}{\partial x} + A_{66} \left(\frac{\partial u}{\partial y} + \frac{\partial v}{\partial x} \right) + A_{26} \frac{\partial v}{\partial y} + \frac{3}{2} A_{16} \left(\frac{\partial w}{\partial x} \right)^2 + (A_{12} + 2 A_{66}) \frac{\partial w}{\partial x} \frac{\partial w}{\partial y} \\
 & + \frac{3}{2} A_{26} \left(\frac{\partial w}{\partial y} \right)^2 + A_{45} + B_{16} \frac{\partial \phi_x}{\partial x} + B_{66} \left(\frac{\partial \phi_x}{\partial y} + \frac{\partial \phi_y}{\partial x} \right) + B_{26} \frac{\partial \phi_y}{\partial y} \quad (156)
 \end{aligned}$$

$$\begin{aligned}
 C^{T333} = & A_{12} \frac{\partial u}{\partial x} + A_{26} \left(\frac{\partial u}{\partial y} + \frac{\partial v}{\partial x} \right) + A_{22} \frac{\partial v}{\partial y} + \left(\frac{A_{12}}{2} + A_{66} \right) \left(\frac{\partial w}{\partial x} \right)^2 + 3 A_{26} \frac{\partial w}{\partial x} \frac{\partial w}{\partial y} \\
 & + \frac{3}{2} A_{22} \left(\frac{\partial w}{\partial y} \right)^2 + A_{44} + B_{12} \frac{\partial \phi_x}{\partial x} + B_{26} \left(\frac{\partial \phi_x}{\partial y} + \frac{\partial \phi_y}{\partial x} \right) + B_{22} \frac{\partial \phi_y}{\partial y} \quad (157)
 \end{aligned}$$

Table A.4 Average Mechanical Parameters (W= 1= Wrap, F= 2= Fill, A= 3= Across-ply Direction, f= Fiber, m= Matrix)

	Composite	Layer
	Modulus = 10^6 psi	Modulus = 10^6 psi
Tension	$E_W = 2.140$	$E_{f1} = 3.780$
	$E_F = 1.190$	$E_{f2} = 2.790$
	** $E_A = .855$	** $E_3 = .855$
	* $E_m = 0.500$	* $E_m = 0.500$
Compression	$E_W = 2.130$	$E_{f1} = 3.700$
	$E_F = 1.500$	$E_{f2} = 3.500$
	** $E_A = .820$	** $E_3 = .820$
	* $E_m = 0.500$	* $E_m = 0.500$
Shear	$G_{WF} = 0.355$	$G_{12} = 0.670$
	$G_{FW} = 0.246$	$G_{21} = 0.290$
	$G_{WA} = 0.357$	$G_{13} = 0.357$
	$G_{FA} = 0.340$	$G_{23} = 0.340$
	$G_{FW} = 0.025$	$G_{31} = 0.025$
	$G_{AF} = 0.018$	$G_{32} = 0.013$
	* $G_{sm} = 0.200$	* $G_{sm} = 0.200$
	Strength psi	Strength psi
Tension	$R_W = 13.400$	$R_{f1} = 24.800$
	$R_F = 5600$	$R_{f2} = 12.000$
	** $R_A = 8800$	** $R_3 = 8800$
	* $R_m = 2000$	* $R_m = 2000$
Compression	$R_W = 8300$	$R_{f1} = 14.000$
	$R_F = 5700$	$R_{f2} = 13.000$
	** $R_A = 24.000$	** $R_3 = 24.000$
	* $R_m = 2000$	* $R_m = 2000$

Table A.4 Continued

	Composite	Layer
Shear	$R_{WF} = 4300$	$R_{f12} = 9900$
	$R_{FW} = 4000$	$R_{21} = 6.400$
	$R_{WA} = 4000$	$R_{13} = 4000$
	$R_{FA} = 4100$	$R_{23} = 4100$
	$R_{AW} = 2000$	$R_{31} = 2000$
	$R_{AF} = 1600$	$R_{32} = 1600$
	${}^*R_{sm} = 1500$	${}^*R_{sm} = 1500$
	Poisson's ratio	Volume fraction
	$\nu_{12} = .048$	$\nu_{f1} = .500$
	$\nu_{21} = .093$	$\nu_{m1} = .500$
	${}^{**}\nu_{21} = .200$	$\nu_{f2} = .333$
	$\nu_{31} = .426$	$\nu_{m2} = .667$
	$\nu_{32} = .203$	
	${}^{**}\nu_{23} = .210$	
	$\nu_m = .250$	

* Estimated values

** From Rickman et al. 1984

Element Stiffness Matrix and Force Vector for Nonlinear Plate Bending Formulation

$$K_{ij}^{11} = \int_{\Omega^e} \left\{ A_{11} \frac{\partial \psi_i}{\partial x} \frac{\partial \psi_j}{\partial x} + A_{16} \left(\frac{\partial \psi_i}{\partial x} \frac{\partial \psi_j}{\partial y} + \frac{\partial \psi_i}{\partial y} \frac{\partial \psi_j}{\partial x} \right) + A_{66} \frac{\partial \psi_i}{\partial y} \frac{\partial \psi_j}{\partial y} \right\} dx dy$$

$$K_{ij}^{12} = \int_{\Omega^e} \left\{ A_{16} \frac{\partial \psi_i}{\partial x} \frac{\partial \psi_j}{\partial x} + A_{12} \frac{\partial \psi_i}{\partial x} \frac{\partial \psi_j}{\partial y} + A_{66} \frac{\partial \psi_i}{\partial y} \frac{\partial \psi_j}{\partial x} + A_{26} \frac{\partial \psi_i}{\partial y} \frac{\partial \psi_j}{\partial y} \right\} dx dy$$

$$K_{ij}^{13} = \int_{\Omega^e} \frac{1}{2} \frac{\partial w}{\partial x} \left\{ A_{11} \frac{\partial \psi_i}{\partial x} \frac{\partial \psi_j}{\partial x} + A_{16} \left(\frac{\partial \psi_i}{\partial x} \frac{\partial \psi_j}{\partial y} + \frac{\partial \psi_i}{\partial y} \frac{\partial \psi_j}{\partial x} \right) + A_{66} \frac{\partial \psi_i}{\partial y} \frac{\partial \psi_j}{\partial y} \right\} dx dy$$

$$+ \int_{\Omega^e} \frac{1}{2} \frac{\partial w}{\partial y} \left\{ A_{16} \frac{\partial \psi_i}{\partial x} \frac{\partial \psi_j}{\partial x} + A_{12} \frac{\partial \psi_i}{\partial x} \frac{\partial \psi_j}{\partial y} + A_{66} \frac{\partial \psi_i}{\partial y} \frac{\partial \psi_j}{\partial x} + A_{26} \frac{\partial \psi_i}{\partial y} \frac{\partial \psi_j}{\partial y} \right\} dx dy$$

$$K_{ij}^{14} = \int_{\Omega^e} \left\{ B_{11} \frac{\partial \psi_i}{\partial x} \frac{\partial \psi_j}{\partial x} + B_{16} \left(\frac{\partial \psi_i}{\partial x} \frac{\partial \psi_j}{\partial y} + \frac{\partial \psi_i}{\partial y} \frac{\partial \psi_j}{\partial x} \right) + B_{66} \frac{\partial \psi_i}{\partial y} \frac{\partial \psi_j}{\partial y} \right\} dx dy$$

$$K_{ij}^{15} = \int_{\Omega^e} \left\{ B_{16} \frac{\partial \psi_i}{\partial x} \frac{\partial \psi_j}{\partial x} + B_{12} \frac{\partial \psi_i}{\partial x} \frac{\partial \psi_j}{\partial y} + B_{66} \frac{\partial \psi_i}{\partial y} \frac{\partial \psi_j}{\partial x} + B_{26} \frac{\partial \psi_i}{\partial y} \frac{\partial \psi_j}{\partial y} \right\} dx dy$$

$$F_i^1 = \int_{r^e} \left\{ \psi_i (N_x n_x + N_{xy} n_y) \right\} ds$$

$$K_{ij}^{21} = K_{ij}^{12}$$

$$K_{ij}^{22} = \int_{\Omega^e} \left\{ A_{66} \frac{\partial \psi_i}{\partial x} \frac{\partial \psi_j}{\partial x} + A_{26} \left(\frac{\partial \psi_i}{\partial x} \frac{\partial \psi_j}{\partial y} + \frac{\partial \psi_i}{\partial y} \frac{\partial \psi_j}{\partial x} \right) + A_{22} \frac{\partial \psi_i}{\partial y} \frac{\partial \psi_j}{\partial y} \right\} dx dy$$

$$K_{ij}^{23} = \int_{\Omega^e} \frac{1}{2} \frac{\partial w}{\partial x} \left\{ A_{16} \frac{\partial \psi_i}{\partial x} \frac{\partial \psi_j}{\partial x} + A_{66} \frac{\partial \psi_i}{\partial x} \frac{\partial \psi_j}{\partial y} + A_{12} \frac{\partial \psi_i}{\partial y} \frac{\partial \psi_j}{\partial x} + A_{26} \frac{\partial \psi_i}{\partial y} \frac{\partial \psi_j}{\partial y} \right\} dx dy$$

$$+ \int_{\Omega^e} \frac{1}{2} \left(\frac{\partial w}{\partial y} \right)^2 \left\{ A_{66} \frac{\partial \psi_i}{\partial x} \frac{\partial \psi_j}{\partial x} + A_{26} \left(\frac{\partial \psi_i}{\partial x} \frac{\partial \psi_j}{\partial y} + \frac{\partial \psi_i}{\partial y} \frac{\partial \psi_j}{\partial x} \right) + A_{22} \frac{\partial \psi_i}{\partial y} \frac{\partial \psi_j}{\partial y} \right\} dx dy$$

$$K_{ij}^{34} = \int_{\Omega^e} \left(A_{55} \frac{\partial \psi_i}{\partial x} \psi_j + A_{45} \frac{\partial \psi_i}{\partial y} \psi_j \right) dx dy$$

$$+ \int_{\Omega^e} \frac{\partial w}{\partial x} \left\{ B_{11} \frac{\partial \psi_i}{\partial x} \frac{\partial \psi_j}{\partial x} + B_{16} \left(\frac{\partial \psi_i}{\partial x} \frac{\partial \psi_j}{\partial y} + \frac{\partial \psi_i}{\partial y} \frac{\partial \psi_j}{\partial x} \right) + B_{66} \frac{\partial \psi_i}{\partial y} \frac{\partial \psi_j}{\partial y} \right\} dx dy$$

$$+ \int_{\Omega^e} \frac{\partial w}{\partial y} \left\{ B_{16} \frac{\partial \psi_i}{\partial x} \frac{\partial \psi_j}{\partial x} + B_{66} \frac{\partial \psi_i}{\partial x} \frac{\partial \psi_j}{\partial y} + B_{12} \frac{\partial \psi_i}{\partial y} \frac{\partial \psi_j}{\partial x} + B_{26} \frac{\partial \psi_i}{\partial y} \frac{\partial \psi_j}{\partial y} \right\} dx dy$$

$$K_{ij}^{35} = \int_{\Omega^e} \left(A_{45} \frac{\partial \psi_i}{\partial x} \psi_j + A_{44} \frac{\partial \psi_i}{\partial y} \psi_j \right) dx dy$$

$$+ \int_{\Omega^e} \frac{\partial w}{\partial x} \left\{ B_{16} \frac{\partial \psi_i}{\partial x} \frac{\partial \psi_j}{\partial x} + B_{12} \frac{\partial \psi_i}{\partial x} \frac{\partial \psi_j}{\partial y} + B_{66} \frac{\partial \psi_i}{\partial y} \frac{\partial \psi_j}{\partial x} + B_{26} \frac{\partial \psi_i}{\partial y} \frac{\partial \psi_j}{\partial y} \right\} dx dy$$

$$+ \int_{\Omega^e} \frac{\partial w}{\partial y} \left\{ B_{66} \frac{\partial \psi_i}{\partial x} \frac{\partial \psi_j}{\partial x} + B_{26} \left(\frac{\partial \psi_i}{\partial x} \frac{\partial \psi_j}{\partial y} + \frac{\partial \psi_i}{\partial y} \frac{\partial \psi_j}{\partial x} \right) + B_{22} \frac{\partial \psi_i}{\partial y} \frac{\partial \psi_j}{\partial y} \right\} dx dy$$

$$F_i^3 = \int_{\Omega^e} \psi_i q_z dx dy - \int_{r^e} \psi_i \left\{ \left(Q_x + N_x \frac{\partial w}{\partial x} + N_{xy} \frac{\partial w}{\partial y} \right) n_x + \left(Q_y + N_{xy} \frac{\partial w}{\partial x} + N_y \frac{\partial w}{\partial y} \right) n_y \right\} ds$$

$$K_{ij}^{41} = K_{ji}^{14}$$

$$K_{ij}^{42} = K_{ji}^{24}$$

$$K_{ij}^{43} = \int_{\Omega^e} \left(A_{55} \psi_i \frac{\partial \psi_j}{\partial x} + A_{45} \psi_i \frac{\partial \psi_j}{\partial y} \right) dx dy$$

$$+ \int_{\Omega^e} \frac{1}{2} \frac{\partial w}{\partial x} \left\{ B_{11} \frac{\partial \psi_i}{\partial x} \frac{\partial \psi_j}{\partial x} + B_{16} \left(\frac{\partial \psi_i}{\partial x} \frac{\partial \psi_j}{\partial y} + \frac{\partial \psi_i}{\partial y} \frac{\partial \psi_j}{\partial x} \right) + B_{66} \frac{\partial \psi_i}{\partial y} \frac{\partial \psi_j}{\partial y} \right\} dx dy$$

$$+ \int_{\Omega^e} \frac{1}{2} \frac{\partial w}{\partial y} \left\{ B_{16} \frac{\partial \psi_i}{\partial x} \frac{\partial \psi_j}{\partial x} + E_{12} \frac{\partial \psi_i}{\partial x} \frac{\partial \psi_j}{\partial y} + B_{66} \frac{\partial \psi_i}{\partial y} \frac{\partial \psi_j}{\partial x} + B_{26} \frac{\partial \psi_i}{\partial y} \frac{\partial \psi_j}{\partial y} \right\} dx dy$$

$$K_{ij}^{44} = \int_{\Omega^e} \left\{ A_{55} \psi_i \psi_j + D_{11} \frac{\partial \psi_i}{\partial x} \frac{\partial \psi_j}{\partial x} + D_{16} \left(\frac{\partial \psi_i}{\partial x} \frac{\partial \psi_j}{\partial y} + \frac{\partial \psi_i}{\partial y} \frac{\partial \psi_j}{\partial x} \right) + D_{66} \frac{\partial \psi_i}{\partial y} \frac{\partial \psi_j}{\partial y} \right\} dx dy$$

$$K_{ij}^{45} = \int_{\Omega^e} \left\{ A_{45} \psi_i \psi_j + D_{16} \frac{\partial \psi_i}{\partial x} \frac{\partial \psi_j}{\partial x} + D_{12} \frac{\partial \psi_i}{\partial x} \frac{\partial \psi_j}{\partial y} + D_{66} \frac{\partial \psi_i}{\partial y} \frac{\partial \psi_j}{\partial x} + D_{26} \frac{\partial \psi_i}{\partial y} \frac{\partial \psi_j}{\partial y} \right\} dx dy$$

$$F_i^4 = \int_{\Gamma_i^e} \left\{ \psi_i (M_x n_x + M_{xy} n_y) \right\} ds$$

$$K_{ij}^{51} = K_{ji}^{15}$$

$$K_{ij}^{52} = K_{ji}^{25}$$

$$K_{ij}^{53} = \int_{\Omega^e} \left(A_{45} \psi_i \frac{\partial \psi_j}{\partial x} + A_{44} \psi_i \frac{\partial \psi_j}{\partial y} \right) dx dy$$

$$+ \int_{\Omega^e} \frac{1}{2} \frac{\partial w}{\partial x} \left\{ B_{16} \frac{\partial \psi_i}{\partial x} \frac{\partial \psi_j}{\partial x} + B_{66} \frac{\partial \psi_i}{\partial x} \frac{\partial \psi_j}{\partial y} + B_{12} \frac{\partial \psi_i}{\partial y} \frac{\partial \psi_j}{\partial x} + B_{26} \frac{\partial \psi_i}{\partial y} \frac{\partial \psi_j}{\partial y} \right\} dx dy$$

$$+ \int_{\Omega^e} \frac{1}{2} \frac{\partial w}{\partial y} \left\{ B_{66} \frac{\partial \psi_i}{\partial x} \frac{\partial \psi_j}{\partial x} + B_{26} \left(\frac{\partial \psi_i}{\partial x} \frac{\partial \psi_j}{\partial y} + \frac{\partial \psi_i}{\partial y} \frac{\partial \psi_j}{\partial x} \right) + B_{22} \frac{\partial \psi_i}{\partial y} \frac{\partial \psi_j}{\partial y} \right\} dx dy$$

$$K_{ij}^{54} = K_{ji}^{45}$$

$$K_{ij}^{55} = \int_{\Omega^e} \left\{ A_{44} \psi_i \psi_j + D_{66} \frac{\partial \psi_i}{\partial x} \frac{\partial \psi_j}{\partial x} + D_{26} \left(\frac{\partial \psi_i}{\partial x} \frac{\partial \psi_j}{\partial y} + \frac{\partial \psi_i}{\partial y} \frac{\partial \psi_j}{\partial x} \right) + D_{22} \frac{\partial \psi_i}{\partial y} \frac{\partial \psi_j}{\partial y} \right\} dx dy$$

$$F_i^S = \int_{r^S} \{ \psi_i (M_{xy} n_x + M_y n_y) \} ds$$